

MASTER THESIS

Low Frequency Second Order Roll of a Semi-Submersible Crane Vessel

B.J. Dubbeldam

Delft University of Technology



This research is supported by

Heerema Marine Contractors (HMC)

Maritime Research Institute Netherlands (MARIN)

MASTER THESIS

Low Frequency Second Order Roll of a Semi-Submersible Crane Vessel

- Estimation of the low frequency second order roll response of the Sleipnir in the frequency and time domain -

by

B.J. Dubbeldam

4333446

A thesis submitted in partial fulfillment of the requirements for the degree of

Master of Science
in Offshore & Dredging Engineering

at the Delft University of Technology,
to be defended publicly on Tuesday May 17, 2016 at 14:00.

April 2015 - May 2016
45 ECTS

Chairman:	Prof. dr. ir. R. H. M. Huijsmans	TU Delft
Thesis committee:	ir. P. Naaijen	TU Delft
	ir. P. de Vos	TU Delft
	ir. J. den Haan	TU Delft
	ir. B. Hoogendoorn	HMC
	ir. O. Waals	MARIN



ABSTRACT

Heerema Marine Contractors is constructing a new semi-submersible crane vessel, the Sleipnir. Due to low initial stability, semi-submersibles may present significant wave induced resonant motions in heave, roll and pitch. For practical reasons, especially the roll motion could play a limiting factor for future lift operations of the Sleipnir. In order to study the hydrodynamic behaviour of the Sleipnir, model tests in waves have been performed at Maritime Research Institute Netherlands. In the tested sea states low frequent second order roll has been observed. In order to evaluate the impact of the low frequent motions of the Sleipnir it is important to create an accurate (low frequent) simulation model.

The aim of this thesis is to investigate if a low frequency roll motion simulation model, in the frequency and time domain, can be created. It is challenging to predict the low frequent second order roll motions in good agreement with the measurements due to two main non-linear phenomenons. In the first place, the (viscous) roll damping is considered to be non-linear. In the second place, the second order wave forces in the vertical plane, which have not been investigated extensively in the past, are non-linear phenomena.

A calculation method in order to simulate the low frequency roll motions is created. This simulation method makes use of a first and second order hydrodynamic data base, first and second order moment spectra and a moment transfer function in order to define the roll motion spectrum. In order to implement viscous roll damping in the frequency domain method, a linearization of the roll damping is necessary. First empirical linear viscous damping values have been obtained for the three tested sea states. The frequency domain method predicts the roll motion energy in good agreement with the measurements, using the empirical linear viscous roll damping values, for the three tested sea states.

In order to predict the low frequent roll motions for any sea state, a calculation scheme is proposed. In this calculation scheme, a linear roll damping prediction method based on linearization techniques, is incorporated. However, the investigated linearization techniques do not predict the linear viscous damping in agreement with the measurements. The energy in the roll motion response spectrum is highly dependent on the amount of added viscous damping in the calculation. Therefore, it will be hard, due to inaccurate linear viscous damping predictions assigned to the linearization techniques, to estimate the low frequency second order roll motions in good agreement with the measurements.

In the time domain simulations non-linear viscous damping terms are incorporated by means of a linear and quadratic damping coefficient. Still water decay test simulations show a very good agreement with the measurements when using damping coefficients obtained from decay tests. However, the statistics of the simulated model tests are not in exact agreement with statistics of the model tests. Possible causes for this mismatch are discussed. It must be noted that the time domain simulations have been validated with only one sea state. It is recommended to validate the time domain model for more sea states.

Although the model tests and simulation methods show significant second order roll motions, which are undesirable for performing a heavy lift, it must be realized that a combination of the tested conditions (very low initial stability, long crested beam waves) will be very rare during a future heavy lift of the Sleipnir. Additionally it is noted, that the tested sea states exceed the typical heavy lift operability limit, used by Heerema.

ACKNOWLEDGEMENTS

This master thesis describes the research performed in order to complete the requirements for the degree of Master of Science, in Offshore & Dredging Engineering, at the Delft University of Technology. The research is performed in cooperation with Heerema Marine Contractors in Leiden and Maritime Research Institute Netherlands in Wageningen, in order to gain more understanding in low frequent roll motions of the Sleipnir, a semi-submersible crane vessel.

During this research, I did not only see a lot of the Netherlands, but I also got an insight in two technical environments. Working in a technical environment has been a new experience for me, due to the fact that I performed a non-technical bachelor in Physics & Astrophysics. On the one hand, I experienced the corporate environment of a marine contractor which operates semi-submersibles with the largest lift capacities in the world. On the other hand, I experienced the technical environment of one of the world's largest independent maritime research institutes. Both organizations have big departments involved with research into the hydrodynamic behaviour of vessels, a subject in which I became very interested during my masters. I would like to express my gratitude to both organizations for the given chance to perform this graduation research.

First and foremost, I would like to thank my supervisors, Bob Hoogendoorn and Olaf Waals, for their helpfulness during the whole research period. Without their support, I would not have been able to get this far. I learned a lot from Bob's practical way of approaching technical problems and I admire Olaf's, seemingly never ending, theoretical knowledge.

Secondly, I would like to thank Radboud van Dijk and Geert Meskers. Their advice and expertise helped me in many stages of this research. Furthermore, I want to thank the other members of my expert panel from Heerema, Eelco Harmsen and Rimmelt Heemskerk, for their input in progress meetings.

From the university, I would like to express my gratitude to professor Huijsmans for supervising this thesis and providing guidance along the way. I would like to thank Peter Naaijen and Peter de Vos for their time and interest in participating in my graduation committee.

Lastly, I would like to thank my family and friends for their support throughout the course of this graduation study.

*Boaz Dubbeldam
Amsterdam, May 2016*

CONTENTS

Abstract	iii
Acknowledgements	v
Introduction	1
Research questions	2
Reading guide	3
1 Theory	5
1.1 Long wave induced by regular wave groups	5
1.2 Second order wave force and moment	7
1.2.1 Quadratic Transfer Functions	8
1.2.2 Calculation methods for the second order potential contribution	8
1.3 Force Spectrum	9
1.4 Motion Response Spectrum	9
1.5 Roll damping	10
1.6 Definition of Ship motions and origin	12
2 Model tests	13
2.1 Model test set up	13
2.2 Most Relevant Results	16
2.3 Most Relevant Conclusions	18
3 Method	19
3.1 Frequency domain study	19
3.1.1 Refinement studies	19
3.2 First Order Analysis	24
3.3 Second Order Analysis	27
3.4 Total response spectrum	30
3.4.1 Validation	30
3.5 Comparison of WAMIT and DIFFRAC	30
3.6 Time domain study	31
4 Results and Discussion	33
4.1 Calculation of the roll damping	33
4.1.1 Discussion	36
4.2 Grid refinement study	39
4.2.1 Quadratic Transfer Function	39
4.2.2 Second Order Moment Spectrum	40
4.2.3 Moment Transfer Function	41
4.2.4 Second order roll response spectrum	42
4.3 Frequency Refinement Study	43
4.3.1 Quadratic Transfer Function	43
4.3.2 Second Order Moment Spectrum	43
4.3.3 Moment Transfer Function	44
4.3.4 Second order roll response spectrum	46
4.4 Viscous Damping Study	48
4.4.1 Quadratic Transfer Function	48
4.4.2 Second Order Moment Spectrum	49
4.4.3 Moment Transfer Function	50
4.4.4 Second order roll response spectrum	52

4.5	Total Roll Response Spectrum	53
4.5.1	Influence of viscous damping on the roll response spectrum	53
4.5.2	Discussion	54
4.6	Comparison of WAMIT and DIFFRAC calculations	57
4.6.1	First Order	57
4.6.2	Second order.	58
4.7	Influence second order contributions on low frequency quadratic transfer function	63
4.7.1	Discussion	65
4.8	Time domain study	69
4.8.1	Decay test simulation	69
4.8.2	Model test simulation	71
5	Conclusions and Recommendations	79
5.1	Refinement Studies	79
5.2	Frequency Domain Simulation Study	80
5.3	Time Domain Simulation Study.	81
5.4	Answer to research question	84
5.5	Second Order Roll Problem in Perspective	84
5.6	Enumeration of Conclusions	85
5.7	Enumeration of Recommendations.	86
	Bibliography	87
A	Appendix Vessel Specifications of Sleipnir	89
B	Appendix Results	93
B.1	Frequency domain study	94
B.1.1	Quadratic Transfer function	94
B.1.2	Comparison method of results WAMIT and DIFFRAC	99
B.1.3	Influence of different p and q values on equivalent damping	103
B.1.4	Estimation of roll damping using the half-power bandwidth method	105
B.1.5	Influence of added viscous damping on roll motion response spectrum	109
B.2	Time domain study	121
B.2.1	Roll time traces of model test simulations	121
B.2.2	Modeltest simulation using JONSWAP with different seeds	125
B.2.3	Simulations using measured wave trains from WAVECL, WAVE180 and WAVE270	128
B.2.4	Time traces and spectra of measured waves during MARIN tests.	130
C	Appendix Theoretical Background	137
C.1	Statistical Analysis	138
C.1.1	Statistical Description of Waves	138
D	Appendix Software	141
E	Appendix Discretized Surface Models	147
E.1	Wetted Body Surface	148
E.2	Free Water Surface	154
F	Appendix Error Analyses Manual	155
G	Appendix Company Profiles	161
G.1	Heerema Marine Contractors	162
G.2	Maritime Research Institute Netherlands	163

INTRODUCTION

Heerema Marine Contractors (HMC) is a marine contractor specialized in transportation, installing and removing offshore facilities. Their current fleet consists of three Semi-Submersible Crane Vessels (SSCV's), a (monohull) deepwater construction vessel, tugs and barges¹. In order to maintain their world leading position as a marine contractor HMC is designing a New Semi-Submersible Crane Vessel (NSCV) with a lift capacity of 20000 tonnes.

According to HMC tradition the new semi-submersible has been named after a figure from Norse mythology. The semi-submersible is named 'Sleipnir', the eight legged steed of Odin. In the mythology Sleipnir is praised for his strength, courage and speed. HMC is focussed to do justice to the vessels name. In Figure 1 an artist impression of the Sleipnir is shown.

The main purpose of the Sleipnir will be to transport, install and remove offshore facilities. In this research the vessel is investigated during installation conditions. Due to its hull shape, the operability of a semi-submersible crane vessel differs from the operability of a 'normal' shaped vessel. A semi-submersible vessel consists of floaters (or pontoons) and an operational deck, connected with structural columns as shown in Figure 1.



Figure 1: Artist impression of the Sleipnir. A semi-submersible crane vessel with eight columns.

The draft of a semi-submersible vessel can be varied by (de)ballasting the pontoons with sea water. In a transit the semi-submersible will use a shallow draft and the pontoons will intersect the water surface. In a transit the semi-submersible experiences less water resistance due to the hydrodynamic shaped pontoons. Performing a heavy lift operation, the semi-submersible will use a deeper (operational) draft, in which only the columns will intersect the water surface. In this situation the semi-submersible is less affected by wave loading than 'normal' shaped ships.

In practice, when performing a heavy lift operation, a Semi-Submersible Crane Vessel (SSCV) is often exposed to beam waves (waves coming from port side or starboard). The reason for this orientation is that large liftable objects, like an integrated topside, are often transported on a barge to the desired offshore location. The barge will be orientated in head waves (waves on the bow) in order to reduce the motions of the barge. Considering the SSCV will perform a dual lift (using both cranes), the vessel will be orientated in beam waves due to the position of the cranes on the vessel. In Figure 2 a schematic overview of this situation is shown. The roll behaviour of the SSCV, due to the beam wave loading, will be an important factor in the operability of a heavy lift operation. The hydrostatic and hydrodynamic properties are, in general, of great importance for the design and the future operability of a vessel. In order to study the hydrodynamic behaviour of the Sleipnir, model tests have been performed at Maritime Research Institute Netherlands (MARIN)¹.

¹Complete company profiles can be found in Appendix G.

In this research the model tests, performed in beam waves, are investigated. The model tests have been performed at operational draft, which is the design draft for a heavy lift operation. The motions of the Sleipnir are measured in three sea states. The natural roll period in operational stability conditions is ≈ 10 s. Due to the long roll period in this condition, the roll motion is expected to be sensitive for the low frequent energy of wave groups (Figure 3). Research already showed that sea states, with peak periods of 7-10 seconds, can cause large roll angles for semi-submersibles with long roll periods [1].

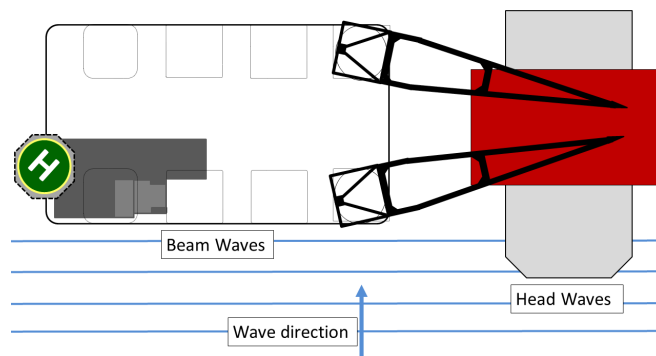


Figure 2: Schematic overview of a semi-submersible crane vessel performing a dual lift while being exposed to beam waves.

In order to investigate if this low frequent roll behaviour also applies for the Sleipnir, model tests have been performed with sea states with peak periods of 7 and 12 seconds and wave heights of 1.5 and 3 meter. As was expected, based on theory and earlier model test results (e.g. [1]), low frequent second order roll motions have been measured during the MARIN model tests.

Before defining the research questions for this research, a short historical review is presented. The first order linear behaviour of vessel motions is investigated for a long time and is assumed to be an understood phenomenon, e.g. [2]. The non-linear second order motions in the horizontal plane (surge, sway, yaw) have been subject of investigation for quite some decades. Horizontal drift forces have a big influence on practical applications, as the loads on mooring lines and risers, and are therefore investigated extensively, e.g. [3], [4], [5]. Although research suggested that the second order phenomena could have a significant effect on the second order roll motions of a semi-submersible [4], [5], the second order (drift) forces in the vertical plane (heave, roll, pitch) have been investigated less extensively. Recent work by Matos et al shows prediction methods for the pitch and heave motions in the frequency domain [6], [7], [8]. In these studies no prediction methods for the viscous damping terms have been used.

Viscous roll damping, due to its non-linear behaviour, is not easy to accurately predict. Viscous roll damping, and roll damping prediction methods, have been subject of investigation for more than sixty years, e.g. [9], [10]. Recent studies, on FPSO roll damping, suggest a calculation method for first order roll motions including a roll prediction technique, e.g. [11].

RESEARCH QUESTIONS

The measured low frequent second order roll behaviour, measured during model tests, contains of two (main) non-linear phenomena. The roll motion excited by second order wave forces and the roll damping. It is challenging to predict the low frequency second order roll motions accurately, due to the dual non-linearity. Therefore the main research question of this study is:

Is it possible to predict the low frequency second order roll motions of the Sleipnir, in good agreement with the model tests, in the frequency and time domain?

In order to answer this question the following subquestions are defined:

- a) The quadratic transfer function is approximated with potential flow theory. The quadratic transfer function will influence the calculation of the roll response spectrum, in the frequency and time domain. What is the influence of the following variables on the calculation of the roll response spectrum?
 - Discretized hull shape of the Sleipnir
 - Frequency resolution
 - Added viscous damping
- b) Is it possible to accurately predict the roll damping in the frequency and time domain?
- c) The quadratic transfer function consist of five contributions. What are the dominant contributions in the roll motion response spectrum, in the tested sea states?

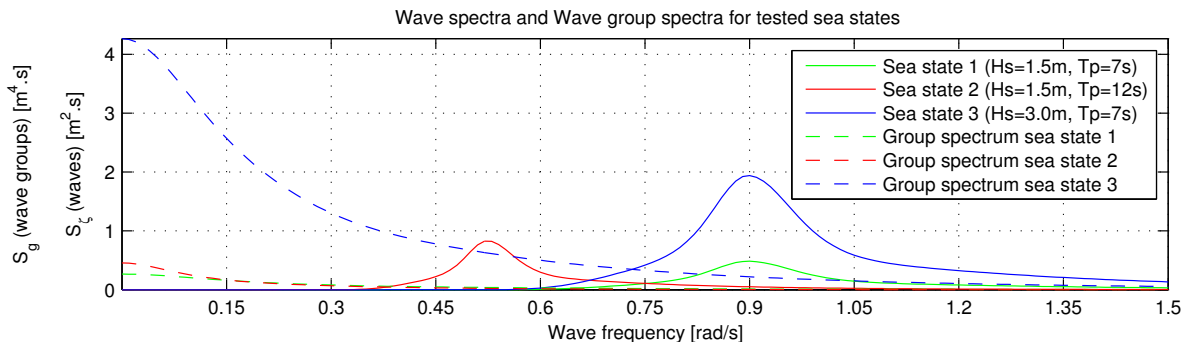


Figure 3: Wave spectrum and wave group spectrum. The shown sea states have been tested during MARIN model tests. Due to the low roll frequency of 0.16 rad/s (~ 40 s), the roll motion is expected to be sensitive for the low frequency energy of wave groups.

READING GUIDE

This thesis is structured in five chapters. In the **first Chapter** all theory, on which the performed work is based, is described. Furthermore the chapter provides insight in physical phenomena, which are useful to understand the low frequency second order wave loading on vessels. The **second Chapter** presents the method and results of the model tests performed at MARIN. In **Chapter 3** the methods, in order to predict the roll response spectrum in the frequency and time domain, are explained. In **Chapter 4** the results are presented and discussed. Lastly the conclusions of the performed work are presented and summarized in **Chapter 5**. The thesis is concluded with recommendations for future research, presented in the same Chapter.

1

THEORY

This chapter describes the theory which is used for this research. First, the low frequent wave induced by the presence of regular wave groups is explained. The different terms, which contribute to the second order wave forces, are presented and explained. Calculation methods for the second order potential contribution are presented. Finally, this chapter describes a theoretical procedure to obtain a first and second order force spectrum, force transfer function and a first and second order response spectrum.

1.1. LONG WAVE INDUCED BY REGULAR WAVE GROUPS

WAVE ENVELOPE

In order to understand the second order behaviour of vessels it is important to be familiar with wave envelopes. A wave envelope arises if multiple waves with a small difference in frequency travel together. These waves that travel together are defined as a wave group. The simplest example of a wave group is a group of two regular waves:

$$\zeta(t) = \sum_{i=1}^2 \zeta_i \cdot \sin(\omega_i t + \epsilon_i) = \zeta_1 \cdot \sin(\omega_1 t + \epsilon_1) + \zeta_2 \cdot \sin(\omega_2 t + \epsilon_2) \quad (1.1)$$

with $\zeta(t)$ the wave elevation, ζ_i the wave amplitude, ω_i the wave frequency and ϵ_i the phase of the wave (See Appendix C.1).

In order to show the behaviour of the resulting wave, first the summation will be done by considering equal amplitudes $\zeta_1 = \zeta_2 = \zeta_a$. The resulting wave is assumed to have the form $A(t) \sin(\omega_3 t + \epsilon_3)$ with A , ω_3 , ϵ_3 the unknown amplitude, frequency and phase. The summation of the two sinusoidal waves in Equation 1.1 can, with the use of trigonometry, be written as:

$$\zeta_a (\sin(\omega_1 t + \epsilon_1) + \sin(\omega_2 t + \epsilon_2)) = \underbrace{2\zeta_a \cdot \cos\left(\frac{(\omega_1 - \omega_2)t + (\epsilon_1 - \epsilon_2)}{2}\right)}_{A(t)} \cdot \underbrace{\sin\left(\frac{(\omega_1 + \omega_2)t + (\epsilon_1 + \epsilon_2)}{2}\right)}_{\sin(\omega_3 t + \epsilon_3)} \quad (1.2)$$

From Equation 1.2 it is shown that $\omega_3 = \frac{(\omega_1 + \omega_2)t}{2}$ and $\epsilon_3 = \frac{(\epsilon_1 + \epsilon_2)}{2}$. The modulating amplitude $A(t)$ is:

$$A(t) = 2\zeta_a \cdot \cos\left(\frac{(\omega_1 - \omega_2)t + (\epsilon_1 - \epsilon_2)}{2}\right) = 2\sqrt{2\zeta_a^2 + 2\zeta_a^2 \cdot \cos((\omega_1 - \omega_2)t + (\epsilon_1 - \epsilon_2))} \quad (1.3)$$

The modulated amplitude $A(t)$ is the wave envelope and modulates the amplitude of the carrier wave ($\sin(\omega_3 t + \epsilon_3)$) with a frequency which is the difference between the two initial wave frequencies. This will be defined as the difference frequency $\mu = \omega_1 - \omega_2$. The frequency of the carrier wave $\omega_3 = \frac{(\omega_1 + \omega_2)}{2}$ is the mean frequency of the initial two wave frequencies.

¹ $\sin \alpha + \sin \beta = 2 \cdot \sin\left(\frac{\alpha + \beta}{2}\right) \cdot \cos\left(\frac{\alpha - \beta}{2}\right)$

² $\cos^2 \alpha = \frac{1 + \cos(2\alpha)}{2}$

Additional to the summation above, the summation of two waves with different wave amplitudes ($\zeta_1 \neq \zeta_2$) as in Equation 1.1 is considered. It can be shown that the wave envelope becomes:

$$\begin{aligned} A(t) &= \sqrt{\zeta_1^2 + \zeta_2^2 + 2\zeta_1\zeta_2 \cdot \cos((\omega_1 - \omega_2)t + (\epsilon_1 - \epsilon_2))} \\ &= \sqrt{\sum_{i=1}^2 \sum_{j=1}^2 \zeta_i \zeta_j \cos((\omega_i - \omega_j)t + (\epsilon_i - \epsilon_j))} \end{aligned} \quad (1.4)$$

Figure 1.1 shows the wave envelope of a regular wave group with small differences between ω_1 and ω_2 . The period of the wave envelope is defined as $T = \frac{2\pi}{\mu}$. Note that in the example above the wave group elevation is is

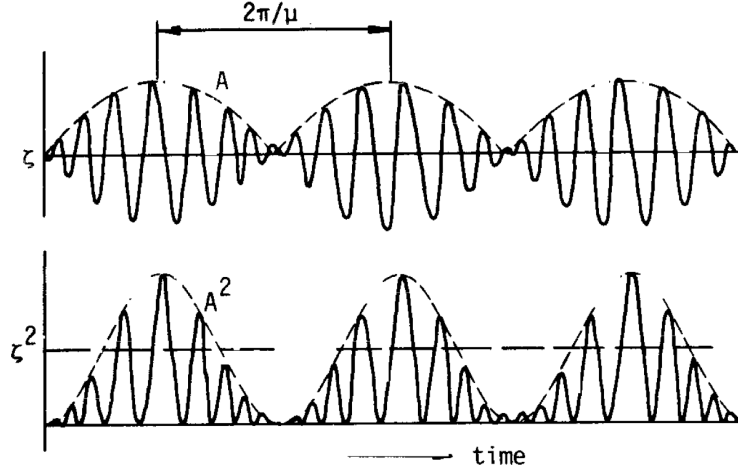


Figure 1.1: Illustration of a regular wave group, $A(t)$, and the square of a regular wave group, $A^2(t)$ [Source: [3]]

shown by the summation of two sinusoidal waves, but the wave elevation can be defined by a summation of N waves, with specific amplitudes, frequencies and phases. The expression for the square of the wave envelope amplitude becomes:

$$A^2(t) = \sum_{i=1}^N \sum_{j=1}^N \zeta_i \zeta_j \cos((\omega_i - \omega_j)t + (\epsilon_i - \epsilon_j)) \quad (1.5)$$

The presence of a regular wave group induces a long (low frequent) wave as is shown in Figure 1.1. The low frequent wave, is important for the second order wave forces.

WAVE GROUP SPECTRUM

With the use of trigonometry³ it can be shown that the square of the wave elevation can be described as:

$$\begin{aligned} \zeta^2(t) &= \sum_{i=1}^N \sum_{j=1}^N \zeta_i \cdot \sin(\omega_i t + \epsilon_i) \cdot \zeta_j \cdot \sin(\omega_j t + \epsilon_j) \\ &= \frac{1}{2} \sum_{i=1}^N \sum_{j=1}^N \zeta_i \zeta_j \left(\underbrace{\cos\{(\omega_i - \omega_j)t + (\epsilon_i - \epsilon_j)\}}_{\text{Low frequency part}} - \underbrace{\cos\{(\omega_i + \omega_j)t + (\epsilon_i + \epsilon_j)\}}_{\text{High frequency part}} \right) \end{aligned} \quad (1.6)$$

The expression in Equation 1.6 contains a high frequency ($^{(+)}$) and a low frequency ($^{(-)}$) part. Equation 1.5 and 1.6 show similarities between the square of the wave envelope amplitude and the low frequency part of the square of the wave elevation. In other words, the square of the wave elevation contains information on wave grouping. From Equation 1.5 and 1.6 follows:

$$A^2(t) = 2 \cdot (\zeta^{(-)}(t))^2 \quad (1.7)$$

For a wave component n the spectral density is given as (See Appendix C.1):

$$S_\zeta(\omega_n) \cdot \Delta\omega = \frac{1}{2} \zeta_n^2(\omega) \quad (1.8)$$

³ $\sin \alpha \sin \beta = \frac{1}{2} \cos(\alpha - \beta) - \frac{1}{2} \cos(\alpha + \beta)$

From Equation 1.4 and 1.8 it follows that the spectral density of the low part of the square of the wave envelope will be:

$$\begin{aligned} S_{A^2(\mu)} \Delta \omega &= \frac{1}{2} (2\zeta_1 \zeta_2)^2 \\ &= 2 \cdot \zeta_1^2 \cdot \zeta_2^2 \\ &= 2 \cdot 2 \cdot 2 \cdot S_\zeta(\omega_1) \Delta \omega \cdot S_\zeta(\omega_1) \Delta \omega \end{aligned} \quad (1.9)$$

Now it can be shown that the expression for the spectral density of wave groups ($S_{A^2}(\mu)$ or $S_g(\mu)$) with difference frequency μ will be in continuous form [3]:

$$S_g(\mu) = 8 \int_0^\infty S_\zeta(\omega) \cdot S_\zeta(\omega + \mu) d\omega \quad (1.10)$$

In Figure 3, the wave spectra and the corresponding group spectra are presented for the tested sea states in this research.

1.2. SECOND ORDER WAVE FORCE AND MOMENT

The second order exciting wave force and moment, $\vec{F}^{(2)}$ and $\vec{M}^{(2)}$, are defined as in Equation 1.11 [12].

$$\begin{aligned} \vec{F}^{(2)} &= -\frac{1}{2} \rho g \oint_{WL} (\zeta_r^{(1)})^2 \cdot \vec{n} \cdot dl & \vec{M}^{(2)} &= -\frac{1}{2} \rho g \oint_{WL} (\zeta_r^{(1)})^2 \cdot (\vec{r} \times \vec{n}) \cdot dl & I \\ &+ \frac{1}{2} \rho g \iint_{S_0} (\nabla \Phi^{(1)})^2 \cdot \vec{n} \cdot dS & &+ \frac{1}{2} \rho g \iint_{S_0} (\nabla \Phi^{(1)})^2 \cdot (\vec{r} \times \vec{n}) \cdot dS & II \\ &+ \rho \iint_{S_0} \left(\vec{X}^{(1)} \cdot \nabla \frac{\partial \Phi^{(1)}}{\partial t} \right) \cdot \vec{n} \cdot dS & &+ \rho \iint_{S_0} \left(\vec{X}^{(1)} \cdot \nabla \frac{\partial \Phi^{(1)}}{\partial t} \right) \cdot (\vec{r} \times \vec{n}) \cdot dS & III \\ &+ m \cdot R^{(1)} \cdot \vec{X}_G^{(1)} & &+ I \cdot R^{(1)} \cdot \vec{X}_G^{(1)} & IV \\ &+ \rho \iint_{S_0} \left(\frac{\partial \Phi^{(2)}}{\partial t} \right) \cdot \vec{n} \cdot dS & &+ \rho \iint_{S_0} \left(\frac{\partial \Phi^{(2)}}{\partial t} \right) \cdot (\vec{r} \times \vec{n}) \cdot dS & V \end{aligned} \quad (1.11)$$

with for	contribution I:	ρ	=	Mass density of fluid.
		g	=	Gravity constant.
		$\zeta_r^{(1)}$	=	First order relative wave elevation.
		\vec{n}	=	Outward normal vector on line segment dl.
		\vec{r}	=	Position vector of waterline segment dl.
	contribution II:	S_0	=	Mean wetted surface.
		$\Phi^{(1)}$	=	First order potential.
		dS	=	Surface element.
	contribution III:	$\vec{X}^{(1)}$	=	First order body motion.
	contribution IV:	m	=	Mass of body.
		$R^{(1)}$	=	Linearized rotation matrix.
		$\vec{X}_G^{(1)}$	=	Oscillatory first order acceleration vector of center of gravity (CoG).
		I	=	Mass moment of inertia.
	contribution V:	$\Phi^{(2)}$	=	Second order potential.

For the derivation of these expressions and extensive explanation of the variables reference is made to the work of Pinkster [12] or Journée et al [13]. As shown in Equation 1.11 the second order force and moment consists of five contributions:

Contribution <i>I</i>	is caused by the effect of the relative wave height.
Contribution <i>II</i>	is caused by the pressure drop due the first order velocity squared.
Contribution <i>III</i>	is caused by the pressure due to the product of the gradient of the first order pressure and the first order motion.
Contribution <i>IV</i>	is caused by the effect of the product of the first order rotational motion and the inertia force.
Contribution <i>V</i>	is the second order potential term and is related to the long wave induced by the presence of regular wave groups (see section 1.1).

Contributions *I*, *II*, *III* and *IV* depend on first order quantities. These four contributions are caused by the quadratic interaction of the first order solution. Therefore, the summation of these four contributions is referred to as the quadratic force and moment.

Contribution *V* depends only on the second order potential. This second order potential contribution is referred to as the second order potential force or moment. This part of the force and moment is the most complex to calculate due to the free surface boundary condition [14].

As can be seen in Equation 1.11 the force and moment are time dependent. In order to perform calculations in the frequency domain time independent quadratic transfer functions (QTF's) of the second order forces and moments are used.

1.2.1. QUADRATIC TRANSFER FUNCTIONS

The quadratic transfer functions are used to determine the second order force spectra in the frequency domain and allow prediction of second order force and moment time histories in the time domain. The quadratic transfer function consists of a time independent in-phase component, P_{ij} , and of an out-phase component, Q_{ij} . Comparing these second order force and moment components with the square of the wave elevation given in Equation 1.6 shows that P_{ij} and Q_{ij} are transfer functions which are the in- and out-of-phase part of the force or moment comparing with the square of the wave elevation.

The amplitude of the quadratic transfer function is defined as:

$$T_{ij} = \sqrt{P_{ij}^2 + Q_{ij}^2} \quad (1.12)$$

In which T_{ij} and P_{ij} are symmetrical and Q_{ij} is asymmetrical [12].

The phase angle ϵ_{ij} of the quadratic transfer function is defined as:

$$\tan(\epsilon_{ij}) = -\frac{Q_{ij}}{P_{ij}} \quad (1.13)$$

The method to determine the quadratic transfer functions from the second order wave forces and moments is shown in, e.g. [12].

1.2.2. CALCULATION METHODS FOR THE SECOND ORDER POTENTIAL CONTRIBUTION

In order to calculate the second order force and moment, software packages WAMIT and DIFFRAC have been used. Contributions *I*, *II*, *III* and *IV* depend on first order quantities, therefore the calculations with both software package are expected to result in equal quadratic second order contributions. The calculation of the second order potential contribution can be solved with different methods. In this research, three methods in order to calculate the second order potential force (Contribution *V*) and moment have been compared.

- The Direct method (WAMIT):

In order to calculate the second order loads, the effects of the second order diffracted potential is are included. This method solves the full second order problem directly by pressure integration. This method of solving the second-order potential is similar to the one used for the first order method. The free-surface integral is calculated. [15])

- The Indirect method (WAMIT):

This method calculates the second order loads through first order quantities introduced by B. Molin (without explicit calculation of second order potential). An assisting potential is used for the solution of the first-order radiation problem. [15]

Using this method the numerical integration over the hull is not a significant problem. The integration over the free surface is much more complicated. The domain is separated in the near-field part and the far-field part. The near-field is integrated numerically and the far-field analytically. [15]
The first order force, evaluated in this way is referred to as, the Haskind exciting force, and the second order force as the indirect force. [14]

- Pinkster approximation (DIFFRAC):

Pinkster uses a ratio coefficient between the second order and the first order incident wave potential in order to calculate the potential part of the quadratic transfer function. The idea is that the main contribution is due to the second order incoming waves [12].

1.3. FORCE SPECTRUM

FIRST ORDER

The first order force spectrum is defined as:

$$S_{F,i}(\omega) = \left| \frac{F_a}{\zeta_a} \right|_i^2(\omega) \cdot S_\zeta(\omega) \quad (1.14)$$

in which i is the mode of the motion, S_ζ is the wave spectrum, $\left| \frac{F_a}{\zeta_a} \right|_i^2(\omega)$ is the first order wave force transfer function with the force amplitude, F_a , and the wave amplitude, ζ_a . This transfer function is referred to as Response Amplitude Operator (RAO) of the first order wave force.

LOW FREQUENCY SECOND ORDER

The low frequency second order order force spectrum or wave drift force spectrum is defined as:

$$S_{F,i}^{(-)}(\mu) = 8 \cdot \int_0^\infty S_\zeta(\omega) \cdot S_\zeta(\omega + \mu) \cdot |T_i^{(-)}(\omega + \mu)|^2 \cdot d\omega \quad (1.15)$$

in which i is the mode of the motion, S_ζ is the wave spectrum, T is the amplitude QTF, μ is the difference frequency ($\mu = \omega_2 - \omega_1$), the (-) in $S_{F,i}^{(-)}(\mu)$ indicates the use of only difference frequencies and no sum frequencies.

The derivation of the second order force spectrum is described by Wichers [3].

1.4. MOTION RESPONSE SPECTRUM

FIRST ORDER

When the wave force spectrum is known the first order response spectrum can be obtained with:

$$S_i(\omega) \cong |H_{ij}(\omega)|^2 \cdot S_{F,i}(\omega) \quad (1.16)$$

in which: $S_i(\omega)$ = Spectral density of first order motion i .
 $H_{ij}(\omega)$ = Force Transfer Function (FTF) for mode ij .
 $S_{F,i}(\omega)$ = Exciting force spectrum (Equation 1.14).

The Force Transfer Function (FTF) $H_{ij}(\omega)$ is given by [6]:

$$H_{ij}(\omega) = \frac{1}{-\omega^2(M_{ij} + A_{ij}(\omega)) + i\omega(B(\omega) + B'_{ij}) + (C_{ij} + C'_{ij})} \quad (1.17)$$

with: i and j = Mode 1 to 6.
 M_{ij} = Mass Matrix.
 $A_{ij}(\omega)$ = Added mass matrix.
 $B_{ij}(\omega)$ = Damping matrix.
 B'_{ij} = Viscous Damping matrix.
 C_{ij} = Hydrostatic restoring spring matrix.
 C'_{ij} = External Spring matrix.

The transfer function in Equation 1.17 is dominated by the variables in the following frequency ranges [13]:

$$for \begin{cases} \omega \rightarrow 0 & H_{ij}(\omega) \text{ is dominated by spring term } C_{ij} + C'_{ij}. \\ \omega \rightarrow \omega_{nat} & H_{ij}(\omega) \text{ is dominated by damping term } B(\omega) + B'_{ij}. \\ \omega \rightarrow \infty & H_{ij}(\omega) \text{ is dominated by mass \setminus inertia term } M_{ij} + A_{ij}(\omega). \end{cases} \quad (1.18)$$

LOW FREQUENCY SECOND ORDER

The second order low frequency motion response spectrum can be approximated by:

$$S_i^{(-)}(\omega) \cong |H_{ij}(\omega)|^2 \cdot S_{F_i}^{(-)}(\omega) \quad (1.19)$$

in which: $S_i^{(-)}(\omega)$ = Spectral density of low frequency motion i .
 $H_{ij}(\omega)$ = Force Transfer Function (FTF) for mode ij (Equation 1.17).
 $S_{F_i}^{(-)}(\omega)$ = Low frequency second order exciting force spectrum (Equation 1.15).

TOTAL RESPONSE SPECTRUM

The total response spectrum can be obtained from the first order and the second order response spectrum.

$$S_{Total,i}(\omega) \cong S_i(\omega) + S_i^{(-)}(\omega) \quad (1.20)$$

in which: $S_{Total,i}(\omega)$ = Spectral density of total motion i .
 $S_i(\omega)$ = Spectral density of first order motion i (Equation 1.16).
 $S_i^{(-)}(\omega)$ = Spectral density of low frequency second order motion i . (Equation 1.19).

1.5. ROLL DAMPING

The equation of motion for the roll motion $\phi(t) = \phi_a \cos(\omega t + \epsilon)$ can be defined as:

$$(I_\phi + A_\phi) \cdot \ddot{\phi} + B_\phi(\dot{\phi}) + C_\phi \cdot \phi = M_\phi \quad (1.21)$$

In which ϕ is the roll angle with amplitude ϕ_a , I_ϕ is the roll mass moment of inertia, A_ϕ the added mass moment for roll, B_ϕ is the roll damping moment, C_ϕ the restoring moment coefficient and M_ϕ is the exciting moment.

The total damping of a system in water is non-linear which cannot be calculated by means of potential theory. The total damping can be described by a potential damping part and an external viscous damping part, as shown in Equation 1.17.

In Equation 1.21 the total non-linear roll damping moment can be described by:

$$B_\phi(\dot{\phi}) = b_\phi^{(1)} \cdot \dot{\phi} + b_\phi^{(2)} \cdot \dot{\phi}|\dot{\phi}| + \dots \quad (1.22)$$

with $b_\phi^{(1)}$, $b_\phi^{(2)}$, ... the non-linear damping coefficients, considered as constants during the concerned motion.

Since it is difficult to strictly analyze the non-linear damping in Equation 1.22, an equivalent linear damping coefficient, b_{eq} , is introduced. Several ways exist to express the coefficient b_{eq} in terms of the damping coefficients $b_\phi^{(1)}$ and $b_\phi^{(2)}$. In the first method, it is assumed that the linear equivalent damping term has the same energy loss as the non-linear damping terms. Using this assumption Equation 1.22 becomes:

$$B_\phi(\dot{\phi}) = b_{eq} \cdot \dot{\phi} \quad (1.23)$$

with:

$$b_{eq} = b_\phi^{(1)} + \frac{8}{3\pi} \cdot \omega \cdot \phi_a \cdot b_\phi^{(2)} + \dots \quad (1.24)$$

in which ω is the wave frequency and ϕ_a is the roll amplitude. This method, is considered as a linearization method for regular waves. In practice the equivalent damping coefficient is linearized around a specific roll amplitude ϕ_a [16].

Secondly in case of irregular roll motion another approach to linearize the roll damping expression exists. Using the assumption that the undulation of the roll angular velocity, $\dot{\phi}$, is subject to a Gaussian process it can be shown that:

$$b_{eq} = b_{\phi}^{(1)} + \sqrt{\frac{8}{\pi}} \cdot \sigma_{\dot{\phi}} \cdot b_{\phi}^{(2)} + \dots \quad (1.25)$$

where $\sigma_{\dot{\phi}}$ is the variance of the angular velocity $\dot{\phi}$. The factor $\sqrt{\frac{8}{\pi}}$ indicates the stochastic linearization in a Gaussian spectrum. [10]

The constants $b_{\phi}^{(1)}$ and $b_{\phi}^{(2)}$ can be obtained by performing decay tests. In Figure 1.2a a typical time trace of roll decay tests is shown. The natural period and the damping constants can be obtained by measuring the decay of a particular motion. The procedure in order to obtain the damping constants, is to plot the decrease of the motion amplitude divided by the mean motion amplitude, versus the mean motion amplitude, as is shown in Figure 1.2b. The linear and quadratic constants p and q can be obtained from the fitted line through

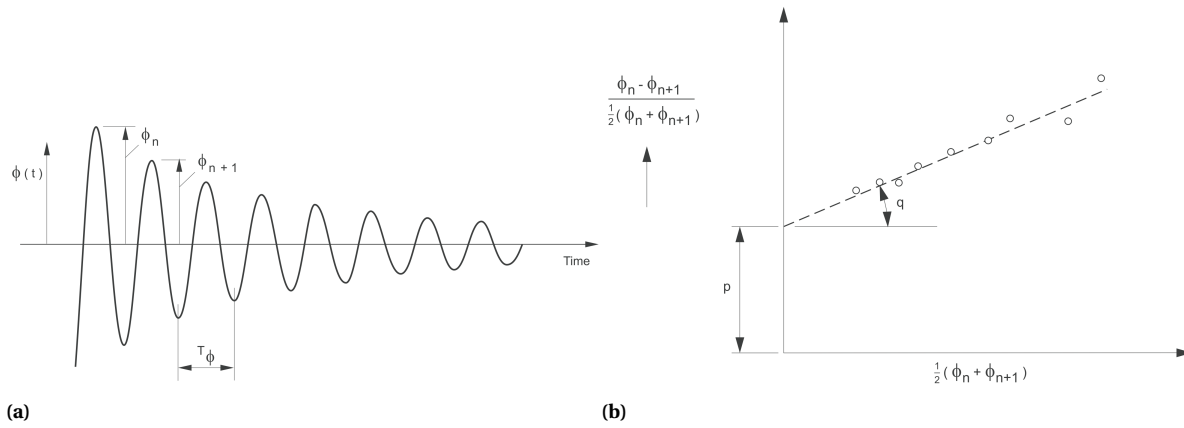


Figure 1.2: (a): Typical time trace of a decay test of a lightly damped motion. (b): Plot of the decrease of the motion amplitude divided by the mean motion amplitude versus the mean motion amplitude in order to obtain the constants p and q . Source: [17]

the data points. The linear and quadratic roll damping constants $b_{\phi}^{(1)}$ and $b_{\phi}^{(2)}$ can be calculated with p and q .

$$\begin{aligned} b_{\phi}^{(1)} &= 2 \cdot \frac{(I_{\phi} + A_{\phi})}{T_n} \cdot p \\ b_{\phi}^{(2)} &= \frac{3}{8} \cdot (I_{\phi} + A_{\phi}) \cdot q \end{aligned} \quad (1.26)$$

in which T_n is the natural period of roll, p the linear damping constant and q the quadratic damping constant.

After determination of b_{eq} the external viscous damping part can be obtained if the potential damping is known:

$$b_{visc} = b_{eq} - b_{pot} \quad (1.27)$$

in which b_{visc} is the viscous damping and b_{pot} is the potential damping.

The added (viscous) damping is often expressed as a ratio of the critical damping coefficient, b_{crit} .

$$\xi = \frac{b_{visc}}{b_{crit}} \quad (1.28)$$

The critical damping is defined as:

$$b_{crit} = 2 \cdot \sqrt{(M + A) \cdot C} \quad (1.29)$$

in which M is the mass, A is the added mass and C is the restoring spring term of the considered motion.

The roll restoring spring term of a floating object is defined as:

$$C_{\phi\phi} = \rho \cdot g \cdot \nabla \cdot GM_T \quad (1.30)$$

in which ∇ is the submerged volume and GM_T is the transverse metacentric height. Using the roll restoring spring term the roll natural frequency can be obtained with:

$$\omega_{nat} = \sqrt{\frac{C_{\phi\phi}}{I_{\phi} + A_{\phi\phi}}} = \sqrt{\frac{C_{\phi\phi}}{k_{xx}^2 \cdot \nabla \cdot \rho + A_{\phi\phi}}} \quad (1.31)$$

in which the mass moment of inertia for roll I_{ϕ} and k_{xx} is the roll radius of gyration.

1.6. DEFINITION OF SHIP MOTIONS AND ORIGIN

In Table 1.1 and Figure 1.3 the ship motions are defined. In Figure 1.4 the hydrodynamic origin is shown. The motions are mainly calculated at this origin in this research.

DoF/ Mode	Name	Symbol	Unit	Description	Force and Moment
1	Surge	x	[m]	Motion in the x-direction	F_x
2	Sway	y	[m]	Motion in the y-direction	F_y
3	Heave	z	[m]	Motion in the z-direction	F_z
4	Roll	ϕ	[rad]	Rotation around the x-axes	M_{ϕ}
5	Pitch	θ	[rad]	Rotation around the y-axes	M_{θ}
6	Yaw	ψ	[rad]	Rotation around the z-axes	M_{ψ}

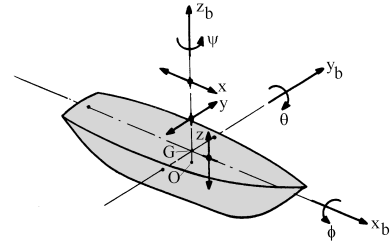


Table 1.1: Degrees of freedom of a floating body.

Figure 1.3: Degrees of freedom of a floating body [13].

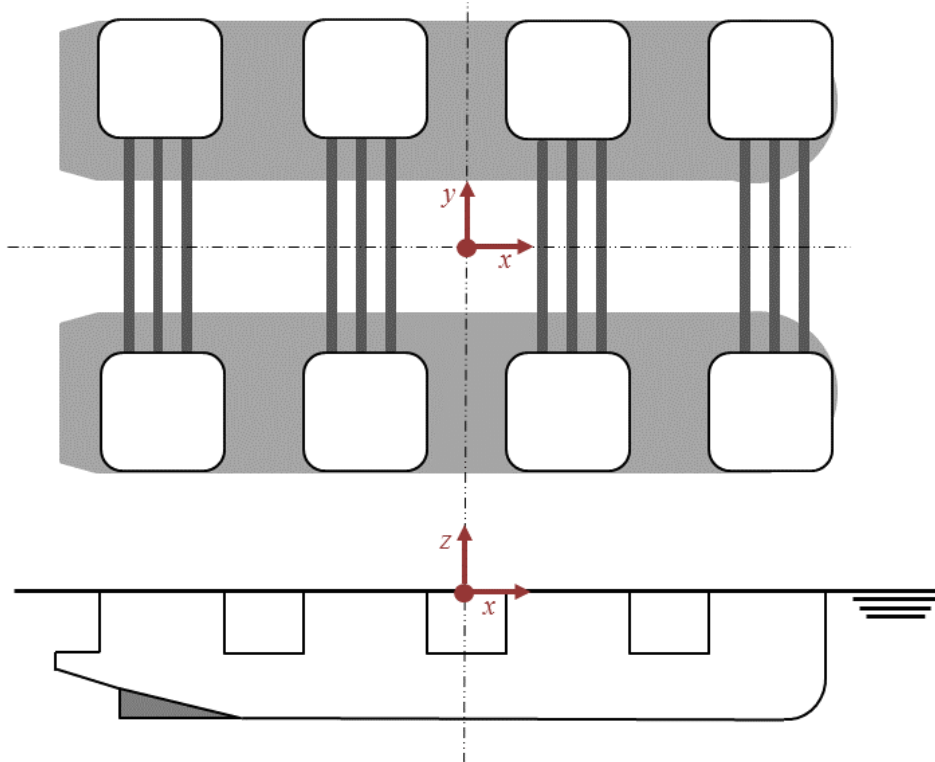


Figure 1.4: Hydrodynamic Origin. The main origin which is used for calculations in this research.

2

MODEL TESTS

In February 2014 Sleipnir model tests have been performed at operational draught. In this time the name 'Sleipnir' had not been introduced. The vessel was referred to as the 'NSCV' (New Semi-submersible Crane Vessel). This chapter is based on the MARIN report 'Operational wave tests of the NSCV' [18] and presents shortly the model test method, results and conclusions.

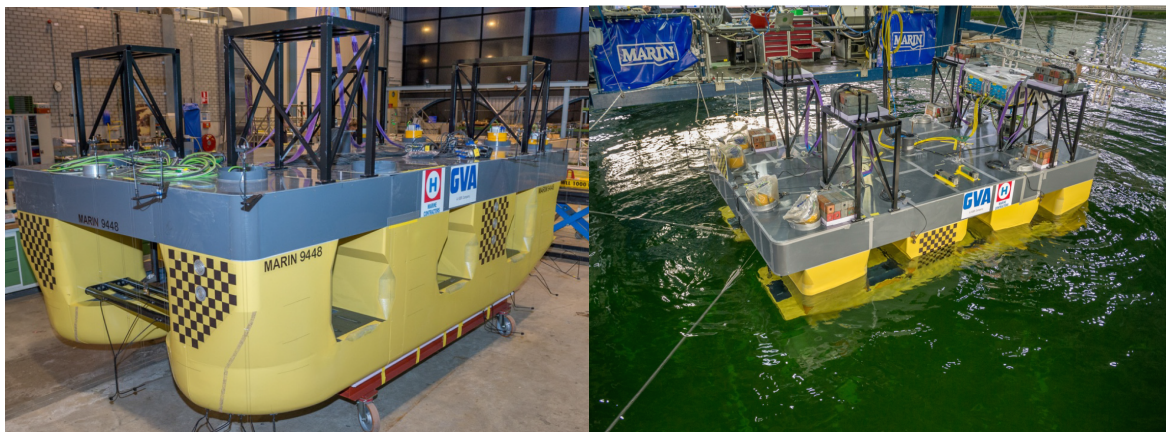
2.1. MODEL TEST SET UP

The model of the Sleipnir was constructed on a geometric scale ratio of 1:40 (Figure 2.1a). The Sleipnir is a eight-column semi submersible crane vessel with three braces at every column. In Table 2.1 the main particulars are shown.

In order to generate a stability condition which is comparable with a heavy lift, the GM value of the model is tuned with extra weights on top of the black constructions on the deck (See Figure 2.1b). Tests have been performed with free floating conditions, a soft spring moored system and with DP. The soft spring mooring system was characterized by a theoretical linearized mooring stiffness off:

- Surge stiffness: $535 \frac{kN}{m}$
- Sway stiffness: $535 \frac{kN}{m}$
- Yaw stiffness: $1.01 \cdot 10^4 \frac{kN \cdot m}{deg}$

The model was instrumented with force panels to measure the impact load, relative wave probes to measure the wave height and thrusters in order to control the vessels position.



(a) Sleipnir model with 8 columns and 3 braces at each column. (b) Soft moored Sleipnir model at operational draught of 27 m.

Figure 2.1: General overview of the Sleipnir model.

Description	Unit	Magnitude	
		Specified	Realized
Length overall of pontoons (L_{pp})	[m]	177.5	177.5
Beam overall (B)	[m]	97.5	97.5
Beam of pontoons	[m]	37.5	37.5
Height of bottom deck box to base line	[m]	37.5	37.5
Column width	[m]	26.25	26.25
Column length	[m]	27.5	27.5
Column corner radius	[m]	3.75	3.75
Draught (even keel)	[m]	27	27
Displacement (Δ)	[tonnes]	242861	241670
Displacement (∇)	[m ³]	236938	235776



Table 2.1: Sleipnir model specifications.

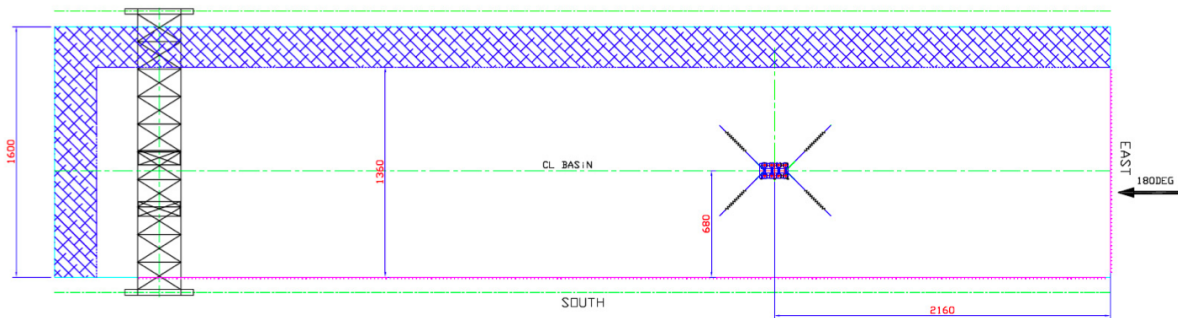


Figure 2.2: Location of the Sleipnir model in the Seakeeping and Manouvring Basin during operational wave tests. 180° incoming waves with the shown model orientation.

MARIN Test No.	Description Wave	IRREGULAR SEA CHARACTERISTICS						
		Duration [hours]	Specified				Calibrated	
			γ [-]	μ [deg]	H_s [m]	T_p [s]	H_s [m]	T_p [s]
201023	White noise 1	3	-	180	4.0	7-50	4.06	-
201019	Operational 1	3	1.0	180	1.5	7.0	1.42	7.24
201013	Operational 2	3	1.0	180	1.5	12.0	1.49	11.32
201016	Operational 3	3	3.0	180	3.0	7.0	2.89	7.10

Table 2.2: Overview of the calibrated operational wave specifications without the Sleipnir model in the basin. In which γ the shape factor of the wave spectrum, μ the incoming wave direction, H_s the significant wave height and T_p the peak period.

ENVIRONMENTAL CONDITIONS

The operational wave model tests have been performed in the Seakeeping and Manoeuvring Basin (SMB) at MARIN. The basin is 170 m long, 40 m wide and a depth of 5 m. The wave generators are located at the south and east side of the basin (See Figure 2.2). During the model tests only the east wave generators have been used. The model was rotated in order to generate incoming waves from different angles. Tests with incoming waves from 135° , 180° and 270° have been performed.

During model tests different sea conditions have been calibrated. Current and wind has not been part of the experimental procedures. The specified and calibrated wave conditions are shown in Table 2.2.

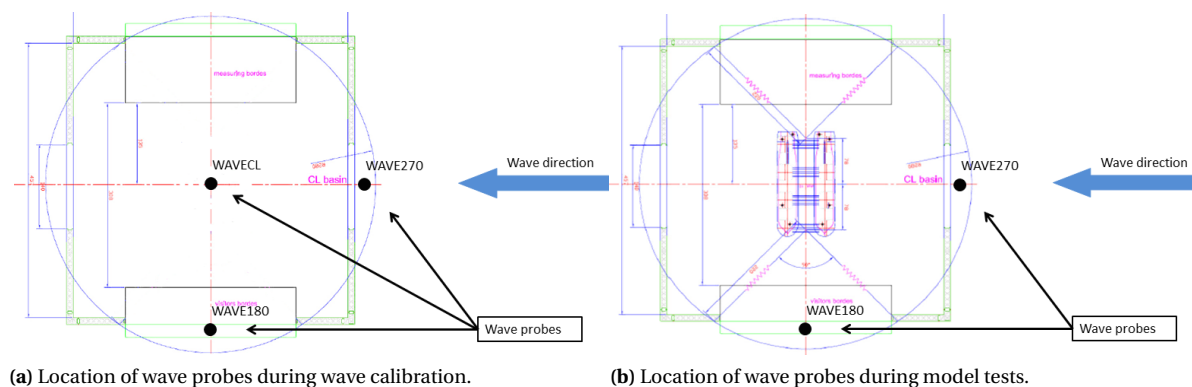


Figure 2.3: (a): Overview of the wave probes during the wave calibration for beam waves. The model and the wave probes are installed at a square measuring construction. Waves for three sea states have been calibrated at position of WAVECL, the location of the model. (b): During model test the waves have been measured at the given locations.

MEASUREMENTS AND MODEL TESTS

During the model tests analogue and digital measurement techniques have been used to obtain the following quantities:

- Wave elevations at reference locations in basin.
- Motions of the Sleipnir in 6 degrees of freedom.
- Accelerations of the Sleipnir.
- Tensions in soft spring mooring lines.
- Forces in soft spring mooring system.
- Relative wave motions with respect to the Sleipnir model at ten locations.
- Six impact pressures.

These measurement techniques have been used during specific model tests. The model tests can be classified by their purpose:

- Estimate the natural periods and damping coefficients for six degrees of freedom.
 - Decay tests in free floating and soft moored scenario.
- Measure ship motions under specified sea conditions.
 - Soft mooring tests in irregular waves.
 - Station keeping tests with dynamic positioning in irregular waves.

2.2. MOST RELEVANT RESULTS

During the model tests the motions of all six degrees of freedom have been measured. However the roll behaviour is especially subject of research for this master thesis study. Therefor the main results for the roll behaviour will be presented here.

First the results of the decay tests will be presented in Table 2.3. The influence of the different environmental conditions on the the roll motions are compared in Table 2.4. Then the motion response will be presented for roll in beam wave conditions in Figure 2.4.

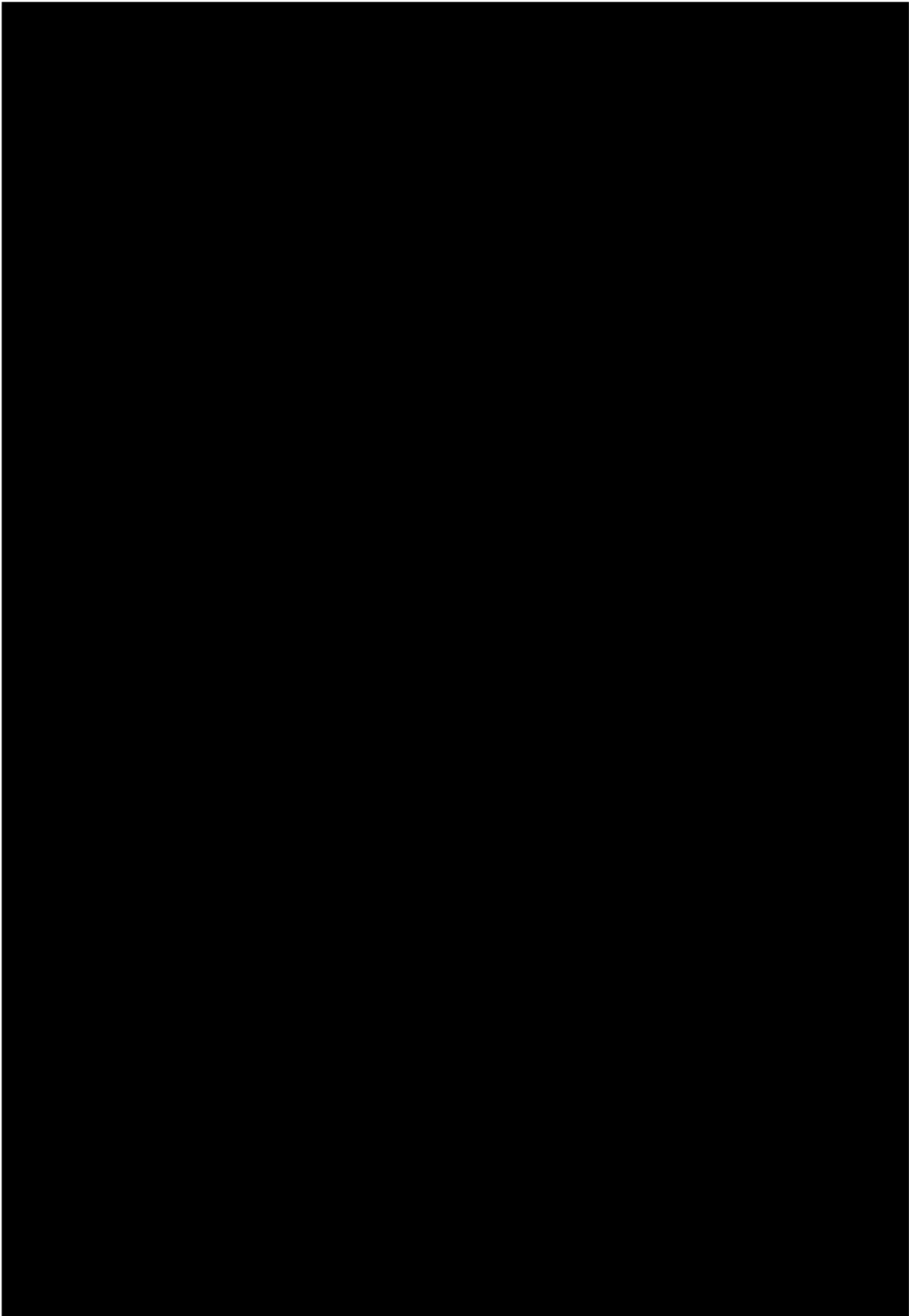
MARIN test No.	
802005	ROLL (5deg)
802006	ROLL (2deg)
802007	ROLL (5deg)
802008	PITCH (3 deg)
802009	PITCH (2deg)
802010	PITCH (3deg)
802012	HEAVE
T = 27	
803008	SURGE
803009	SWAY
803007	HEAVE
803005	ROLL (5deg)
803006	PITCH (3deg)
803010	YAW
T = 27	
803012	SURGE
803011	SWAY
T = 27	
402033	SURGE

* In the above table between brackets

Table 2.3: Results of the decay tests. The graphs from which the proportional and quadratic damping coefficients p and q are obtained for decay test 803005 are presented in Figure 2.5 and 2.6.

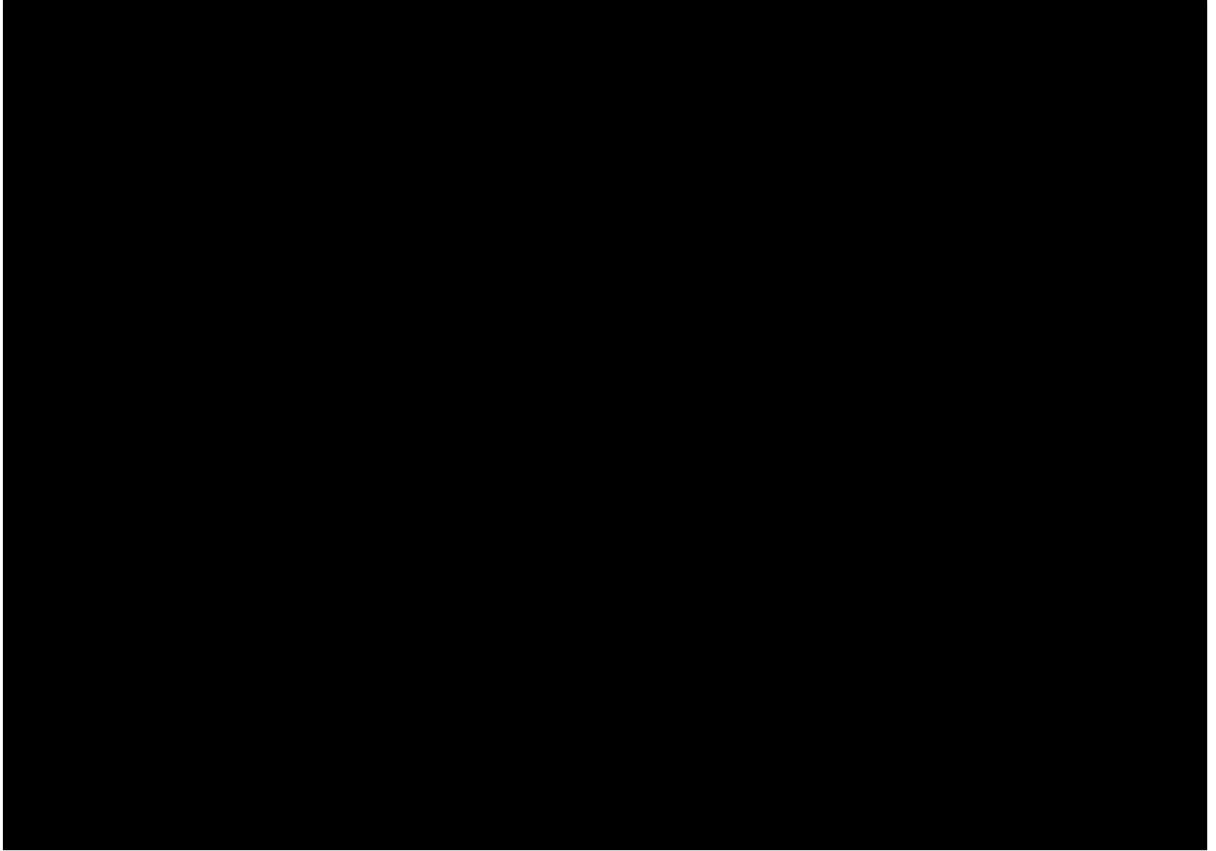
Test No.	Mode	Roll motions operational 1 wave ($H_s = 1.5$ m and $T_p = 7.0$ s)					
		Mean [deg]	St. Dev. [deg]	Max. + [deg]	Max. - [deg]	MPM (max)	MPM (min)
806001	Soft mooring						
805001	Soft mooring						
803004	Soft mooring						

Table 2.4: Comparison roll motions during soft mooring tests in beam conditions.



2.3. MOST RELEVANT CONCLUSIONS

In August 2014 the manager of MARIN's offshore department (ir. O. Waals) approved the following ten conclusions based on the results of the model tests:



3

METHOD

In the previous chapter the model tests of the Sleipnir are described. In this chapter a calculation method is described to predict the roll response spectra with the use of diffraction software. The aim of this research is to obtain a method to predict the roll motions in an acceptable agreement with respect to the measured roll motions during model tests.

Firstly, the research method in the frequency domain is described in this chapter. Secondly a method to compare the roll QTF for two diffraction software packages is discussed. The method to present the separate contributions of the QTF is explained. Lastly, the method for simulations in the time domain is presented.

3.1. FREQUENCY DOMAIN STUDY

In this research a theoretical calculation method is used in order to predict the roll motion response in the frequency domain. A schematic overview of the analysis is presented in a flowchart in Figure 3.1.

At first, a hydrodynamic analysis has been set up in order to calculate the hydrodynamic coefficients, first and second order wave forces and moments. This output combined with the sea conditions (used during model tests) is used to calculate the wave force and moment spectrum and the drift force and moment spectrum. The first and second order motion response spectra can be obtained using the force or moment spectra and a force or moment transfer function (FTF or MTF). Finally, the theoretical calculated total motion response spectrum can be compared with the model test motion response spectrum.

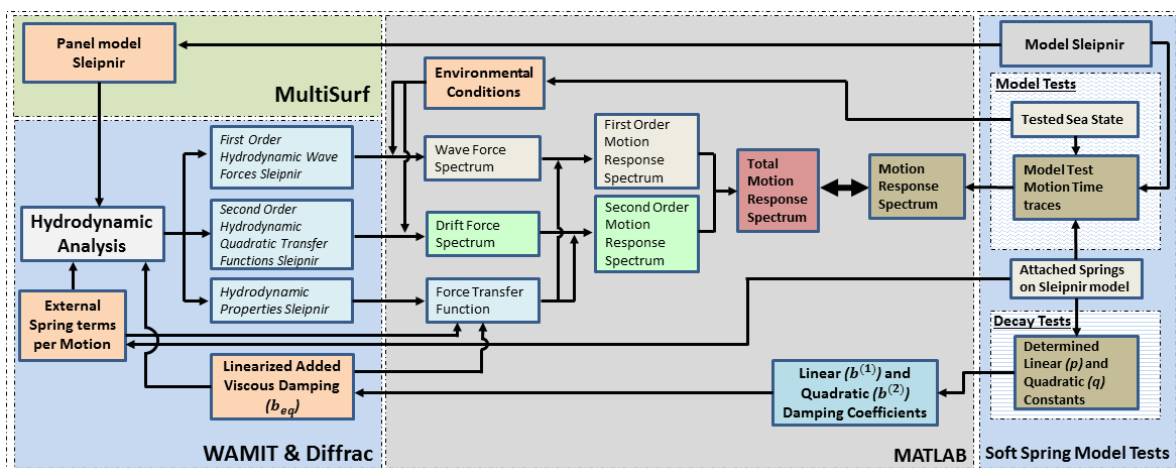


Figure 3.1: Flowchart of the frequency domain analysis.

3.1.1. REFINEMENT STUDIES

In order to calculate the hydrodynamic coefficients, first and second order forces and moments the software packages WAMIT and DIFFRAC are used. An detailed and extensive description of the used software is given

in Appendix D.

In order to run a simulation, variables as the water depth, range of interested wave frequencies, frequency step and the position of the body in the global coordinate system must be defined. In this study the conditions of the model tests have been used as input for the hydrodynamic analyses software.

Three (main) input variables have been studied by means of refinement studies. The influence of the discretized geometric model, the frequency resolution and the added viscous damping, on the calculation of the quadratic transfer function are investigated.

The grid refinement and damping refinement method are described in this section. The process of designing a discretized geometric hull model is described. Finally, the method for stochastic viscous damping linearization is presented.

GRID REFINEMENT STUDY

GEOMETRIC DATA SLEIPNIR

In order to perform hydrodynamic analyses a discretized geometric model of the submerged part of the Sleipnir is necessary. This discretized hull model is used to describe the potential flow around the body based on the principle of Green's integral theorem. The Green's function describes the potential flow by assigning pulsating sources on each panel on the wetted surface satisfying the Laplace equation. This principle is described in Appendix E.6.

DESIGN

The discretized hull model is created using Multisurf, a software package for parametric design of 3D geometric objects. During the design of the hull shape the size and therefore the amount of panels must be considered. The computation time of the hydrodynamic analyses depends on the amount of panels defined on the hull shape. Increasing the amount of panels increases the computation time. Basically the calculation solves a set of linear equation with N (amount of panels) unknowns and the computation time is proportional to N^2 [19].

However the accuracy of the results depend on the size of the panels. The size of the panels should be chosen such that the pressure disturbance due to waves on a single panel can be evaluated accurately by the software. Near the wave impact zone a panel size of $\frac{1}{8}$ to $\frac{1}{6}$ of the wavelength must be considered [13]:

$$panel\ size = \left(\frac{1}{6} \leftrightarrow \frac{1}{8}\right) \cdot \lambda \quad (3.1)$$

$$\lambda = \frac{2\pi}{k} \quad (3.2)$$

$$k = \frac{\omega^2}{g} \quad (3.3)$$

In which λ is the wave length in meter and k is the wave number in radians per meter. Equation 3.3 is the dispersion relation for deep water waves. Using the dispersion relation the panel size can be calculated. The maximum wave frequency which is considered in this research is 2 rad/s corresponding with a wave length of 15.4 meters. The panel size near the wave zone should be between the 1.93 and 2.57 meters.

An other design technique in order to obtain accurate results with less panels is using 'stretched' panels to the waterline. The model consist of stretched (column)panels to the waterline as is shown in Appendix E.1. The wave forces are larger closer to the waterline. By stretching the panels to the waterline the pressure gradient per panel is more equal which results in faster convergence of wave forces. In Figure 3.2 a visualization of this principle is given.

Furthermore irregular frequency lids have been used in order to reduce the effects of irregular frequencies on the free surface inside the columns (See Figure 3.3). Irregular frequencies are a set of infinite discrete resonance frequencies of the nonphysical interior flow [20].

In order to investigate for which discretization of the hull shape the calculated forces and moments are converged, a grid refinement study is performed.

Three models with different panel sizes have been compared for this research. A coarse, a base and a fine panel model have been investigated (See Table 3.1 and Figure 3.3).

Model	Number of panels [-]	Panel size waterline (length x height) [m]
NSCVcoarse	2482	6.88 x 1.57
NSCVbase	9982	3.44 x 0.64
NSCVfine	22338	2.29 x 0.4

Table 3.1: Geometric model specifications.

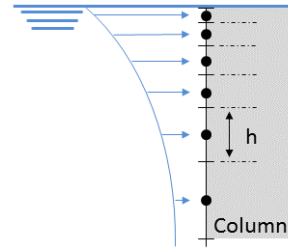


Figure 3.2: Panel height, h , is stretched to the waterline.

The submerged part of the vessel is symmetrical around the XZ-plane. For this reason, only half of the vessel is defined. This decreases the design time of the model and calculation time. The details of the specific geometric models can be found in Appendix E.1.

The hydrodynamic origin (Figure 3.3) of the body is located with respect to the stern, centre line and keel at [92.5, 0, 27] m.

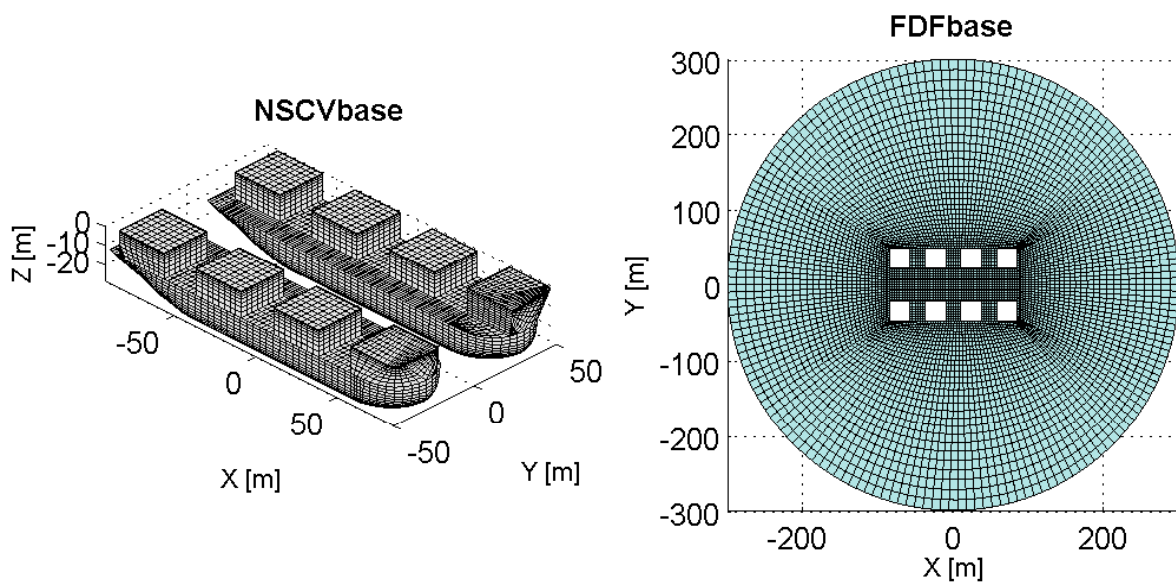


Figure 3.3: *Left:* Geometric NSCVbase model of the submerged part of the Sleipnir including the irregular frequency lids on top of the columns and (column)panels stretched to the waterline. *Right:* Geometric model of the free surface around the vessel model. More detailed figures of the discretized surfaces, can be found in Appendix E

DAMPING REFINEMENT STUDY

VISCOUS DAMPING

The software packages WAMIT and Diffrac are based on potential theory and do not take viscous effects in account. In order to determine the damping coefficients of the Sleipnir motion decay tests have been performed (See Table 2.3 for the motion decay test results).

The total damping can be obtained from the model decay tests as explained in Chapter 1.5. Using WAMIT the theoretical potential damping coefficient and de added mass coefficient can be calculated. An expression for the viscous damping is found by subtracting the potential damping from the total equivalent damping (See Equation 1.27).

It is possible in WAMIT to add external (viscous) damping. In this study the influence of different damping levels on the response motion density spectrum have been investigated. Calculations with zero viscous damping, viscous damping based on b_{eq} and viscous damping which is five percent of the critical damping have been performed.

LINEARIZATION OF ROLL AMPLITUDE

The calculated total equivalent damping b_{eq} depends on frequency and on the motion amplitude (See Equation 1.24). In Figure 3.4 the dependency of amplitude ϕ_a on the viscous damping based on b_{eq} is shown. The operational tests of the Sleipnir with beam wave conditions show a maximal roll amplitude of 0.5, 0.6 and 1.5 degrees (See Table 2.4). In order to calculate the equivalent damping this maximum roll amplitude is used for linearization. In Table 3.2 the calculated viscous damping is shown for the six degrees of freedom. The added damping levels shown in Table 3.2 have been used as input for diffraction calculation. Although the the added viscous damping is added for all degrees of freedom, only the uncoupled roll output is used for analysis in this research.

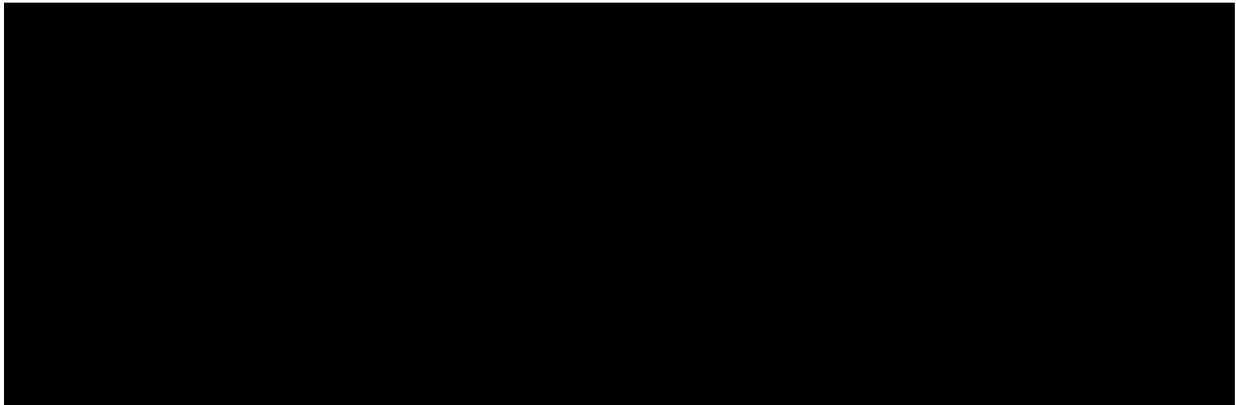


Table 3.2: Calculated added viscous damping for WAMIT calculations. The added viscous damping based on b_{eq} and 5 percent of the critical damping has been used for WAMIT calculations.

IRREGULAR ROLL MOTION

In Figure 3.5 the time traces of the measured roll from three model tests with different sea conditions are shown. The comparison of roll motions during soft mooring model tests in beam conditions are presented in Table 2.4. The roll velocity time traces have been calculated from the measured roll motion time traces using:

$$\dot{\phi}(t) = \frac{\Delta\phi}{\Delta t} = \frac{\phi_{i+1} - \phi_i}{t_{i+1} - t_i} \quad (3.4)$$

The roll velocity spectral density function, $S_{\dot{\phi}}$, can be obtained from the roll velocity time traces in Figure 3.5. The variance for roll velocity, $\sigma_{\dot{\phi}}$, is calculated from the zero order moment of the roll velocity spectral density function as defined in Equation 3.5:

$$m_{0,\dot{\phi}} = \int_0^{\infty} S_{\dot{\phi}} \cdot d\omega$$

$$\sigma_{\dot{\phi}} = \sqrt{m_{0,\dot{\phi}}} \quad (3.5)$$

An expression for b_{eq} with irregular roll motion can now be found using equation 1.25.

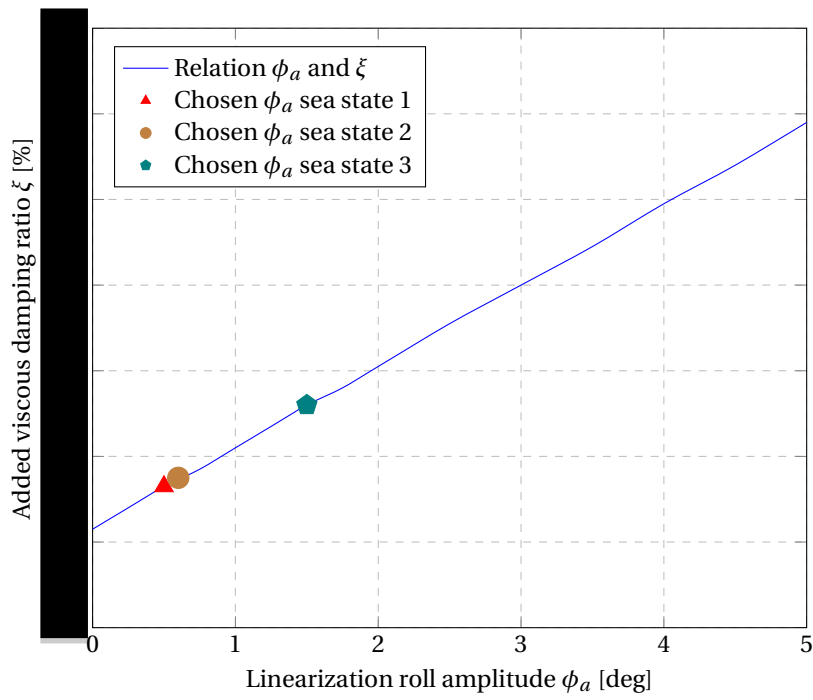


Figure 3.4: Influence of the linearization amplitude on the viscous damping ratio using the harmonic linearation technique. The chosen linearization roll amplitudes are indicated.

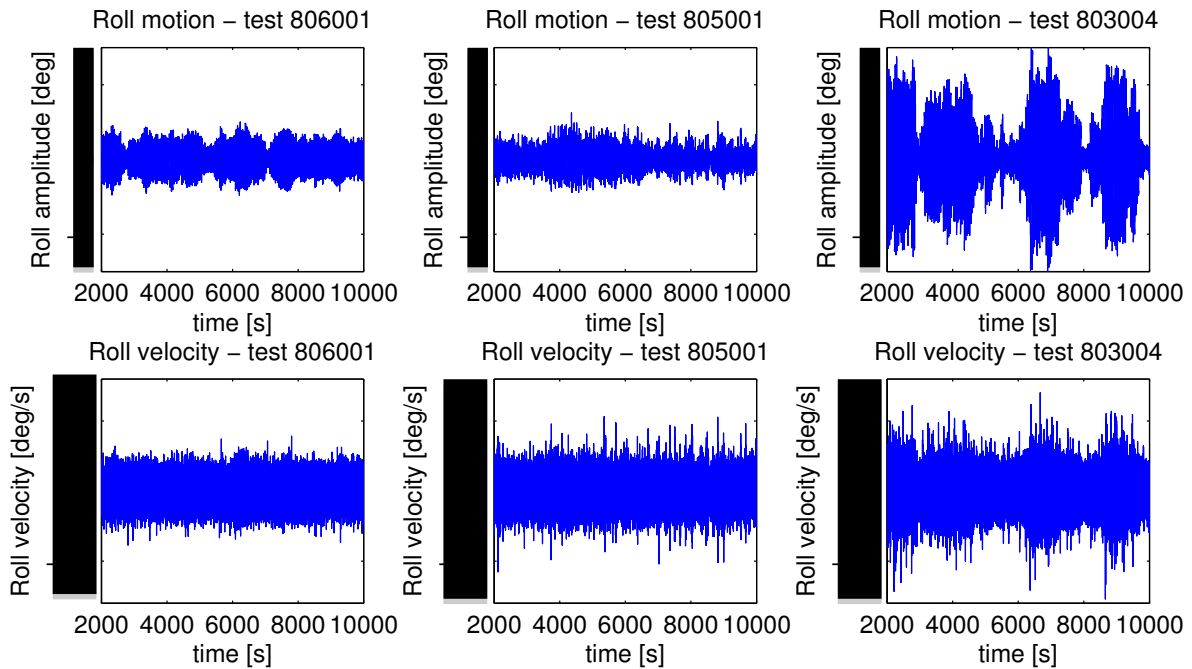


Figure 3.5: Time traces of the measured roll motion and the calculated roll velocity for different sea conditions. Sea conditions: test 806001 - $H_s=1.5$ m, $T_p=7$ s; test 805001 - $H_s=1.5$ m, $T_p=12$ s; test 803004 - $H_s=3$ m, $T_p=7$ s.

3.2. FIRST ORDER ANALYSIS

The software packages WAMIT and DIFFRAC have been used for the first order hydrodynamic analysis. Both software packages are based on the 3D panel method therefore, first order output is expected to be similar. First the roll response spectra is calculated with WAMIT output. Then the first and second order output of WAMIT and DIFFRAC is compared. Finally, the different contributions of the quadratic transfer function are studied.

ADDED MASS, DAMPING AND EXCITING WAVE FORCE

As shown in the flowchart in Figure 3.1 the first order output of the hydrodynamic analysis has been used in order to calculate the first order roll response spectrum of the Sleipnir. The first order output used for the first order analysis consists of the added mass and damping moment shown in Figure 3.6.

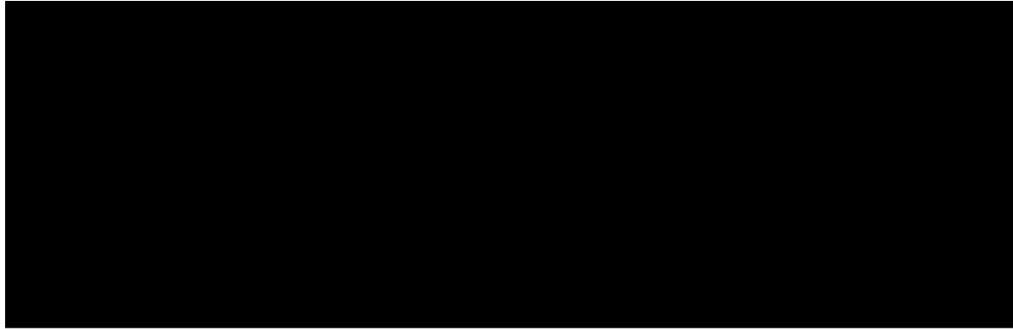


Figure 3.6: Added mass and damping moment for roll calculated with a WAMIT NSCVfine run.

Secondly the calculated wave force is used in order to calculate the first order wave force spectrum using Equation 1.14. The wave moment for roll is shown in Figure 3.7. In order to calculate the first order wave moment spectrum a wave spectrum is needed.

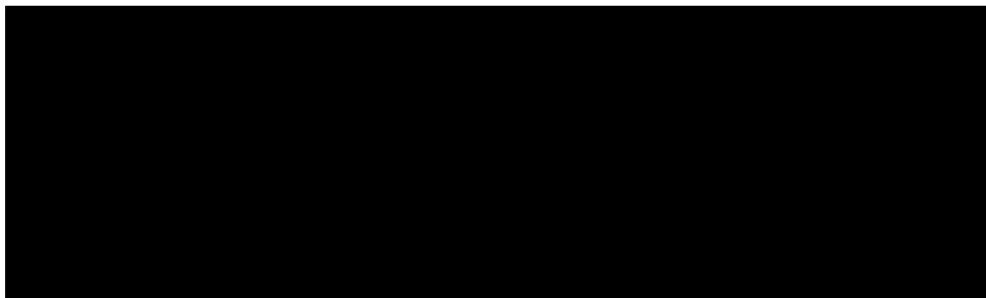


Figure 3.7: RAO of exciting wave moment for roll calculated with a WAMIT NSCVfine run.

ENVIRONMENTAL CONDITIONS

The tested sea conditions (see Table 2.2) have been used to calculate the exciting wave force spectrum. Current and wind have not been part of the experimental procedures. Three sea conditions have been used to calculate the roll response spectra. The theoretical JONSWAP spectra and the calibrated wave spectra are used for the explanation of the analysis. These spectra are shown in Figure 3.8. The calibrated wave spectra of test 201019 - $H_s=1.5$ m, $T_p=7$ s, test 201013 - $H_s=1.5$ m, $T_p=12$ s and test 201016 - $H_s=3$ m, $T_p=7$ s have been used. In order to define the first order roll response spectrum the moment transfer function must be defined.

MOMENT TRANSFER FUNCTION

The moment transfer function is defined as in Equation 1.17. In this case the uncoupled roll motion is considered. The moment transfer function has been calculated by interpolation of the added mass and damping moment of a NSCVfine run with a frequency step $\Delta\omega = 0.01$ rad/s. The added mass and damping for roll are shown in Figure 3.6.

The motion response around the natural frequency is the focus of this research. In Equation 1.17, the added

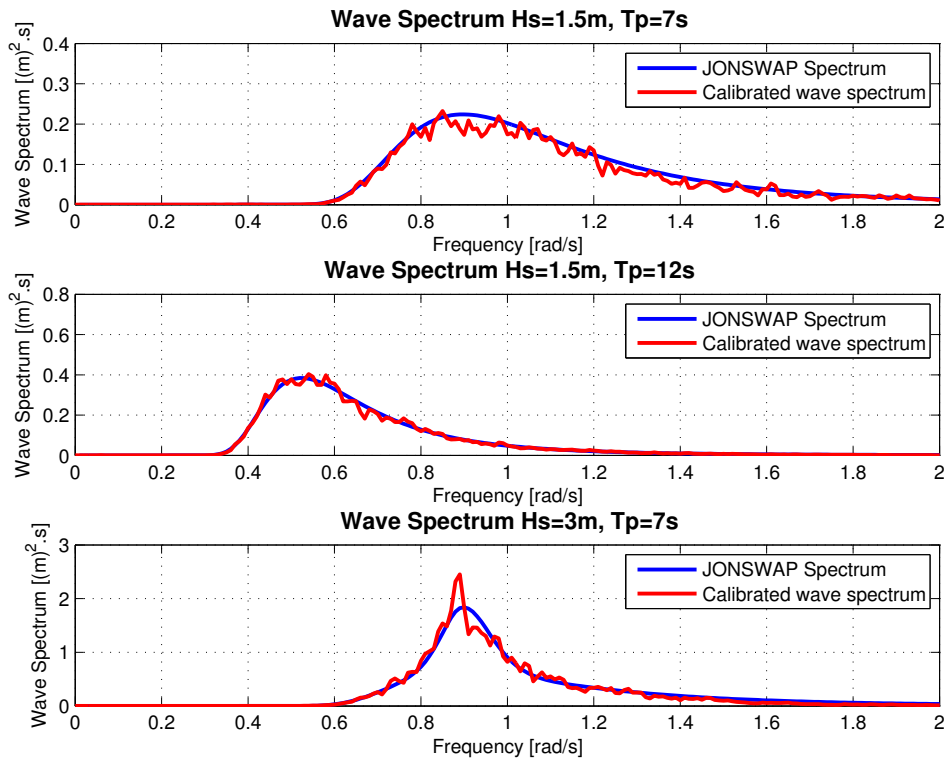


Figure 3.8: Theoretical JONSWAP wave spectra and the calibrated wave spectra for the tested sea conditions. The calibrated wave spectra of test 201019 - H_s=1.5 m, T_p=7 s, test 201013 - H_s=1.5 m, T_p=12 s and test 201016 - H_s=3 m, T_p=7 s are shown.

viscous damping is included. The dominant parameter near the natural frequency for the moment transfer function is damping. From Equation 1.17, it follows that with a non-damped system the moment transfer function will increase to infinity at the natural frequency (with infinitesimal frequency steps). In Figure 3.9 an example of the absolute moment transfer function is shown with an added viscous damping of 5% b_{crit} . In Figure 3.1 it is shown that the added viscous damping can be added in the diffraction software packages but also is used in the moment transfer function. For this reason the influence of the added viscous damping on the total roll response spectrum is investigated for three damping levels. This raises the question whether it is necessary for future analysis to add the viscous damping in the diffraction software or is it sufficient to use the viscous damping only in the moment transfer function?

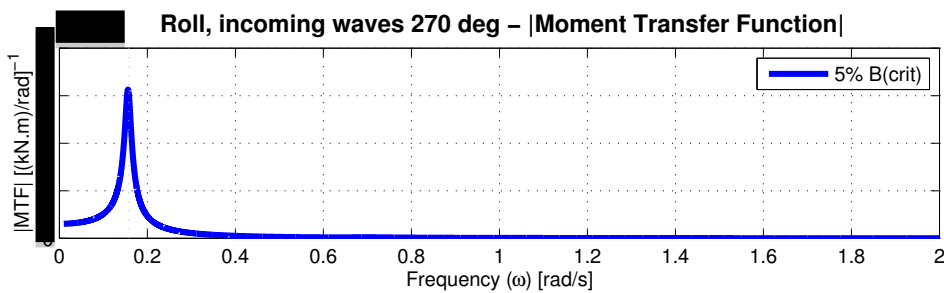


Figure 3.9: Example of the absolute moment transfer function for roll in beam waves. An added viscous damping of 5% b_{crit} has been used.

RESPONSE SPECTRUM

By calculating the wave exciting moment spectrum and the moment transfer function, the first order response spectrum can be obtained. The first order roll response spectrum is defined as in Equation 1.16.

The method for calculating the first order response spectrum is presented in Figure 3.15.

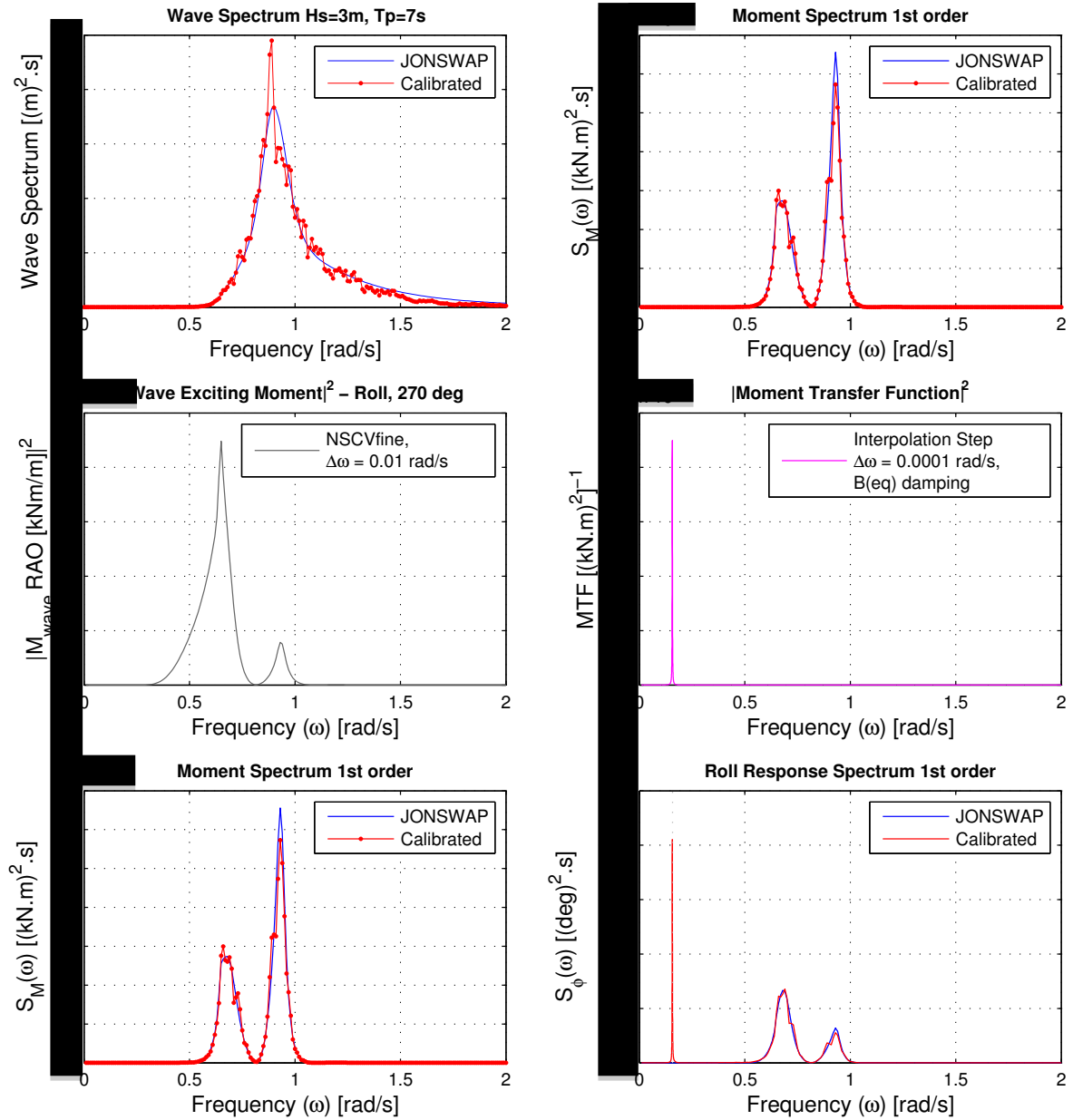


Figure 3.10: Method of calculating the first order roll response spectrum in beam waves. **Left:** On the left side this figure shows how to calculate the first order moment spectrum by multiplying the sea spectra with the wave exciting moment RAO squared. In this figure the theoretical JONSWAP spectrum and calibrated spectrum with $H_s = 3\text{m}$, $T_p = 7\text{s}$ are shown. **Right:** On the right side of the figure is shown how to obtain the first order roll response spectrum from the wave moment spectrum and the moment transfer function (b_{eq} is 0.52% b_{crit}).

3.3. SECOND ORDER ANALYSIS

The second order analysis have been performed using WAMIT and DIFFRAC. The second order velocity potential is calculated with a different method in both software packages. The diffraction and radiation problem can not be considered separately for the second order solution. WAMIT is able to calculate the complete second order velocity potential using a discretized free water surface as shown in Figure 3.3. DIFFRAC approximates the second order velocity potential using first order quantities described by Pinkster [12].

In order to calculate the second order roll response, the second order velocity potential calculated by WAMIT, is used. Then the first and second order output of WAMIT and DIFFRAC is compared. Finally the different contributions of the quadratic transfer function calculated by DIFFRAC will be studied.

QUADRATIC TRANSFER FUNCTION

The second order output of the hydrodynamic analysis consists of the quadratic transfer functions. In this study only the low frequency quadratic transfer function is calculated. The second order high (sum) frequency QTF is not subject of research because these sum frequencies do not influence the motion behaviour around the natural periods of the Sleipnir. The software packages calculate only the upper triangle of the QTF. In order to obtain the whole QTF symmetry, as explained in Chapter 1.2.1, has been used.

Firstly, runs have been done with coarse frequency steps of 0.05 rad/s and 0.025 rad/s in order to obtain a complete QTF landscape for a frequency domain of $[0 \leq \omega_1 \leq 2]$ rad/s and $[0 \leq \omega_2 \leq 2]$ rad/s.

However, only a small range of difference frequency combinations are important to predict the roll motion response spectrum around the natural frequency. The frequency range, in which the difference frequencies are essential to calculate, is around the natural frequency of the motion (for roll $\mu = 0.16$ rad/s). The second order roll response spectrum of the Sleipnir consist of a small width and high peak (See Figure 2.4b) because it is a low damped system.

The natural frequency for roll is 0.16 (0.158) rad/s. It is important to choose the frequency step in a manner that the QTF is calculated where the difference frequency is equal to the natural frequency. In this research the QTF is calculated for a range of difference frequencies from $0.13 \leq \mu \leq 0.18$ rad/s, with a frequency step of 0.01 rad/s. The duration of the calculation, of this QTF, with the geometric models NSCVcoarse, NSCVbase and NSCVfine was respectively, 5.5 hours, 9.5 days and 91.5 days. The chosen range encloses the diagonal $\mu = 0.16$ rad/s. Furthermore, the range encloses the width of the moment transfer function, defined in Equation 1.17, which is important in order to calculate the roll response spectrum.

ENVIRONMENTAL CONDITIONS

In the second order analysis the same environmental conditions have been used as in the first order analysis. The wave spectra in Figure 3.8 consists of a set of data related to the wave frequency. If the wave spectra $S_\zeta(\omega)$ can be considered as a vector, a , the following statement holds:

$$S_\zeta(\omega) \cdot S_\zeta(\omega + \mu) = aa^T \quad (3.6)$$

In Figure 3.12 this 'multiplication' is shown for the theoretical JONSWAP spectrum and the calibrated measured wave spectrum with $H_s = 3$ m, $T_p = 7$ s (presented in Figure 3.8).

WAVE DRIFT FORCE SPECTRUM

The wave drift force spectrum is calculated using Equation 1.15. Inside the integration, the 'multiplied' sea spectrum, which has been discussed in the previous paragraph, is multiplied with the amplitude of the calculated QTF squared (Figure 3.11). The resulting matrix is shown in Figure 3.13.

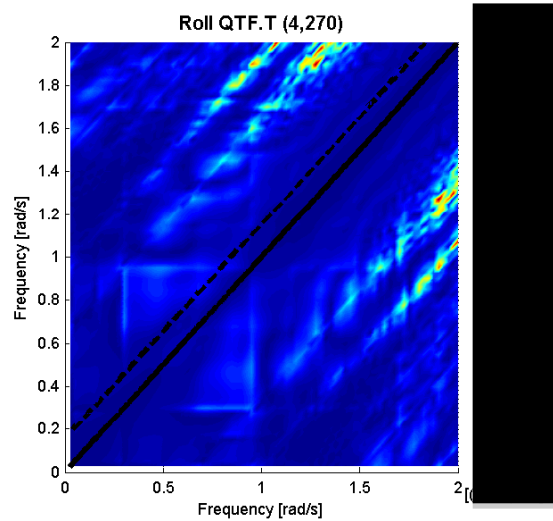


Figure 3.11: Example of a calculated amplitude quadratic transfer function by WAMIT. The black diagonal for difference frequency $\mu = 0$ rad/s and the black dotted diagonal at of $\mu = 0.16$ rad/s is included.

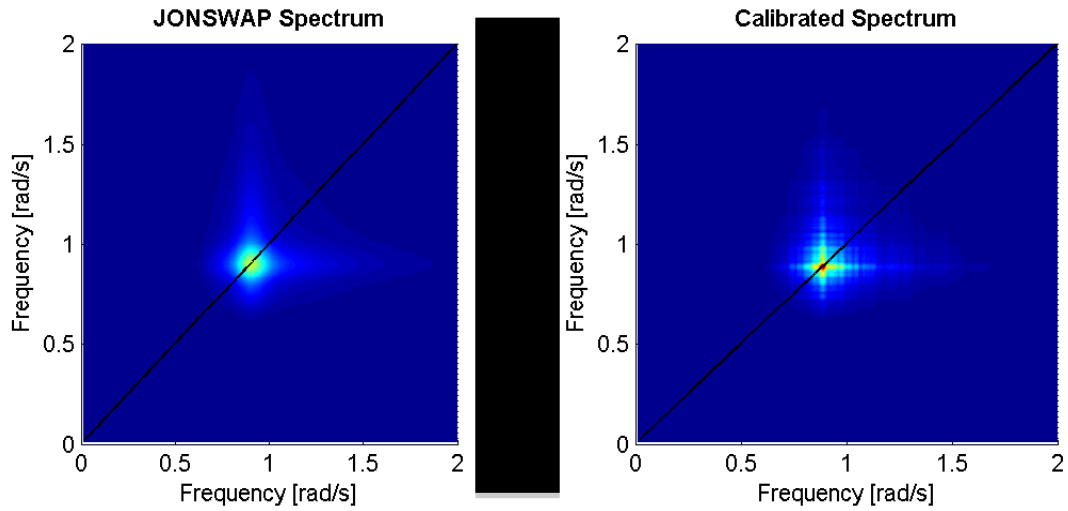


Figure 3.12: In this figure the multiplied JONSWAP spectrum and the multiplied calibrated spectrum with $H_s=3$ m, $T_p=7$ s. The colorbar is applicable for both spectra. The black line is the diagonal where the difference frequency $\mu = 0$.

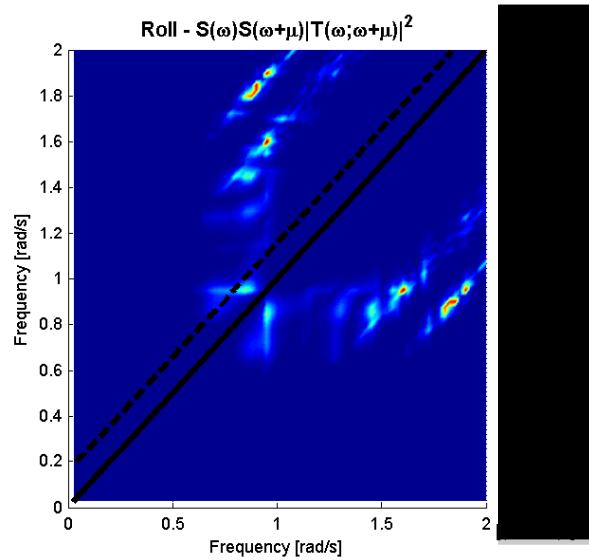


Figure 3.13: In this figure the $S_{\zeta}(\omega) \cdot S_{\zeta}(\omega + \mu) \cdot |T(\omega + \mu, \omega)|^2$ for roll with a $H_s=3$ m, $T_p=7$ s is plotted. This Figure is the multiplication of the spectrum left in Figure 3.12 and the amplitude (T) QTF in Figure 3.11. The black line is the diagonal where the difference frequency $\mu = 0$. The black dotted line is the diagonal with $\mu = 0.16$ rad/s.

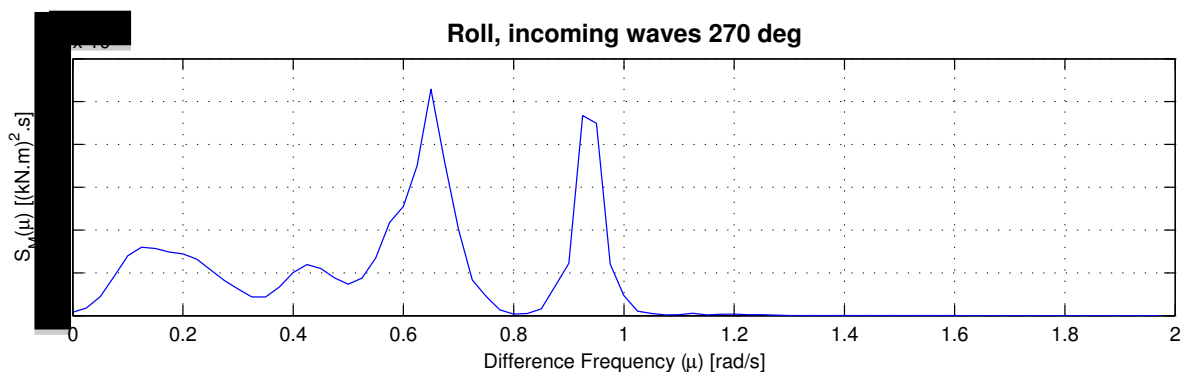


Figure 3.14: Example of drift moment spectrum for roll calculated from the matrix in Figure 3.13.

In order to calculate the wave drift moment spectrum for roll, the diagonals in the matrix $S_{\zeta}(\omega) \cdot S_{\zeta}(\omega + \mu) \cdot |T(\omega + \mu, \omega)|^2$ are integrated, and multiplied with eight for a range of μ . In other words, the matrix consists of a diagonal for every difference frequency μ . Performing the integral for every diagonal results in the moment drift force spectrum as in Figure 3.14. In Figure 3.14 an example of this procedure on the matrix in Figure 3.13 is given.

RESPONSE SPECTRUM

In order to calculate the second order response spectrum the wave drift force spectrum is multiplied with the absolute moment transfer function squared (See Equation 1.19). This moment transfer function is identical with the moment transfer function in the first order analysis.

The method for calculating the second order response spectrum is presented in Figure 3.15.

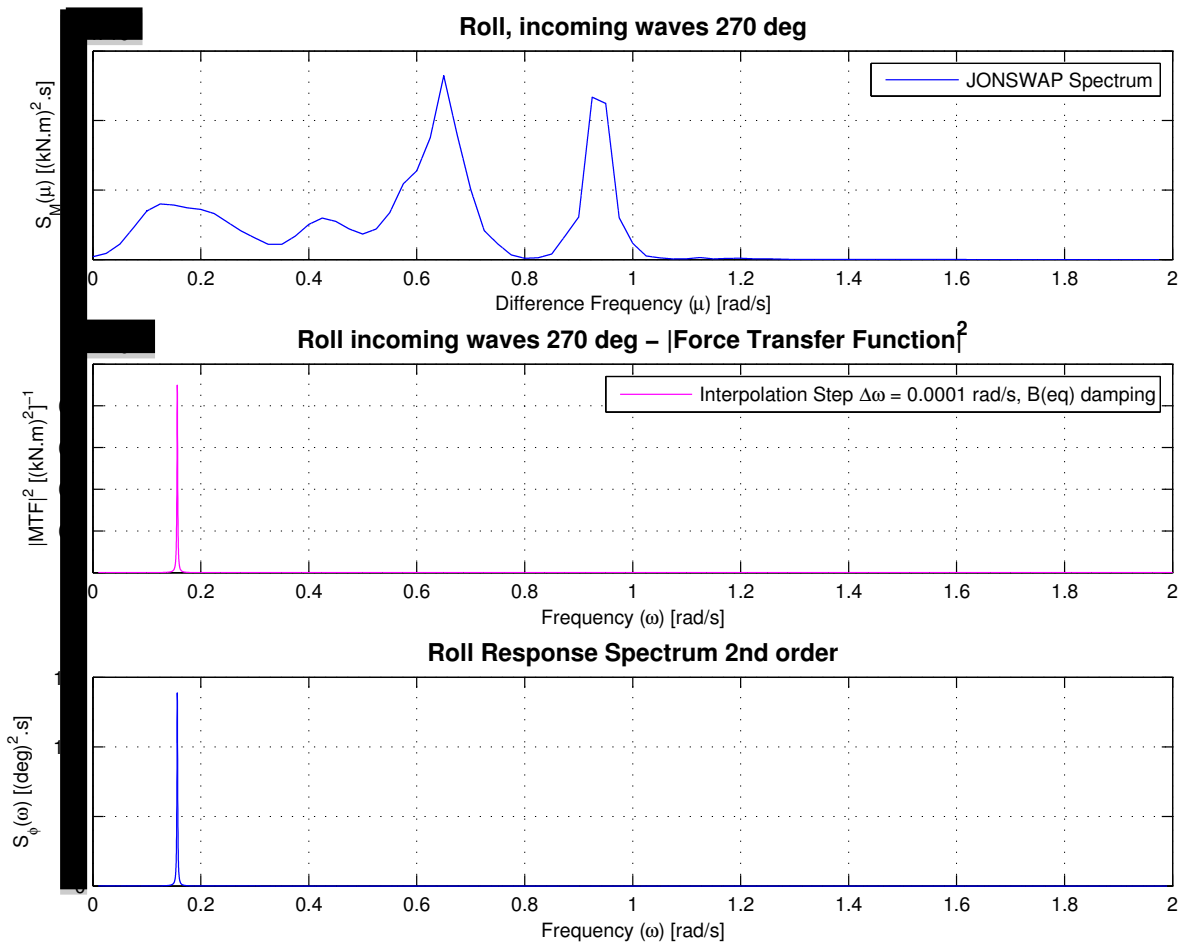


Figure 3.15: Method of calculating the second order roll response spectrum in beam waves. **Top:** Wave drift moment spectrum for roll. This spectrum is calculated using a QTF with a $\Delta\omega = 0.025$ rad/s. The theoretical JONSWAP spectrum with $H_s = 3$ m, $T_p = 7$ s has been used. **Middle:** In this figure the moment transfer function squared is shown. The equivalent damping b_{eq} is $0.52\% b_{crit}$. **Bottom:** Low frequency second order roll response spectrum.

3.4. TOTAL RESPONSE SPECTRUM

The total motion response spectrum is obtained with Equation 1.20. The summation of the first and second order spectra is shown in Figure 3.16.

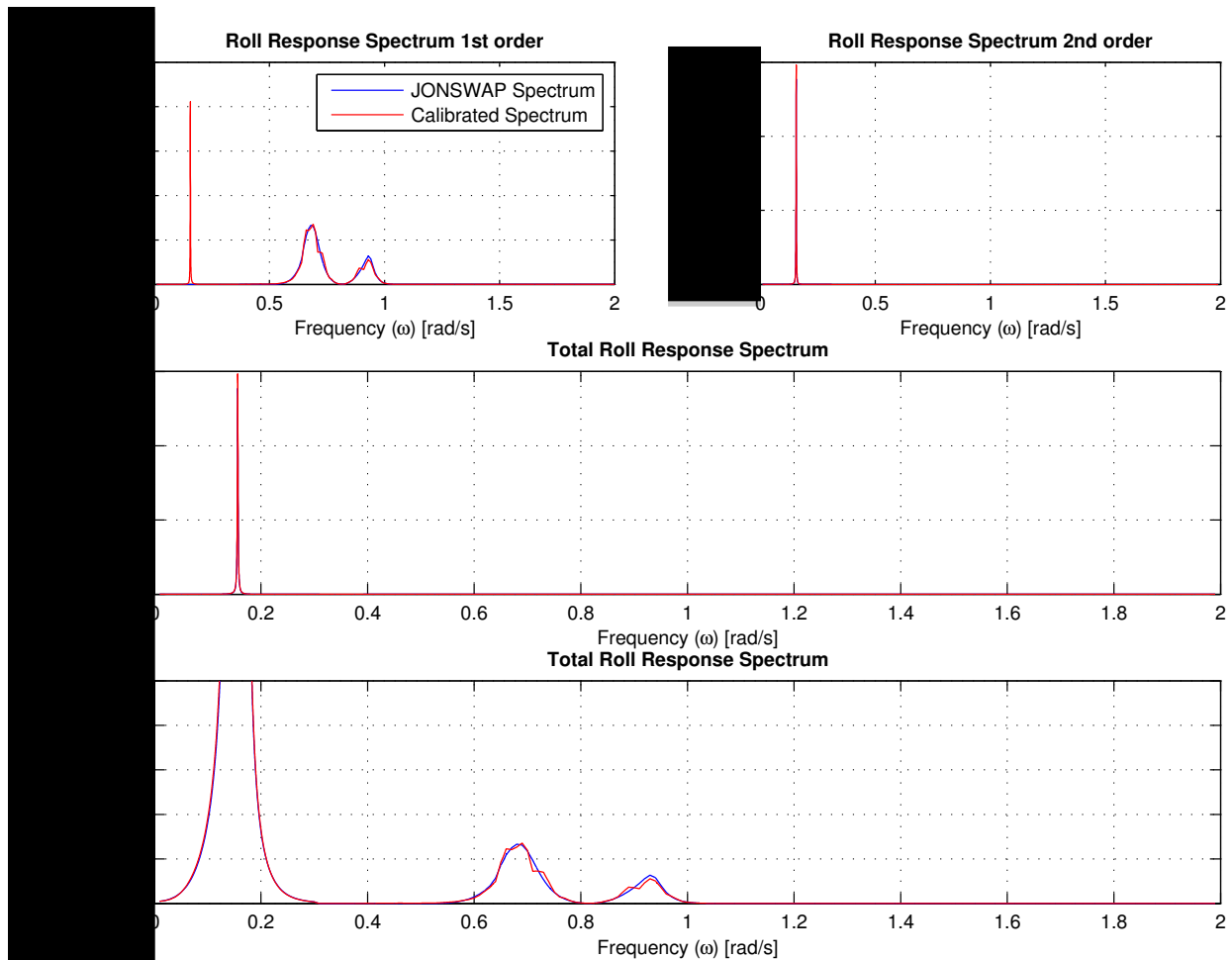


Figure 3.16: Method of calculating the total roll response spectrum in beam waves. **Top:** *Left* - First order roll spectrum. *Right* - Second order roll spectrum. **Middle:** Total roll response spectrum. **Bottom:** Total roll response spectrum with a different scale. The first order response in frequency range $0.6 \text{ rad/s} \lesssim \omega \lesssim 1 \text{ rad/s}$

3.4.1. VALIDATION

The calculated roll response spectrum is validated with the measured motion response of the model tests. During model tests the roll motion is measured. The roll response spectrum is created from the roll motion time traces, using two spectral density functions. These are described in Appendix B.2.4.

3.5. COMPARISON OF WAMIT AND DIFFRAC

The software package WAMIT calculates the motions around the hydrodynamic origin (CoH). This is a point between the two columns in the middle at the waterline. DIFFRAC calculates the motions around the centre of gravity (CoG). In order to compare the results of the hydrodynamic calculations of the different software packages the origin around which the motions and the wave loads have been calculated must be similar. The motions and wave loads calculated for the CoG in DIFFRAC are transformed to the CoH. The transformation method is extensively explained in Appendix B.1.2.

3.6. TIME DOMAIN STUDY

The computer program aNySIM is used to simulate the motions of the Sleipnir in the time domain. The hydrodynamic coefficients, first and second order forces, calculated with diffraction software, are needed as a hydrodynamic input file (.hyd file) for aNySIM.

In the time domain simulations with aNySIM a linear and quadratic damping term can be included. Comparing the roll responses calculated with aNySIM and the roll response calculated in the frequency domain could give an inside in the accuracy of the linearized damping value b_{eq} .

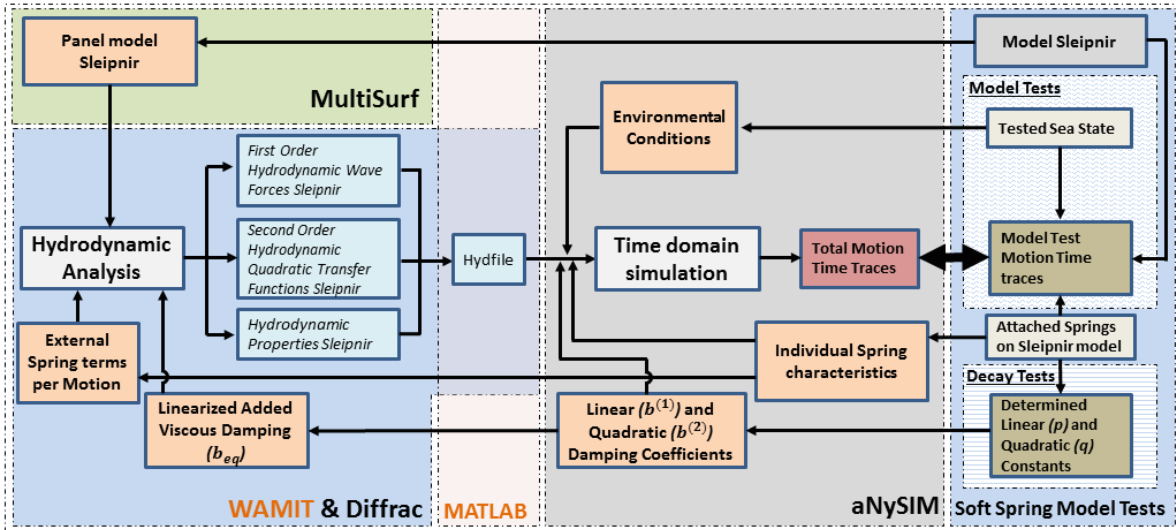


Figure 3.17: Flowchart of the time domain analysis.

DECAY TEST SIMULATION

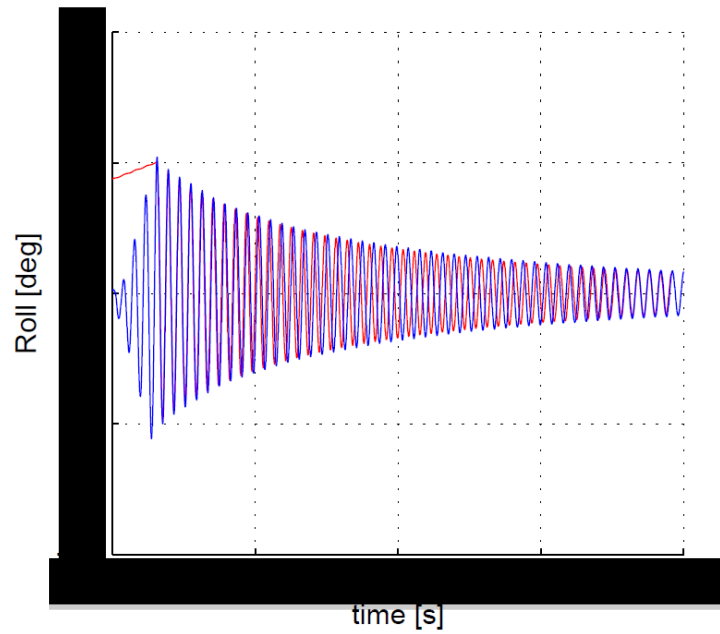
The decay test are simulated by applying a force or moment on the body, which stops acting on a certain time. The body will start to perform a damped oscillation, with a characteristic oscillation period and damping values. In order to estimate the correct damping values for roll the decay tests performed at MARIN are simulated with aNySIM.

As a first approach the linear and quadratic damping constants are calculated with the p and q values obtained from the MARIN soft spring decay tests. In order to simulate the forces in the springs four separate spring lines are defined. The position where the springs act on the body, the line stiffness and the pretension of the springs are incorporated.

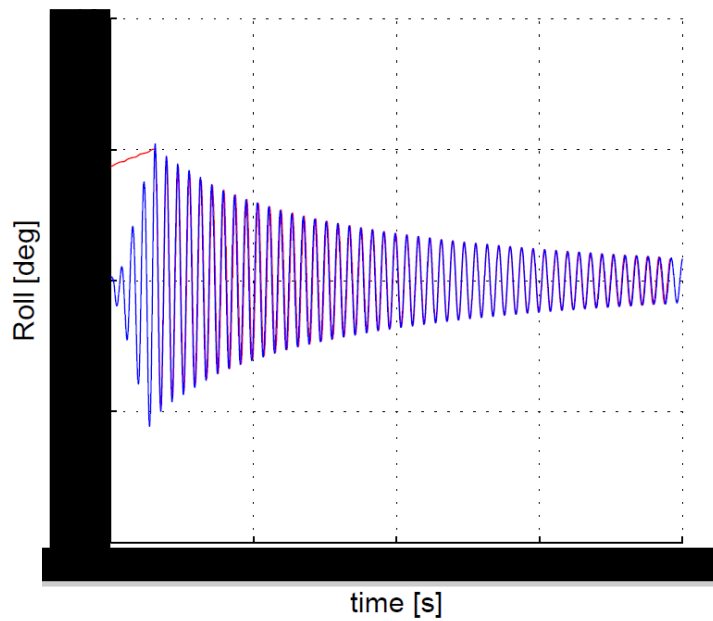
In Figure 3.18a the results of the first run are shown. The natural period of roll is not corresponding with the natural period during the measured decay tests. In Figure 3.18b the natural period is 'tuned' by varying the roll radius of gyration k_{xx} .

MODEL TEST SIMULATION

The model test with sea state $H_s = 3\text{m}$ and $T_p = 7\text{s}$ is simulated using similar linear and quadratic damping constants as in the decay test simulations. The time trace of the measured wave at WAVECL (See Figure 2.3) during calibration tests is used as input value for the first simulation. Thereafter simulations with the time traces measured at WAVE180 and WAVE270 during model tests are performed (See Figure 2.3).



(a) Roll decay simulation with roll radius of gyration k_{xx} of 42,5 m.



(b) Roll decay simulation with a tuned roll radius of gyration k_{xx} of 44.6 m.

Figure 3.18: Simulation of the roll decay tests performed at MARIN. Decay test nr. 803005.

4

RESULTS AND DISCUSSION

In this chapter the results of the frequency domain study and of the time domain study are presented. First the results of three estimation methods of the viscous roll damping are presented. Secondly a grid refinement study, a frequency refinement study and a damping level study is shown. The studies are presented in a manner in which the influence of the tested variables on the quadratic transfer function, second order moment spectrum, moment transfer function and the calculated roll response spectrum is shown. In these studies the sea state $H_s = 3\text{m}$, $T_p = 7\text{s}$ for beam wave loading is used in order to calculate the roll response behaviour of the Sleipnir.

Based on the findings in the refinement studies the total response spectrum is calculated consisting of a first and second order part. The results are compared with the measured roll response spectra during model tests. The influence of (linearized) added viscous damping on the estimated roll response spectrum is presented for three tested sea states.

Then the results of the calculation of first and second order forces using WAMIT and DIFFRAC presented. The different contribution of the low frequency quadratic transfer function are shown.

Finally results of the time domain simulations are presented. In these simulations a linear and quadratic damping coefficient, calculated from the still water p and q values, are used. The resulting roll response spectra are compared with the roll density function from the measurements and the frequency domain calculations.

4.1. CALCULATION OF THE ROLL DAMPING

The roll damping of a vessel is a non-linear phenomenon. In order to implement damping in the equation of motion it is necessary to linearize the non-linear damping. This linearized total damping term is referred to as the equivalent damping. In this research three different methods are used in order to estimate the (linear) equivalent damping based on performed model tests of the Sleipnir. The hydrostatic and hydrodynamic properties of the Sleipnir model are calculated with WAMIT and shown in Table 4.1.

First equivalent damping estimations, which are based on the linear ($b^{(1)}$) and quadratic ($b^{(2)}$) damping coefficients, are shown. These damping coefficients are calculated with the results of the performed still water decay tests (Table 2.3) and are shown in Table 4.2.

In Table 4.3 the results of the harmonic linearization (for regular waves) approach are shown. In this linearization method the equivalent damping term is related to the quadratic damping term ($b^{(2)}$) through a roll amplitude. In this case the maximal roll amplitude measured during model tests for each specific sea state is used for the linearization.

In Table 4.4 the results of the stochastic linearization (for irregular waves) approach are presented. The equivalent damping term in this method is related to the quadratic damping term ($b^{(2)}$) through the variance of the global roll velocity ($\sigma_{\dot{\phi}}$). The roll motion time traces of the three model tests have been used in order to calculate roll velocity time traces. The roll variance is obtained from the velocity spectra.

The results of the damping estimation using the half-power bandwidth method on the spectral density functions for roll are presented in Table 4.5. In Appendix B.1.4 an extensive description of obtaining these results is presented.

The influence of three different damping levels on the roll response spectrum is investigated (See Section

3.1.1). The damping levels are defined as 0% of the critical damping or $\xi = 0\%$ ($\xi = b/b_{crit}$), 5% of the critical damping and the (harmonic linearized) equivalent damping (b_{eq}). The values of the first two damping levels can be found in Table 4.1. The equivalent damping used in this damping study is presented in Table 4.3.

Linear Spring Coefficient	Added Mass	Potential Damping	Mass Moment of Inertia	Critical Damping	5% of b_{crit}
$C_{\phi\phi}$ [kNm/rad]	$A_{\phi\phi}(\omega_n)$ [t·m ²]	$b_{pot}(\omega_n)$ [kNm/(rad/s)]	I_{ϕ} [t·m ²]	b_{crit} [kNm/(rad/s)]	[kNm/(rad/s)]
18681768	295681648	2467	439397047	234372092	11718604

Table 4.1: Hydrostatic and hydrodynamic coefficients. The spring coefficient is calculated using the realized displacement and transverse metacentric height of the MARIN Sleipnir model (Table 2.1). The added mass and potential damping at the natural frequency (0.16 rad/s) is calculated with WAMIT.

Period	Proportional Damping	Quadratic Damping	Logarithmic Decrement	Linear Damping Coefficient	% of $b^{(1)}$ relative to b_{crit}	Quadratic Damping Coefficient	% of $b^{(2)}$ relative to b_{crit}
T [s]	p [-]	q [1/rad]	δ [-]	$b^{(1)}$ [kNm/(rad/s)]	[%]	$b^{(2)}$ [kNm/(rad ² /s ²)]	[%]

Table 4.2: Results of MARIN decay test 803005 for roll motion.

Operational Wave	Linearization roll amplitude	Equivalent damping	Added viscous damping	% of b_{visc} relative to b_{crit}
H_s, T_p [m], [s]	ϕ_a [deg] / [rad]	b_{eq} [kNm/(rad/s)]	b_{visc} [kNm/(rad/s)]	[%]

Table 4.3: Results of added viscous damping calculation using linearization of the roll amplitude ϕ_a . The ϕ_a is chosen based on the maximal measured roll amplitude during model tests. The potential damping is calculated with WAMIT.

Operational Wave	Variance of roll velocity	Equivalent damping	Added viscous damping	% of b_{visc} relative to b_{crit}
H_s, T_p [m], [s]	$\sigma_{\dot{\phi}}$ [rad/s]	b_{eq} [kNm/(rad/s)]	b_{visc} [kNm/(rad/s)]	[%]

Table 4.4: Results of added viscous damping estimation using stochastic linearization for an irregular roll motion. The $\sigma_{\dot{\phi}}$ is calculated from the roll velocity time trace. The potential damping is calculated with WAMIT.

Operational Wave	Damping ratio	Damping ratio
H_s, T_p [m], [s]	ξ_c [%]	ξ_{cc} [%]

Table 4.5: Damping ratio's calculated from the roll response spectra of the model tests in three tested sea states with the half-power bandwidth method. See Appendix B.1.4 for a description of the calculation method.

4.1.1. DISCUSSION

In the harmonic and stochastic linearization method the linear and quadratic coefficients are constants. These constants are calculated with the p and q values obtained from still water decay tests. Three free floating and one soft mooring still water roll decay tests are performed at MARIN. The obtained p and q values differ for every still water decay tests. In Appendix B.1.3 the influence of these different values of p and q on the calculation of the equivalent damping is discussed. The viscous damping ratio calculated with the p and q values of still water decay test 803005 is approximately the resulting mean damping ratio. Therefore is chosen to use these p and q values (Table 4.2) for the research of the harmonic and stochastic linearization.

The maximal measured roll amplitudes during model tests have used in order to find an linearized equivalent damping term with the harmonic linearization technique. The influence of the choice of the roll amplitude for linearization on the viscous damping ratio is plotted in Figure 4.1. In this Figure the chosen linearization roll amplitudes for the tested sea states are indicated. The corresponding added viscous damping ratio's can be obtained from the graph.

Furthermore the 'necessary linearization roll amplitude' are indicated. These linearization roll amplitudes correspond to the linear viscous damping ratios which are necessary in order to match the zero order moment of the measured roll response spectrum for each sea state. These statements are based on Figure 4.20, 4.21 and 4.22. The linear damping constant $b^{(1)}$ can be determined from Figure 4.1 at $\phi_a = 0$, which equals $\xi = 0.23\%$.

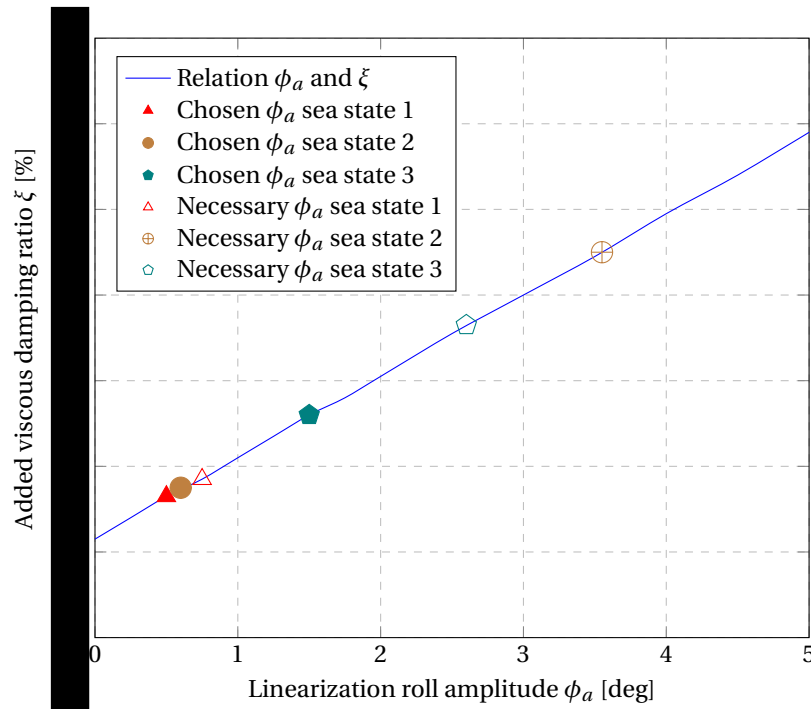


Figure 4.1: Influence of the linearization amplitude on the viscous damping ratio using the harmonic linearization technique. The chosen linearization roll amplitudes are indicated. Furthermore the linearization amplitudes which are necessary to match the roll measurements based on Figure 4.20, 4.21 and 4.22 are plotted.

The harmonic and stochastic roll damping linearization techniques have been subject of investigation for more than sixty years, e.g. [9] [10]. In the late 1970's Japanese researches published several papers summarizing the research on roll damping so far and presented practical estimation techniques for roll damping [16] [21]. For extensive historical reviews about the research on roll damping of vessels reference is made to [22] [23].

In order to predict roll motions of large offshore vessels in irregular seas the stochastic linearization technique for roll damping is used in more recent work. Although stochastic linearization research is often applied on the non-linear drag term of the Morison's equation, as also by Borgman, the linearization technique is also applicable for the estimation of a global equivalent damping term. The stochastic linearization suggested by Borgman is applicable for global roll damping estimation of vessels, as stated in e.g. [24] [11].

The factor which indicates a stochastic linearization in a Gaussian spectrum is suggested as $\sqrt{8/\pi}$ by Borgman

[10]. However also the stochastic linearization factor $\frac{8}{\pi}$ is suggested by others [16] [23]. In Haijarab's dissertation study is discussed that the assumption of the linearization factor $\sqrt{8/\pi}$ is not clear. Using Borgman's derivation method Haijarab finds the linearization factors $(8\sqrt{2})/3\pi$ and $\pi/\sqrt{8}$ [22].

In Figure 4.2 the influence of the stochastic linearization factor (K) on the calculation of the added viscous damping ratio is plotted. In this Figure the linear and quadratic constants $b^{(1)}$ and $b^{(2)}$ are assumed constant. Note that the linear damping constant $b^{(1)}$ can also be determined from Figure 4.2 at $K = 0$, which equals $\xi = 0.23\%$.

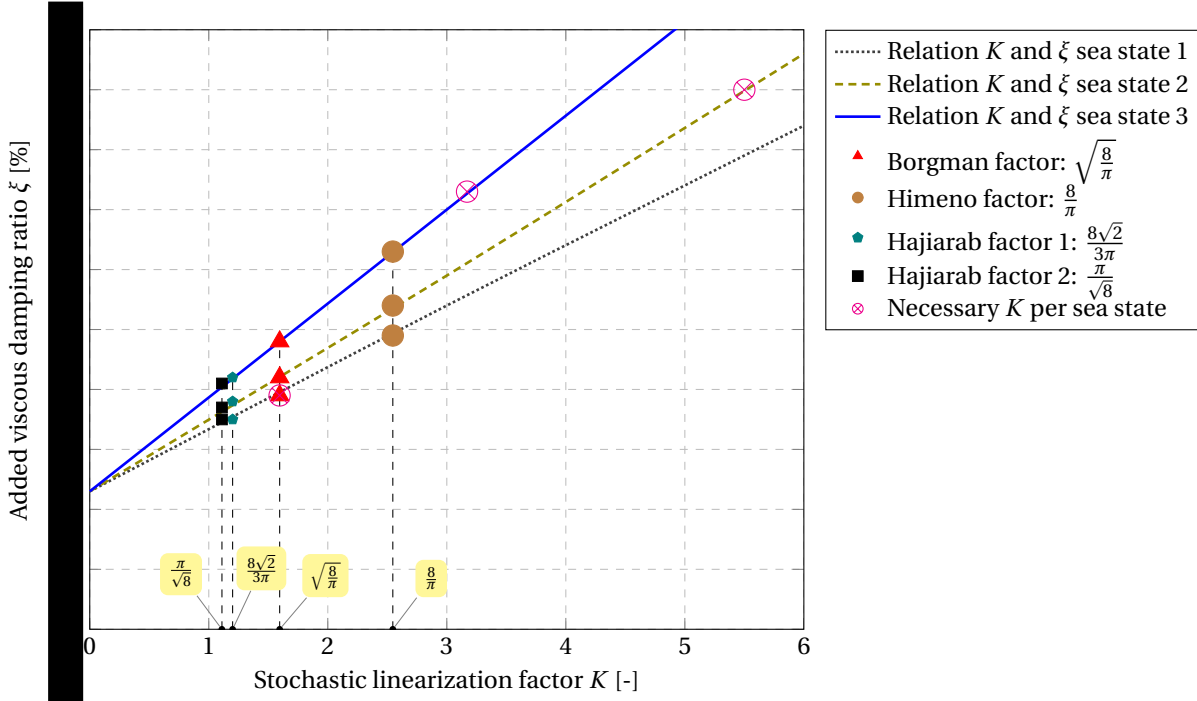


Figure 4.2: Influence of the stochastic linearization factor on the viscous damping ratio. The stochastic linearization factor is indicated with K . The linearization factors suggested by Borgman [10], Himeno [16] and Haijarab [22] are shown. Furthermore the K values which are necessary to match the roll measurements based on Figure 4.20, 4.21 and 4.22 are plotted.

In this study is found that the Borgman stochastic linearization underestimates the damping for two sea states compared with the model tests, see Figure 4.21 and 4.22. This is also indicated in Figure 4.2. Only for sea state one the estimated linear roll damping ratio corresponds with the linear damping ratio found from model tests. The under prediction of the roll damping is, in comparing with the Borgman linearization, for sea state two a factor ~ 2 and for sea state three a factor ~ 1.5 .

The above findings suggest that for certain sea states the Borgman linearization is an accurate roll damping estimation method, while for other sea states the roll damping is under predicted. However in this study only three sea states are tested during model tests. In order to investigate for which sea states the Borgman estimation method is applicable more Sleipnir model tests with different sea states are needed. In other studies the under prediction of roll damping associated with the Borgman linearization is also found [24]. In the article of Wolfram is stated that some earlier researches produced curves that correct the linear predictions in some cases. However the referred research is applied for the linearized form of the Morison's equation and it could be investigated if those findings also are applicable for this specific roll damping study about the Sleipnir.

Please note that the half-power bandwidth method provides a first rough estimation for the total damping of a system. Two main arguments must be taken into account in order to determine the value of the damping estimation results.

As explained in Appendix B.1.4 the advantage of the half-power bandwidth estimation method is simplicity in application. However this damping estimation method is highly dependent on the resolution of the spectral density function. Especially for low damped systems the response spectral density is characterized with a high peak value and a small bandwidth at the resonance frequency. The choice of the resolution of the roll response spectrum influences the bandwidth at the resonance frequency and therefore the estimation of the damping.

Secondly the damping is estimated from the roll response spectra of model tests. Though the method is mathematically correct for application on the frequency response transfer function [25]. As shown in this report (e.g. section 3.3) the roll response spectrum is dependent on a moment spectrum and a moment (response) transfer function. So by applying the half-power bandwidth method on the roll response spectrum the moment drift spectrum is also incorporated. Therefore the results of the estimation technique provide strictly speaking not purely information about the damping but about the damping and excitation combined. On the other hand the damping in the roll response spectrum is dominated by the damping in the response transfer function as shown in this research (See section 4.4.4). Therefore the method applied on the roll response spectrum will provide information about the order of magnitude of the global damping of the system.

4.2. GRID REFINEMENT STUDY

First the quadratic transfer function needs to be calculated in order to calculate the roll response spectrum. The results from the calculation of the forces and moments (QTF's) by diffraction software depend on the grid size of the discretized hull shape. Relevant in this case is to investigate for which grid size the quadratic transfer function is converged. In other words what is the minimal grid size for which the magnitude of the calculated quadratic transfer functions per wave frequency do not increase or decrease.

In Figure 4.3 the diagonal of the quadratic transfer function where the difference frequency μ is equal to the natural frequency (0.16 rad/s) is plotted. As earlier explained this is the most important diagonal in the quadratic transfer function because this diagonal, the sea spectrum and the moment transfer function will define the roll response at the natural frequency. The results of calculations with three different grid sizes (geometric models NSCVcoarse, NSCVbase and NSCVfine) are plotted.

4.2.1. QUADRATIC TRANSFER FUNCTION

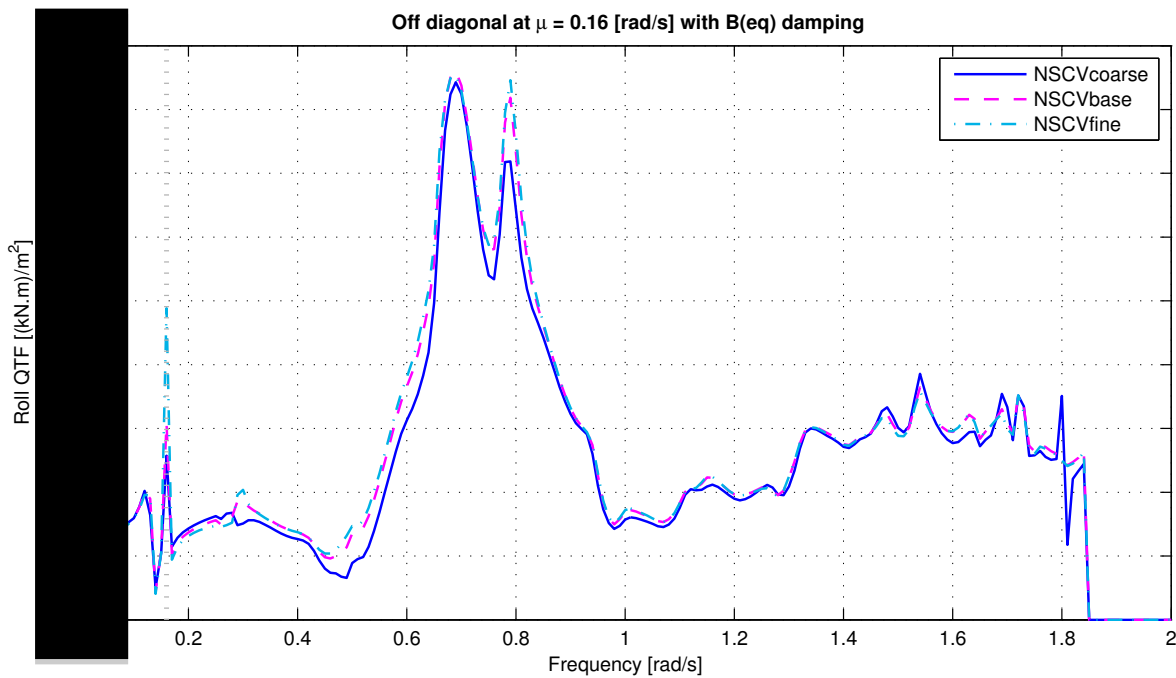


Figure 4.3: The quadratic transfer function calculated with WAMIT for a geometric model with different grid sizes (NSCVcoarse, NSCVbase and NSCVfine). The quadratic transfer function is calculated with a frequency step of $\Delta\omega = 0.01$ rad/s. The diagonal of the difference frequency μ at the natural frequency is plotted. An added viscous damping calculated from the equivalent damping is used in this calculation.

Figure 4.3 shows that the quadratic transfer function is more or less converged for geometric model NSCVbase and NSCVfine. The NSCVcoarse model underestimates the quadratic transfer function in many areas on the frequency range.

4.2.2. SECOND ORDER MOMENT SPECTRUM

The second order moment spectrum or drift moment spectrum is calculated for a sea state of $H_s = 3\text{m}$, $T_p = 7\text{s}$. The drift moment spectrum is plotted versus wave frequency for three different grid sizes of the discretized hull shape in Figure 4.4. As can be seen in this Figure the quadratic transfer function has been calculated in a range only around the natural frequency. The natural frequency is at 0.16 rad/s indicated with the dotted line. In general it can be seen that the drift force spectra of the NSCVbase and NSCVfine are converged. The

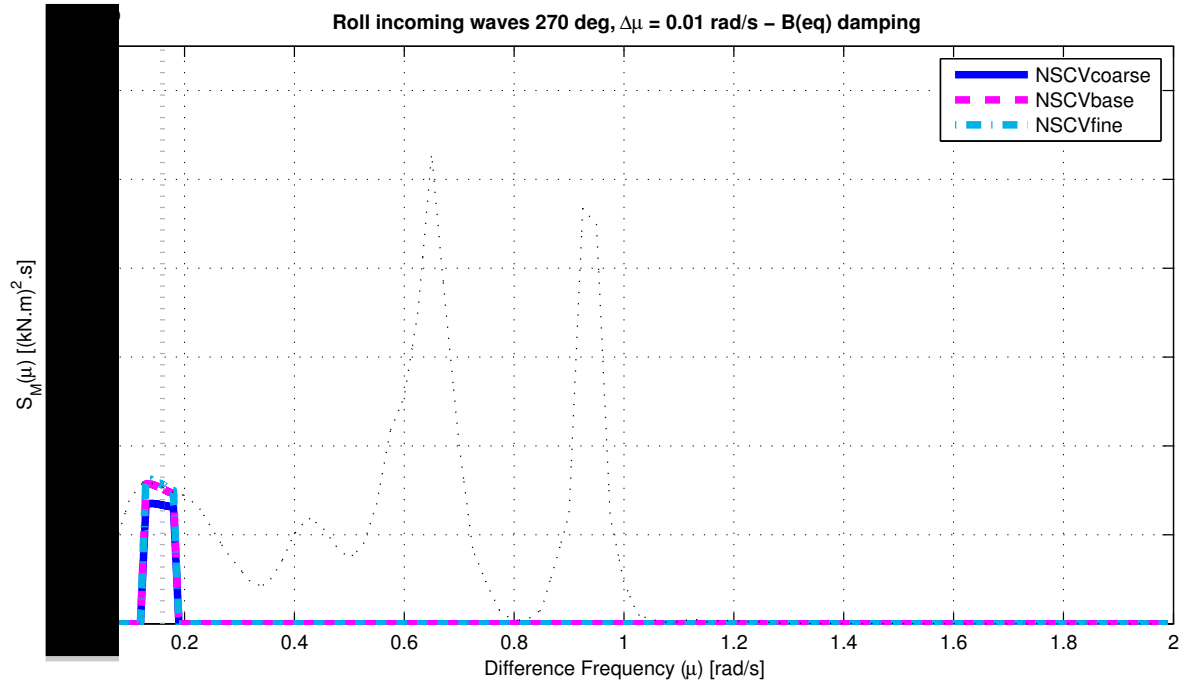


Figure 4.4: Wave drift moment spectrum for roll for geometric models NSCVcoarse, NSCVbase and NSCVfine. Dotted grey line indicates the difference frequency μ at the natural frequency 0.16 rad/s .

value of the drift force spectrum at the natural frequency has a difference of -3.1% for the NSCVbase model and a difference of -16.6% for the NSCVcoarse model compared to the NSCVfine model (See Table 4.6).

Geometric Model	$S_M(\mu_{nat})$ [(kNm) ² s]	Deviation with NSCVfine [%]
NSCVcoarse	$1.43 \cdot 10^9$	-16.6
NSCVbase	$1.66 \cdot 10^9$	-3.1
NSCVfine	$1.72 \cdot 10^9$	-

Table 4.6: Difference in wave drift force spectrum at the natural frequency calculated with WAMIT for three geometric models.

4.2.3. MOMENT TRANSFER FUNCTION

The moment transfer function is used in order to calculate the roll response spectrum. The moment transfer function is depends on inertia, added mass, damping and spring terms. In Figure 4.5 the added mass and potential damping are plotted for the three grid sizes of the discretized hull of the vessel. In order to create the moment transfer function the added mass and potential damping have been interpolated with a frequency step of 0.0001 rad/s. In Figure 4.6 the absolute squared moment transfer function is presented.

ADDED MASS AND DAMPING



Figure 4.5: Added mass and damping for NSCVcoarse, NSCVbase and NSCVfine run with WAMIT.

MOMENT TRANSFER FUNCTION

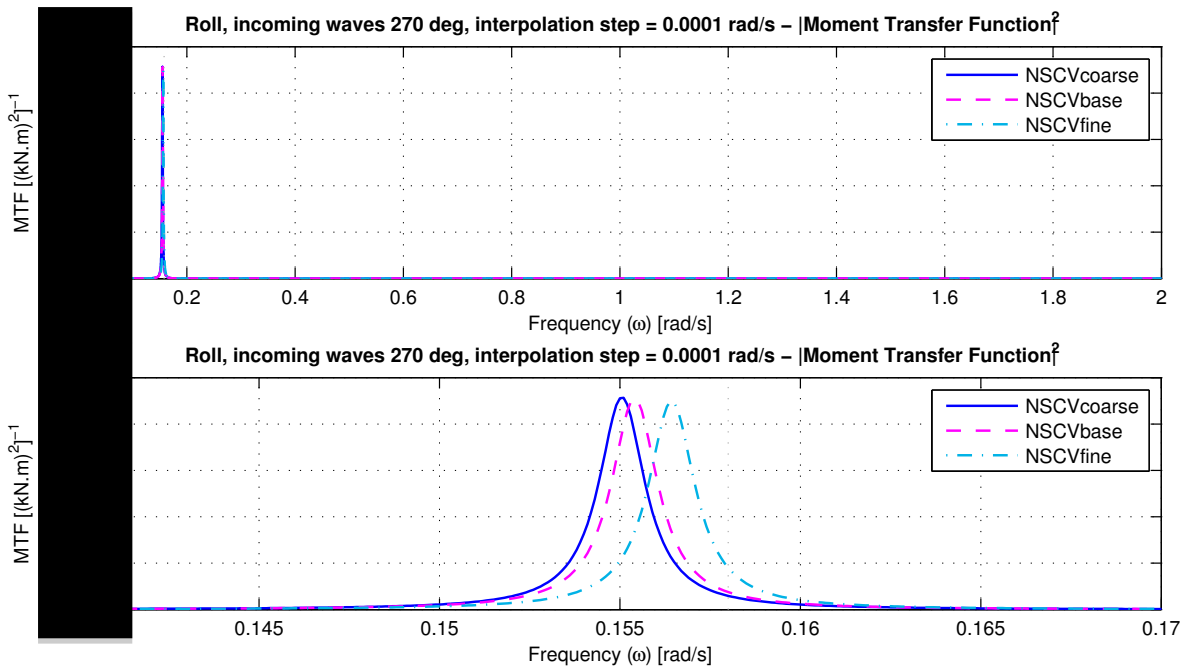


Figure 4.6: Moment transfer function for the three grid sizes. **Top:** Total frequency range is shown. **Bottom:** Frequency range around the natural period is shown.

Figure 4.5 shows a small overestimation of the added mass and potential damping for the NSCVcoarse and the NSCVbase model. Consequently the position of the second order resonance roll motion response peaks of the NSCVcoarse and NSCVbase model are underestimated comparing with the NSCVfine model in Figure 4.6.

4.2.4. SECOND ORDER ROLL RESPONSE SPECTRUM

Finally the second order roll response spectrum is calculated. The roll response spectra are presented in Figure 4.7. The roll response spectrum from the measured roll time traces is plotted in the same Figure. The

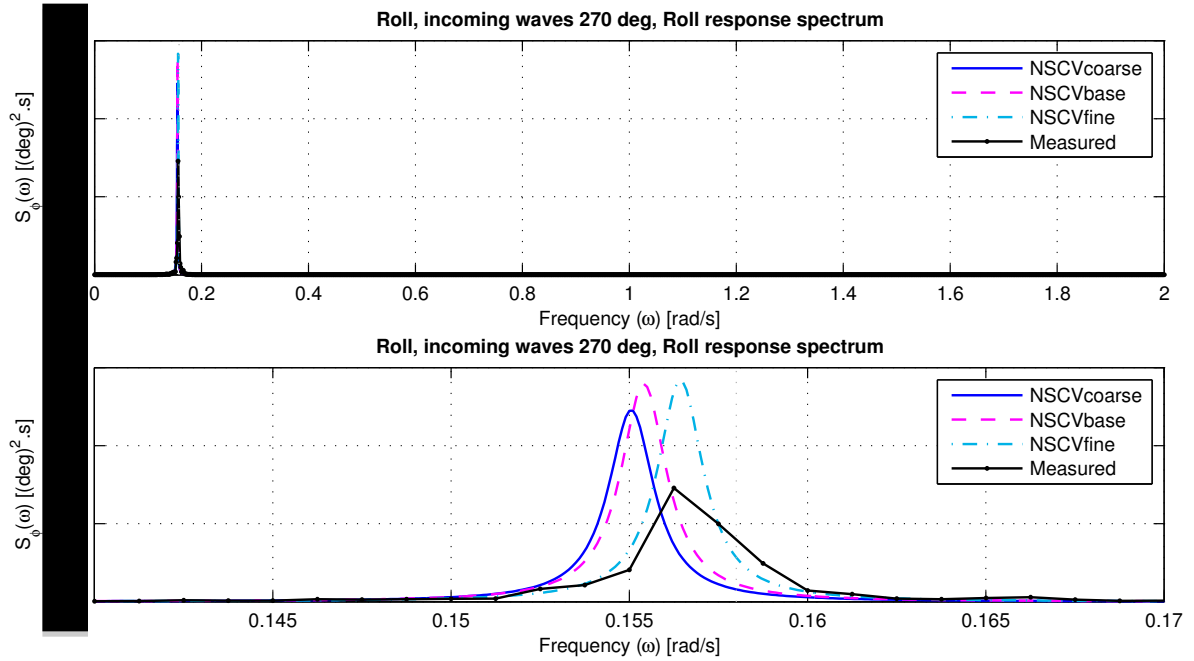


Figure 4.7: The calculated roll response spectra and the measured roll response spectrum are shown. **Top:** Total frequency range is plotted. **Bottom:** Frequency range around the natural frequency is shown.

observations from Figure 4.7 are a summation of the comments on Figure 4.4, 4.5 and 4.6. The roll response spectrum peak is underestimated in magnitude for the NSCVcoarse model. The roll response calculated with the NSCVcoarse and NSCVbase model are underestimated in the frequency position of the resonance peak. The roll motion response spectrum calculated with the NSCVfine model shows the best comparison with the measured roll response spectrum.

The shape of the calculated and measured roll response spectra differ. The theoretically calculated roll response spectrum is smooth and symmetrical but the measured roll motion density function is not symmetrical and less smooth. The shape of the spectral density function of the measurements is influenced by the chosen frequency resolution, as described in Appendix B.2.4.

4.3. FREQUENCY REFINEMENT STUDY

A similar procedure as in the grid refinement study is performed in the frequency refinement study. The influence of three frequency steps on the calculation of the roll response spectrum is presented. In Figure 4.8 the quadratic transfer function is plotted calculated with different frequency steps, $\Delta\omega = 0.05$ rad/s, $\Delta\omega = 0.025$ rad/s and $\Delta\omega = 0.01$ rad/s.

4.3.1. QUADRATIC TRANSFER FUNCTION

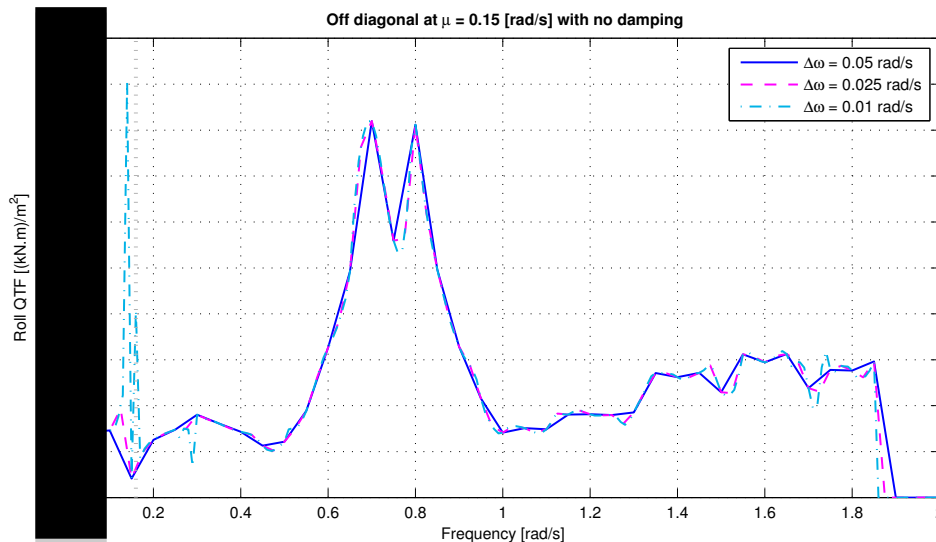


Figure 4.8: The diagonal of difference frequency $\mu = 0.15$ rad/s from the quadratic transfer function calculated with WAMIT for a NSCVbase run. No added viscous damping is used in the calculation.

Figure 4.8 shows that the quadratic transfer function calculated with 0.05 rad/s frequency step 'misses information' on several areas of the frequency domain. This is to a lesser extent also the case for the quadratic transfer function calculated with a 0.025 rad/s frequency step.

4.3.2. SECOND ORDER MOMENT SPECTRUM

In Figure 4.9 the roll moment drift force spectrum calculated for sea state $H_s = 3$ m, $T_p = 7$ s is plotted. The drift moment spectrum is plotted versus wave frequency for three calculations with different frequency steps. As shown in Figure 4.9 the calculation with the finest frequency step is performed for a smaller frequency range. The natural frequency is at 0.16 rad/s indicated with the dotted line.

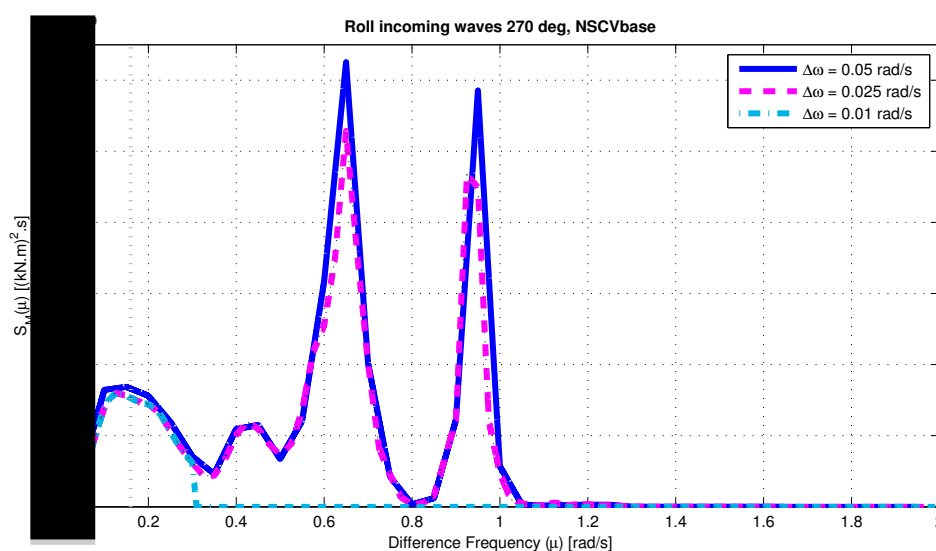


Figure 4.9: Moment drift force spectrum for roll.

The moment drift force spectrum at the natural frequency 0.16 rad/s is important for the calculation of the roll motion response spectrum. Figure 4.9 shows that the second order roll moment spectrum seems to be converged for the calculation with 0.025 rad/s and 0.01 rad/s. Note that the peaks (around $\omega \approx 0.16$ rad/s) in the quadratic transfer function (Figure 4.8) for the 0.01 rad/s frequency step run do not influence the moment spectrum significantly. This is because in the calculation of the drift moment spectrum an integration of the diagonals is incorporated (See Equation 1.15). The value of the three second order force spectra in Figure 4.9 at the natural frequency are presented in Table 4.7. From Table 4.7 it can be concluded that the second order

Geometric Model	$S_M(\mu_{nat})$ [(kNm) ² s]	Deviation with $\Delta\omega = 0.01$ rad/s [%]
$\Delta\omega = 0.05$ rad/s	$1.66 \cdot 10^9$	8.5
$\Delta\omega = 0.025$ rad/s	$1.54 \cdot 10^9$	0.3
$\Delta\omega = 0.01$ rad/s	$1.53 \cdot 10^9$	-

Table 4.7: Difference in wave drift force spectrum at the natural frequency calculated with WAMIT for three frequency steps.

moment spectrum is converged for a frequency step of 0.025 rad/s. The value of the drift moment spectrum at the natural frequency differs 0.3 % with the compared drift moment spectrum calculated with 0.01 rad/s frequency step.

4.3.3. MOMENT TRANSFER FUNCTION

In Figure 4.10 the added mass and potential damping are shown.

ADDED MASS AND DAMPING

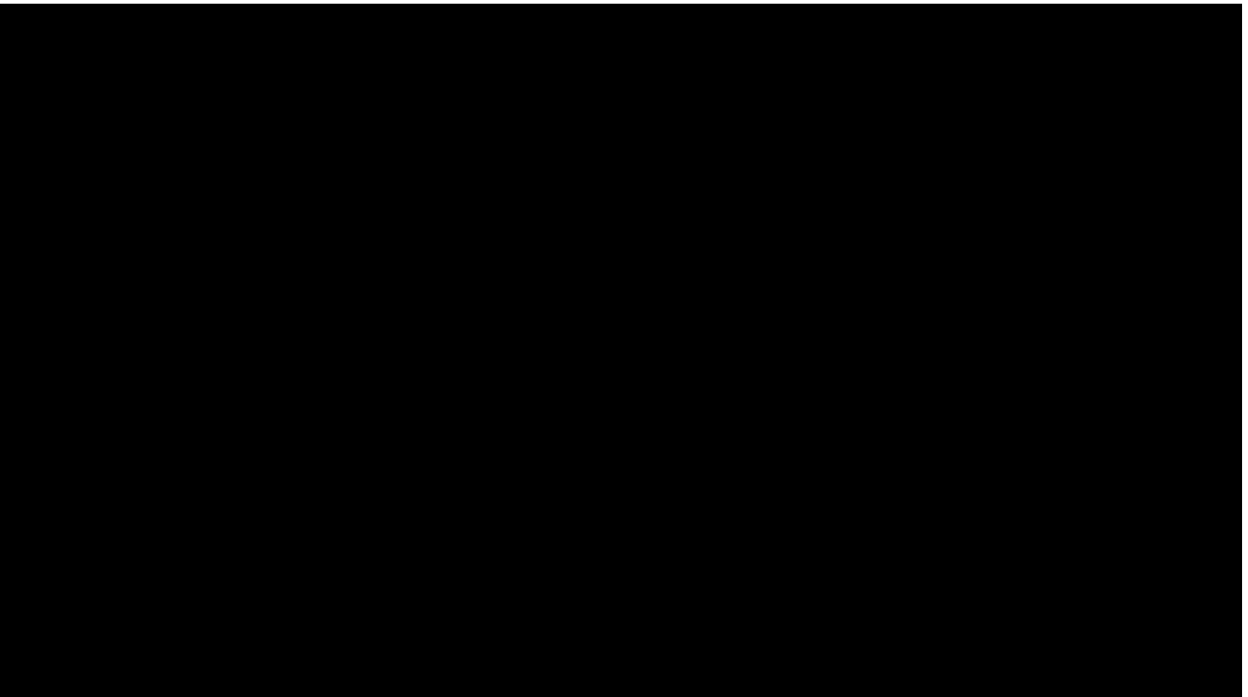


Figure 4.10: Added mass and damping for roll calculated with three different frequency steps.

Figure 4.10 shows that the different frequency steps do not influence the calculation of the added mass and potential damping significantly. However the calculation with the frequency step of 0.05 rad/s show some 'loss of information' in the added mass and potential damping near local maxima (and minima).

MOMENT TRANSFER FUNCTION

The moment transfer function calculated with different frequency steps and no added viscous damping is presented in Figure 4.11. In Figure 4.11 it is shown that the location of the resonance peak of the moment

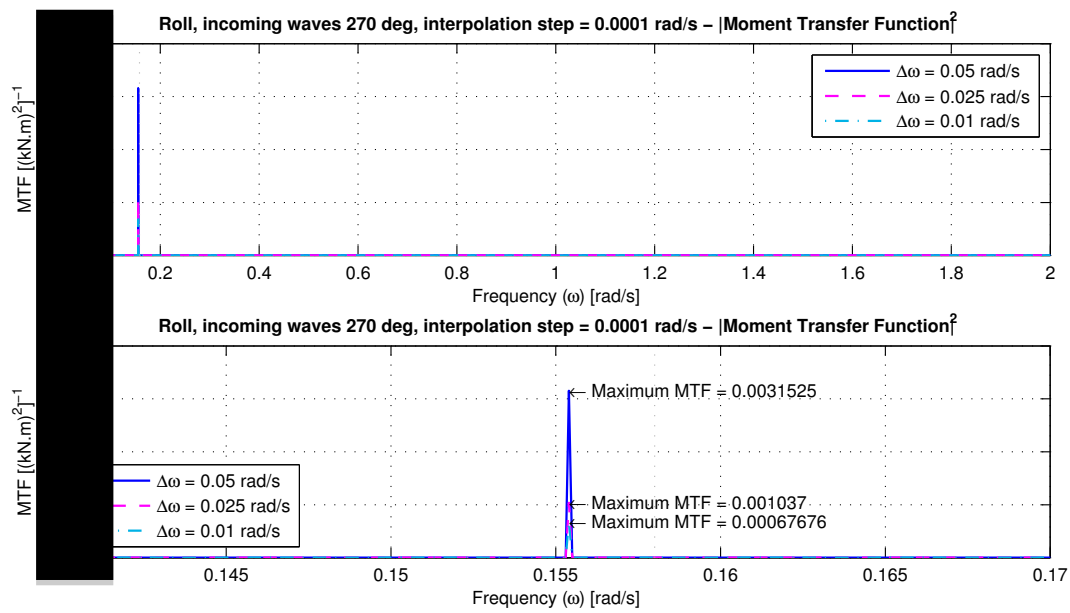


Figure 4.11: Moment transfer function for roll calculated with frequency steps of $\Delta\omega = 0.05$ rad/s, $\Delta\omega = 0.025$ rad/s and $\Delta\omega = 0.01$ rad/s. No viscous damping is added in the calculation. **Top:** Total frequency range is plotted. **Bottom:** Frequency range around the natural frequency is shown.

transfer function is equal for the calculation with the three different frequency steps. From Figure 4.11 it can also be concluded that the moment transfer function is very sensitive for the 'information loss' in the added mass and potential damping in Figure 4.10. Please note that in the calculation of moment transfer functions in Figure 4.11 a viscous damping level of $\zeta = 0\%$ is used. This is an unrealistic assumptions because there will always be some viscous damping in water. Therefore the moment transfer functions are also calculated with a very small amount of viscous damping.

In Figure 4.12 the moment transfer function calculated for the same three different frequency steps but with an added viscous damping level of $\zeta = 0.05\%$ is shown.

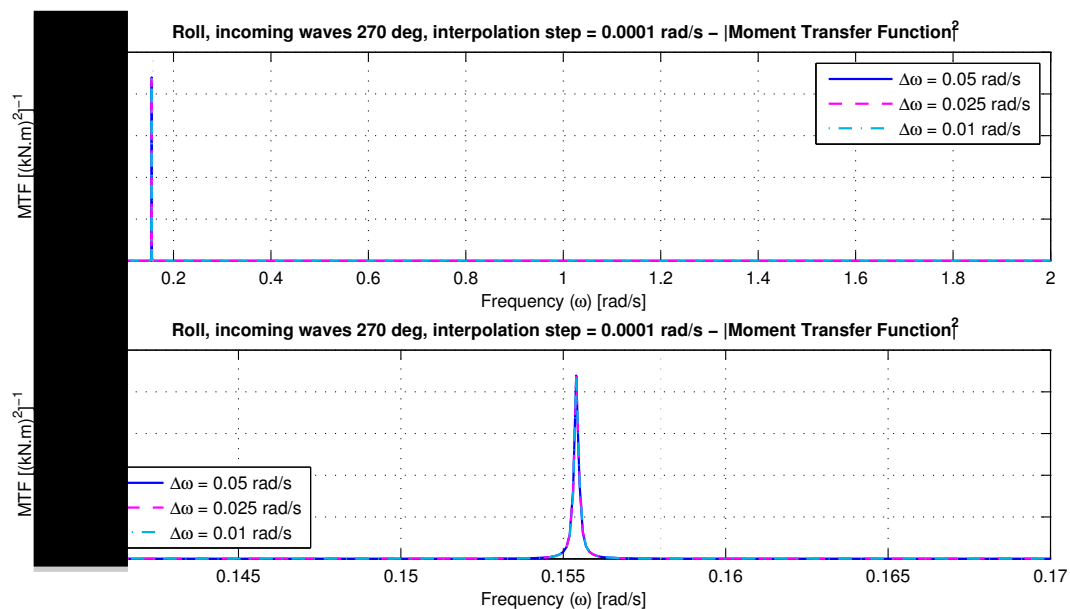


Figure 4.12: Moment transfer function for roll calculated with frequency steps of $\Delta\omega = 0.05$ rad/s, $\Delta\omega = 0.025$ rad/s and $\Delta\omega = 0.01$ rad/s. A viscous damping level of 0.05% of the critical damping is added in the calculation. **Top:** Total frequency range is plotted. **Bottom:** Frequency range around the natural frequency is shown.

In Table 4.8 the values of the moment transfer function maxima at the natural frequency from Figure 4.11 and 4.12 are shown.

Frequency step $\Delta\omega$ [rad/s]	MTF at nat. frequency $MTF(\omega_{nat})$ [(kNm) ²] ⁻¹	Deviation with $\Delta\omega = 0.01$ rad/s, no added viscous damping [%]	Deviation with $\Delta\omega = 0.01$ rad/s, $\xi = 0.05$ % added viscous damping [%]
0.05	██████████	365.8	6.4
0.025	██████████	53.2	2.3
0.01	██████████	-	-

Table 4.8: Moment transfer function values at the natural frequency calculated with a frequency step of 0.05 rad/s, 0.025 rad/s and 0.01 rad/s. The deviation in percentage in the moment transfer function without added viscous damping are calculated with the values in Figure 4.11.

It can be concluded that the calculation of the moment transfer function is very sensitive for damping. Furthermore it can be concluded that the damping is dominated by the viscous damping, this is because the potential damping is a very small fraction (0.001 %) of the critical damping. In other words it is necessary to add viscous damping in the calculation of the moment transfer function for accurate results.

4.3.4. SECOND ORDER ROLL RESPONSE SPECTRUM

In Figure 4.13 the calculated roll response spectrum is plotted without added viscous damping. In Figure 4.14 the calculated roll response spectrum is shown with a viscous damping level level of $\xi = 0.05$ %.

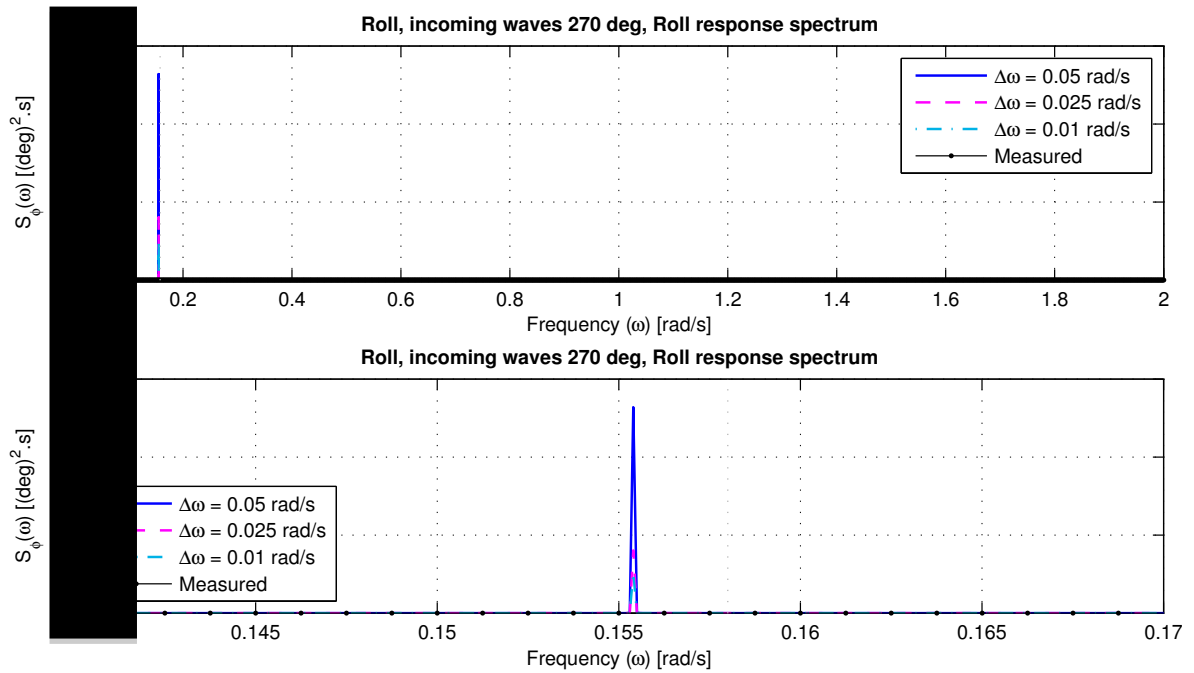


Figure 4.13: The calculated roll response spectra with different frequency steps and the measured roll response spectrum are shown. No viscous damping is added in this calculation. **Top:** Total frequency range is plotted. **Bottom:** Frequency range around the natural frequency is shown.

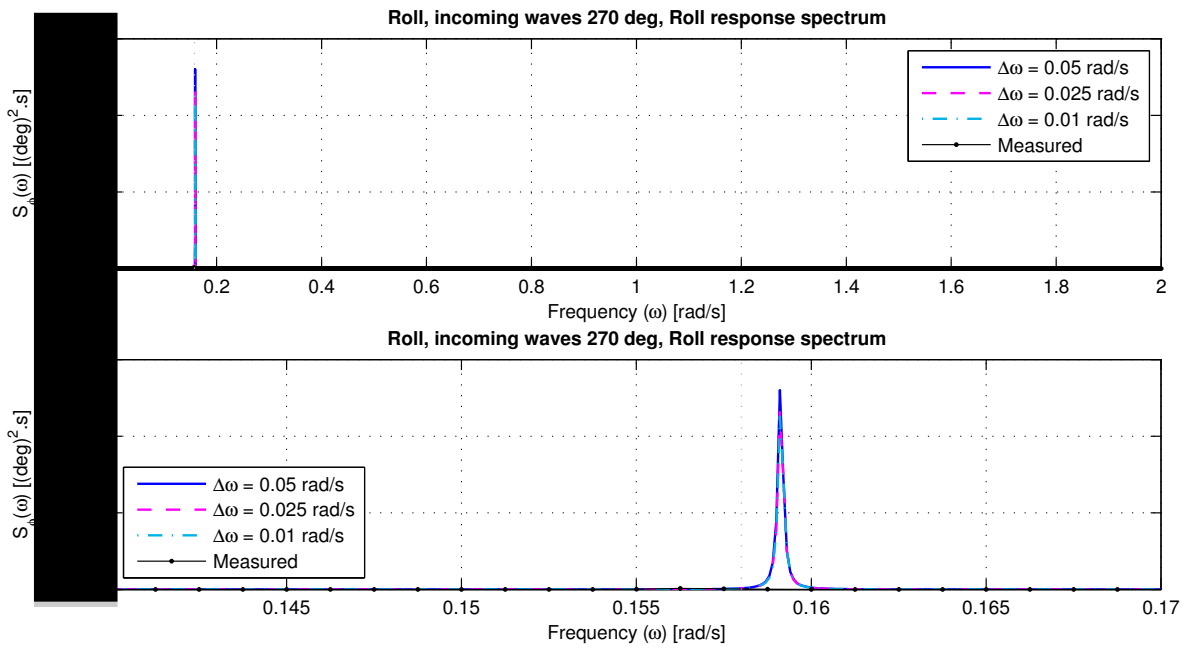


Figure 4.14: The calculated roll response spectra with different frequency steps and the measured roll response spectrum are shown. An viscous damping level of $\xi = 0.05\%$ is added in this calculation. **Top:** Total frequency range is plotted. **Bottom:** Frequency range around the natural frequency is shown.

The zero order moments of the roll response spectra of Figure 4.13 and 4.14 are shown in Table 4.9.

[Table content is obscured by a black box]

Table 4.9: Zero order moments of roll motion response spectra calculated with and without damping.

Summarizing the observations above, the frequency refinement study results in the following conclusions. The second order roll moment spectrum is converted for a quadratic transfer function calculated with a frequency step of 0.025 rad/s. The potential damping is a very small fraction of the critical damping and consequently in order to calculate the transfer function it is necessary to add (some) viscous damping. The calculated roll response spectrum must be calculated with added viscous damping. The zero order moment of the roll motion response spectrum is converted for a frequency step of 0.025 rad/s.

The above conclusions of the frequency refinement study contains also statements about the damping level. In order to prevent unclarities the influence of the damping level is extensively discussed in the next section. The main conclusion on the frequency study is that the zero order moment of the roll motion response spectrum is converted for a frequency step of 0.025 rad/s.

4.4. VISCOUS DAMPING STUDY

4.4.1. QUADRATIC TRANSFER FUNCTION

When theoretically calculating the roll response spectrum an additional viscous damping level can be incorporated twice in the calculation. In the diffraction calculation, a viscous damping level can be added, and in the calculation of the moment transfer function. Is it necessary to incorporate the viscous damping both times? In order to answer this question the influence of different viscous damping levels on the drift moment spectrum and the moment transfer function are calculated.

First the diagonal of the natural frequency of the amplitude quadratic transfer function, calculated with three added viscous damping levels, is presented in Figure 4.15. The equivalent damping level is calculated with harmonic linearization as described in section 4.1.

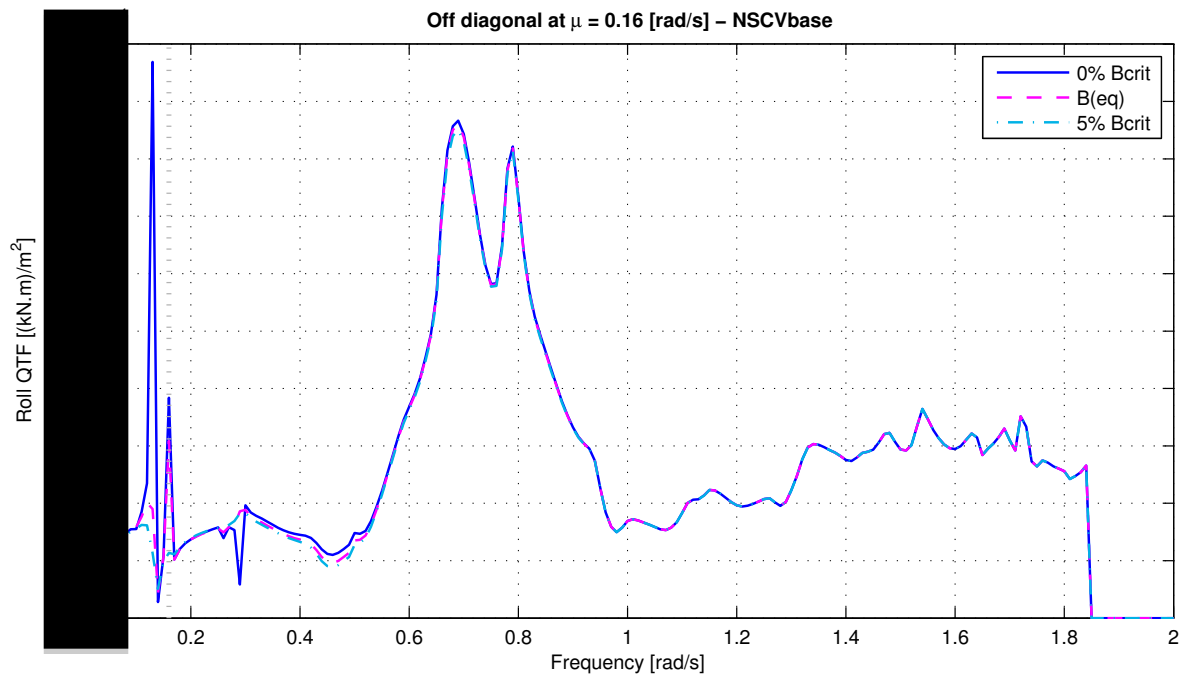


Figure 4.15: Quadratic transfer function. NSCVbase model and $\Delta\omega = 0.01$ rad/s is used for calculations with WAMIT. The diagonal of the difference frequency equal to the natural frequency $\mu = 0.16$ rad/s is plotted.

Figure 4.15 shows that calculating of the quadratic transfer function with several viscous damping levels results in differences at sharp local extremes at $\omega = 0.13$ rad/s, $\omega = 0.16$ rad/s and $\omega = 0.29$ rad/s. The peak at $\omega = 0.16$ rad/s is related to the natural roll frequency. The damping level of $\xi = 0\%$ ($\xi = b/b_{crit}$) overestimates the transfer function at this point, while a damping level of $\xi = 5\%$ totally suppresses the peak at 0.16 rad/s. The difficulty is choosing a damping level (equivalent damping) which is somewhere in between these two values. The research on the estimation of a 'realistic' equivalent damping level using linearization techniques is extensively discussed in section 4.1.

Similar behaviour as with the peak at 0.16 rad/s occurs at the peak at $\omega = 0.13$ rad/s and the dip at $\omega = 0.29$ rad/s. The calculation with 0% added viscous damping overestimates the maxima (and minima) and the calculation with $\xi = 5\%$ added damping suppresses the local extremes. The origin of the local extremes at these frequencies is unclear. The extremes could be related to the diameter of the discretized free water surface used in the calculation of the quadratic transfer function with WAMIT (see Figure 3.3). The diameter of the discretized free surface is 300 m. Consider a standing wave with one antinode and two nodes at both ends of the center line of the discretized water surface. Using the dispersion relation for deep water this standing wave with $1/2 \lambda = 300$ m (λ is the wavelength) correspond to a wave frequency of approximately 0.3 rad/s. This could cause the peak in the quadratic transfer function at $\omega \approx 0.3$ rad/s.

While the origin of the peak at $\omega = 0.29$ rad/s is unclear, it is clear that the peaks at $\omega = 0.13$ rad/s and $\omega = 0.29$ rad/s are directly correlated as shown in Figure B.2 in Appendix B.1.1 on 95. In this amplitude quadratic

transfer function it is clear that the peak at $\omega_1 = 0.29$ rad/s causes the peak in the diagonal at $\omega = 0.13$ rad/s. The diagonal from Figure 4.15 is plotted as the black line in Figure B.2. The minimum of the peak at $\omega = 0.29$ rad/s in the diagonal is caused by the peak at $\omega_2 = 0.29$ rad/s.

The findings in Figure 4.15 show that it is undesirable to add no damping at all because this leads to irregularities in the quadratic transfer function. It is advised to use at least a small amount of damping in the calculations. The estimation of a 'realistic' damping level, which is most desirable to incorporate in the calculation, is described in section 4.1.

4.4.2. SECOND ORDER MOMENT SPECTRUM

In Figure 4.16 the calculated drift moment spectrum with a sea state of $H_s = 3$ m, $T_p = 7$ s for different added viscous damping levels is plotted. In the Figure the natural frequency is plotted at 0.16 rad/s. The black dotted line is the shape of the drift force spectrum for roll for a difference frequency domain of $0 \leq \mu \leq 2$ rad/s. In order to reduce calculation time of the quadratic transfer function the run with a damping level of $\xi = 0\%$ ($\xi = b/b_{crit}$) has a difference frequency range of $0 \leq \mu \leq 0.3$ rad/s. The two other WAMIT runs with damping levels of b_{eq} and $\xi = 5\%$ have a difference frequency range of $0.13 \leq \mu \leq 0.18$ rad/s. The quadratic transfer functions used for the calculation of the drift moment spectra are presented in Figure B.2, B.3 and B.4 in Appendix B.1.1.

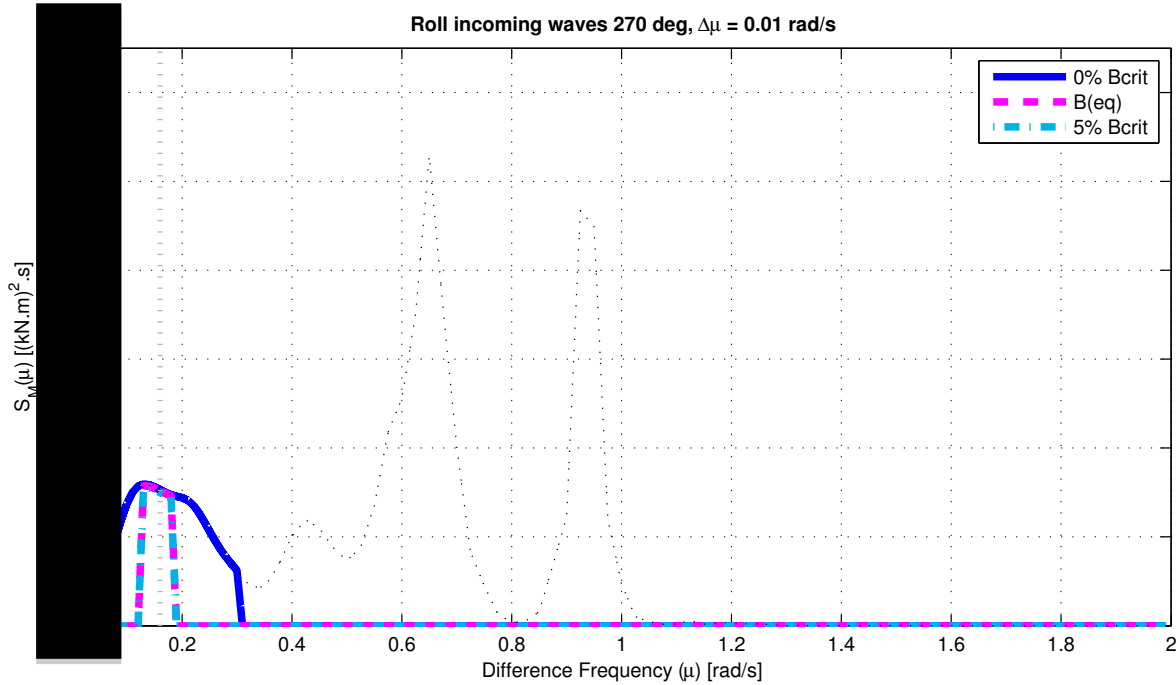


Figure 4.16: Wave drift moment spectrum for roll. The influence of adding different damping levels in WAMIT is shown in this figure. Black dotted line indicates shape of 'complete' drift force spectrum. Grey dotted line indicates the natural frequency at 0.16 rad/s. The WAMIT runs have been done with a frequency step of $\Delta\omega = 0.01$ rad/s.

The difference in value of the wave drift force spectrum at the natural frequency is compared with the calculated force spectrum with $\xi = 0\%$ added damping. The value of the drift force spectrum of the b_{eq} run has a difference of -0.8% and the $\xi = 5\%$ run differs with -2% compared to the $\xi = 0\%$ added damping run (See Table 4.10). It can be concluded that the different damping levels do not have a significant influence on the second order moment spectrum. In order to define the second order moment spectrum an integration of the multiplication of the quadratic transfer function and the sea state needs to be performed (See Equation 1.15). For this reason the extreme values related to the damping levels in Figure 4.15 do not have a significant influence on the second order roll moment spectrum.

Added viscous damping level in WAMIT	$S_M(\mu_{nat})$ [(kNm) ² s]	Deviation with 0% B_{crit} [%]
0% B_{crit}	$1.53 \cdot 10^9$	-
B_{eq}	$1.52 \cdot 10^9$	-0.8
5% B_{crit}	$1.50 \cdot 10^9$	-1.9

Table 4.10: Difference in second order moment spectrum at the natural frequency calculated for three added viscous damping levels with WAMIT.

4.4.3. MOMENT TRANSFER FUNCTION

In Figure 4.17 the added mass and potential damping are shown for the different viscous damping levels. It is shown that the added viscous damping does not influence the added mass and damping as is expected from theory.

ADDED MASS AND DAMPING

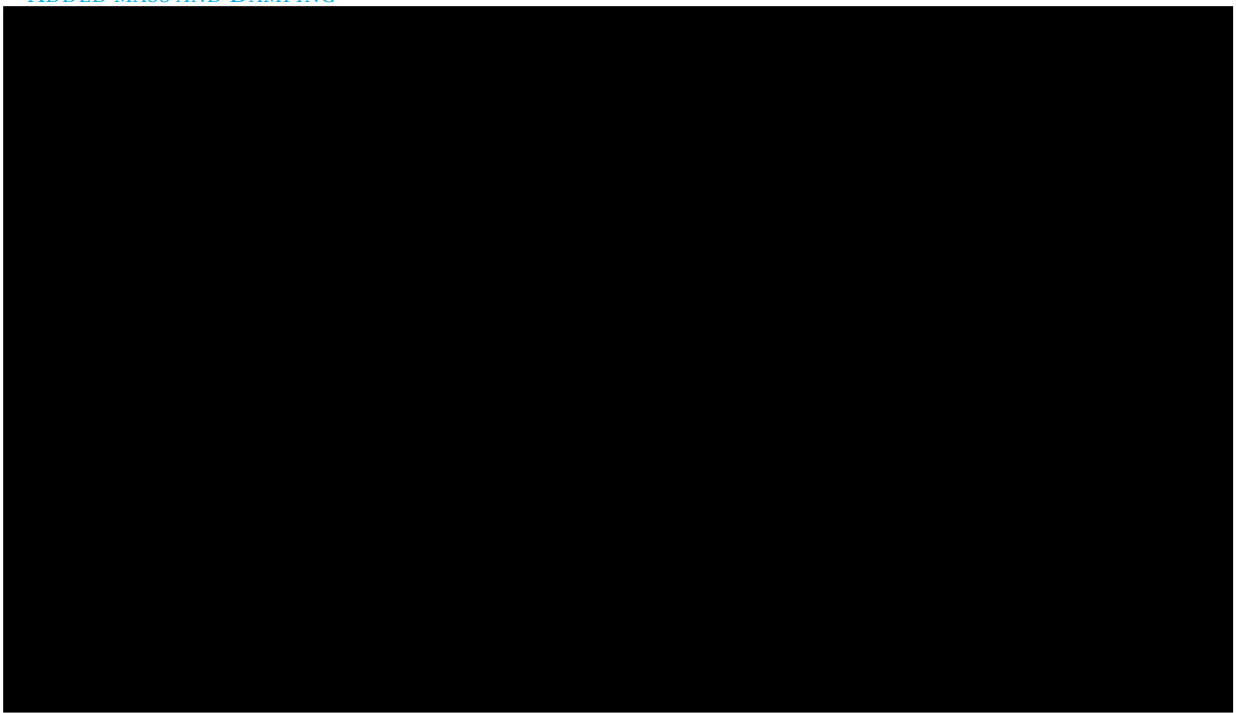


Figure 4.17: Added mass and damping for roll calculating with different damping levels.

MOMENT TRANSFER FUNCTION

The Moment Transfer Function for roll is shown in Figure 4.18 calculated with three added viscous damping levels.

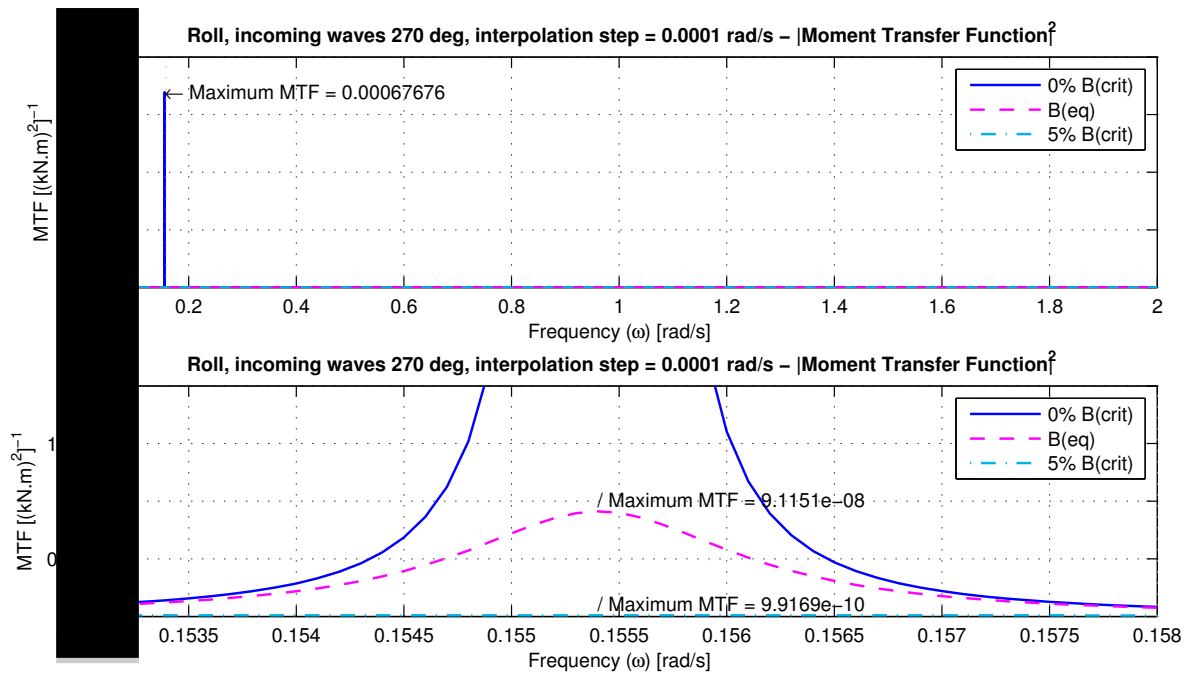


Figure 4.18: The absolute squared moment transfer function for roll. Three moment transfer functions with different damping levels are plotted. The maximum moment transfer functions values are shown for the damping levels. **Bottom:** Frequency range around the natural frequency is shown.

Figure 4.18 shows that the maxima of the moment transfer function at the natural frequency highly depend on the amount of added damping as predicted by theory. More specific it can be concluded that the maxima of the moment transfer function are highly dependent on the added viscous damping, because the potential damping at the natural frequency is only $\xi = 0.001\%$. In other words the viscous damping is dominant for the calculation of the moment transfer function. In Table 4.11 the maximum values of the squared moment transfer function are presented.

Damping Level	Maximum MTF
0% B(crit)	0.00067676
B(eq)	9.1151e-08
5% B(crit)	9.9169e-10

Table 4.11: Difference in absolute squared moment transfer function at the natural frequency calculated for three added viscous damping levels.

Firstly the deviation in percentage in Table 4.11 shows that the calculation of the moment transfer function is very sensitive for the amount of added viscous damping. Secondly the high deviation in percentage of the calculation with $\xi = 0\%$ comparing with the other calculations shows that it is undesirable to calculate the moment transfer function without added viscous damping. The function will overestimate the amount of 'transferred moment' when no viscous damping is added. Additionally the calculation of the moment transfer function for a vessel without any viscous damping is very unrealistic and therefore undesirable.

4.4.4. SECOND ORDER ROLL RESPONSE SPECTRUM

The roll response spectrum for the three different damping levels is presented in Figure 4.19. In Table 4.12 the zero order moment of the roll motion response spectrum and the extreme value at the natural frequency are shown.

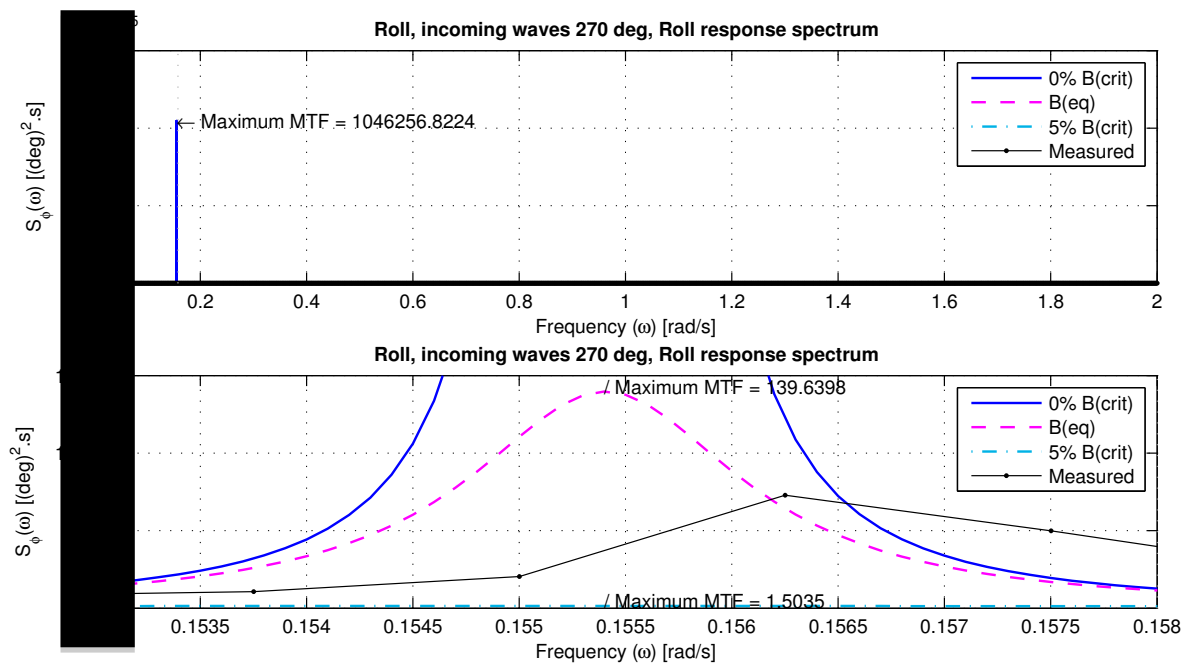


Figure 4.19: The calculated roll response spectra with different damping levels and the measured roll response spectrum are shown. **Bottom:** Frequency range around the natural frequency is shown.

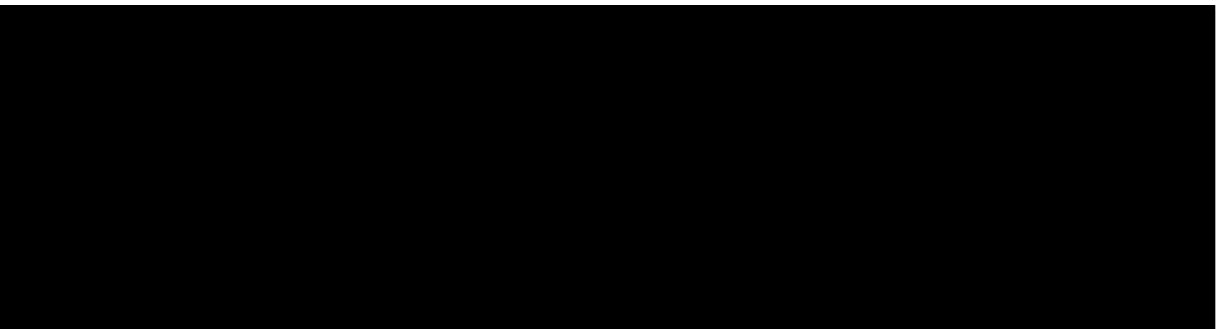


Table 4.12: Differences in roll response spectrum at the natural frequency calculated for three added viscous damping levels.

Table 4.12 shows that the roll motion response is highly dependent of added damping level in the moment transfer function. The amount of added viscous damping is dominant in the calculation of the roll motion response spectrum. In Figure 4.19 the measured roll motion response spectrum is plotted. It can be concluded that the roll motions calculated with only potential damping, without any added viscous damping term, highly overestimates the roll motion response of the Sleipnir. The phenomenon of overestimation of the roll motions is attributable to the absence of viscous damping in the calculation, which is also found in other research, i.e. [26]. Furthermore it can be noticed that none of the roll response spectra is in agreement with the measured roll response spectrum. In the next section the answer on the following question is given. For which damping level is the theoretically calculated roll response spectrum in best agreement with the measured roll response spectrum?

4.5. TOTAL ROLL RESPONSE SPECTRUM

4.5.1. INFLUENCE OF VISCOUS DAMPING ON THE ROLL RESPONSE SPECTRUM

In this section the influence of the added viscous damping on the total roll motion response spectrum is presented. In Figure 4.20, 4.21 and 4.22 the zero order moment is plotted versus the added viscous damping. Additionally the variance (or root mean square (RMS)), which is directly related to the zero order moment, is plotted versus the added viscous damping. Each of the figures is related to a specific sea state. The model tests have been performed with three sea states. The total roll response spectrum is calculated for these specific three sea states. The total roll motion response spectrum is calculated as the sum of the first and second order roll motion response spectrum. In Appendix B.1.5 the tables, on which the figures in this section are based, are presented from page 112.

In Figure 4.20, 4.21 and 4.22 the roll response spectrum calculated with a JONSWAP wave spectrum and with the calibrated wave spectrum are shown. The wave is calibrated without the model in the basin at wave probe WAVECL as shown in Figure 2.3. The calibrated is included in the graphs because of the following. The calibrated wave spectrum contains in contrast to the JONSWAP spectrum (some) wave energy at low frequencies ($0 < \omega < 0.5$ rad/s) as shown in Figure 3.15. This first order wave energy in the low frequency range results in a low frequency roll response at the natural frequency (Figure 3.15)¹. In Figure 4.20, 4.21 and 4.22 the influence of the added viscous damping on the total roll response spectrum, calculated with both wave spectra, is plotted. Furthermore the zero order moment calculated from the measured roll motion time trace during model tests is plotted in each graph. The estimated equivalent roll damping using the harmonic, stochastic and bandwidth linearization technique is indicated with the dotted lines.

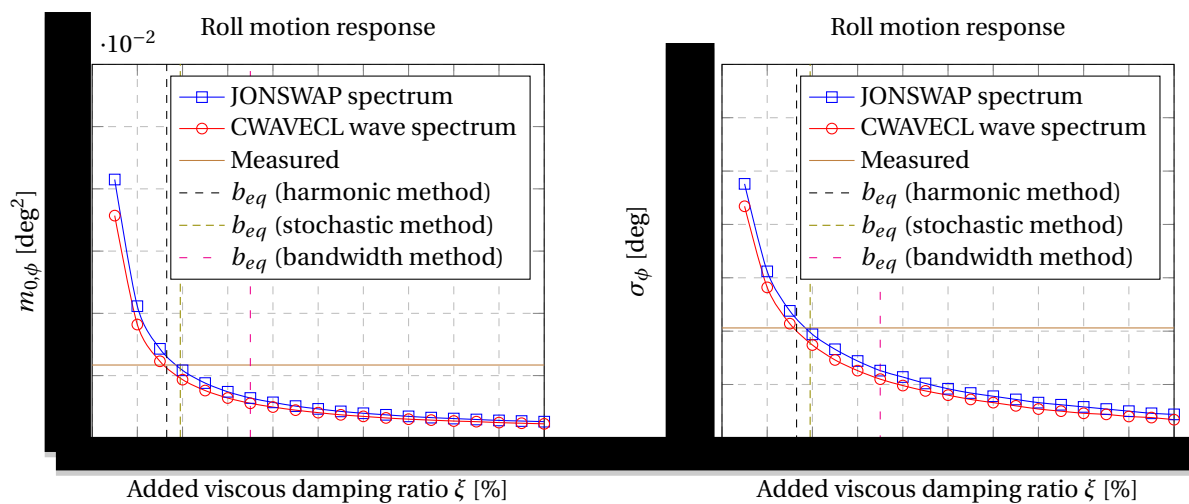


Figure 4.20: Sea state $H_s = 1.5\text{m}$, $T_p = 7\text{s}$. The influence of the added viscous damping in terms of the critical damping on the zero order moment and the variance of the roll motion response spectrum. The roll response spectrum is calculated making use of the theoretical JONSWAP wave spectrum and the calibrated wave spectrum. The zero order moment and variance of the measured roll response during model test is indicated. The calculated equivalent damping as well.

¹The roll response spectrum is not only calculated for the JONSWAP and calibrated wave spectrum but for all measured wave spectra during model tests. The results can be found in Appendix B.1.5 in Figures B.14, B.15 and B.16.

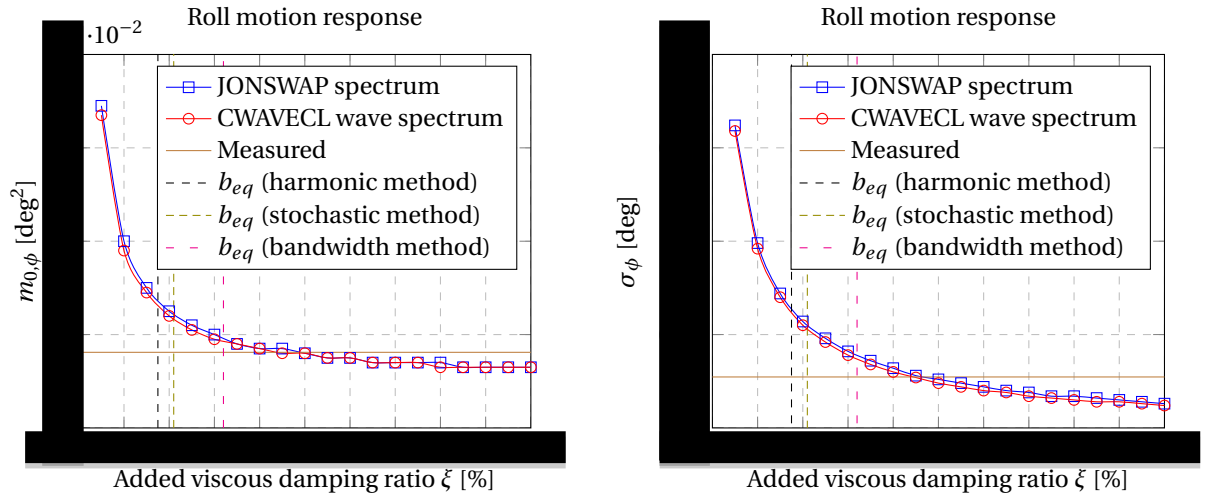


Figure 4.21: Sea state $H_s = 1.5\text{m}$, $T_p = 12\text{s}$. The influence of the added viscous damping in terms of the critical damping on the zero order moment and the variance of the roll motion response spectrum. The roll response spectrum is calculated making use of the theoretical JONSWAP wave spectrum and the calibrated wave spectrum. The zero order moment and variance of the measured roll response during model test is indicated. The calculated equivalent damping as well.

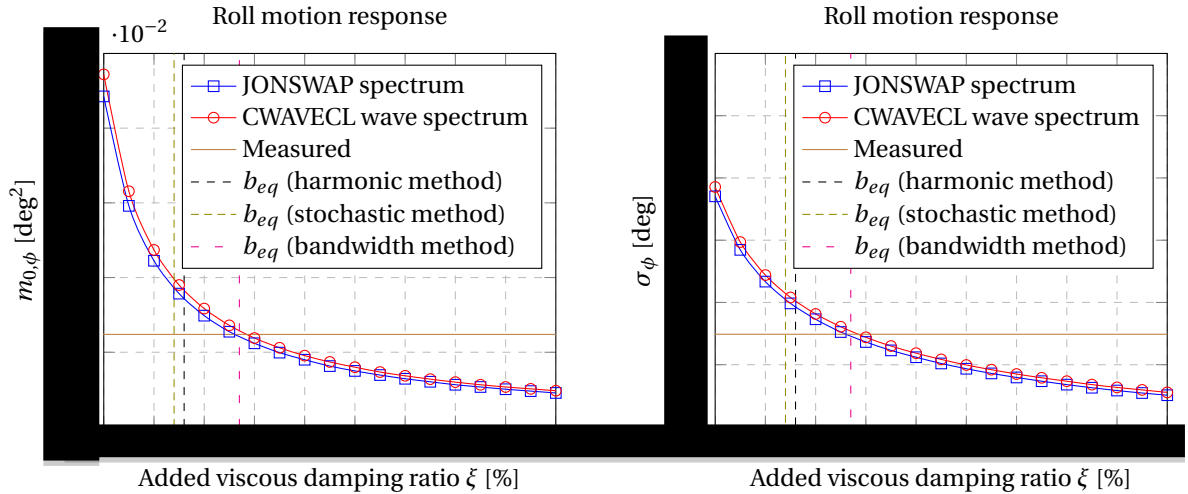


Figure 4.22: Sea state $H_s = 3\text{m}$, $T_p = 7\text{s}$. The influence of the added viscous damping in terms of the critical damping on the zero order moment and the variance of the roll motion response spectrum. The roll response spectrum is calculated making use of the theoretical JONSWAP wave spectrum and the calibrated wave spectrum. The zero order moment and variance of the measured roll response during model test is indicated. The calculated equivalent damping as well.

4.5.2. DISCUSSION

Firstly, it can be noted that in Figure 4.20, 4.21 and 4.22 the zero order moment of the roll motion response spectra calculated with the JONSWAP wave spectrum and the calibrated wave spectrum are almost similar. The influence of the viscous damping on the zero order moment of the roll motion response shows an identical trend for both spectra.

Secondly, it can be noticed that in Figure 4.20, 4.21 and 4.22 the zero order moment converges to a certain value which is not equal to zero. The lines converge to the zero order moment of the first order response spectrum. This is because the added viscous damping in the moment transfer function suppresses eventually only the roll response at the natural frequency. So the second order roll response is suppressed when adding a substantial amount of damping but the first order roll response is not influenced by the damping. The damping in the moment transfer function does not influence the first order response because the response is located in a higher frequency range than the natural frequency.

As described in the second paragraph of this chapter Figure 3.15 shows how the first order roll response spectrum is calculated from two wave spectra. The first order wave energy in the low frequency range results in a low frequency roll response at the natural frequency as shown in this figure. In Figure 4.20, 4.21 and 4.22 only the zero order moment of the total roll response spectrum is plotted, however in Table B.8 up to B.25 in Appendix B.1.5 also the zero order moments of the first and second order response spectra are presented separately. Using these tables it can be shown that the zero order moment of the roll response, calculated with the calibrated wave spectrum, consist of 99.7% (average value of results from the three sea states) zero order moment originating from the second order roll response at the natural frequency. So it can be concluded that the calibrated wave spectrum has a influence on the roll response at the natural frequency. However the roll response at the natural frequency is dominated by the second order forces.

Furthermore in an ideal world the three lines, considering only the JONSWAP spectrum, measured m_0 line and one equivalent damping line, would intersect in a point on the blue curve. This would mean that the roll motion response spectrum calculated with the estimated equivalent damping would be in exact agreement with the model tests in terms of the zero order moment of the roll motion response spectrum. Considering Figure 4.20, 4.21 and 4.22 it can be seen that this is only (approximately) the case in Figure 4.20. In Figure 4.21 and 4.22 the brown line corresponding with the measured zero order moment intersects the blue line in a different point then as the black dotted line. In other words the estimation of the equivalent damping under predicts the damping for the sea states in Figure 4.21 and 4.21. The above findings suggest that for certain sea states the stochastic linearization is an accurate roll damping estimation method, while for other sea states the roll damping is under predicted. However in this study only three sea states are tested during model tests. In order to investigate for which sea states the stochastic linearization estimation method is applicable more Sleipnir model tests with different sea states are needed, as also stated in section 4.1.1.

In this research only three sea states have been investigated. However it is in the interest of Heerema to be able to calculate the roll motion response (which depends on the roll damping) of the Sleipnir for every possible sea state. The roll motion response estimation method, described in this study, is highly dependent on the amount of damping added in the calculation. On the other hand the estimation of the irregular (equivalent) roll damping depends on the variance of the roll velocity response spectrum. Consequently the calculation of the roll response motion will be an iterative process. This process is described in many references, e.g. [11] [24]. The calculation scheme suggested in these articles is shown in Figure 4.23. R. van 't Veer states that the iterative process converges rapidly. However the sharp reader must already have noted that the calculation scheme in Figure 4.23 is only applied to the calculation of the first order roll response motions. This study shows that the roll response motion of the Sleipnir is sensitive to second order moments due to the low roll natural frequency and furthermore a different method is used in order to calculate the roll response spectrum. Not the RAO but the moment transfer function has been used in order to calculate the first and second order roll response motions. Therefore the calculation scheme in Figure 4.23 needs to be expended to second order motions.

The calculation scheme in which the total response spectrum is calculated, including the second order responses, would have the form of the scheme presented in Figure 4.24. The calculation process would be a double iterative process because the calculation of the roll response is dependent on the (equivalent) stochastic linearized roll damping used in the calculation of the moment spectra and the moment transfer function. However this research (see section 4.4) shows that the damping added in the moment transfer function is dominant in order to calculate the roll motion response. As a consequence the calculation scheme would show a single iterative process, indicated with the thick red arrow in Figure 4.24. It must be noted that the scheme in Figure 4.24 has not been validated. The suggested calculation scheme should be investigated and tested for practical use. However the findings in Figure 4.20, 4.21 and 4.22 suggest that the zero order moments of the roll motion response converge to the value of the first order zero order moment by increasing the damping. The zero order moment obtained from the model test is located in a highly non-converged part of the curve in the Figures. This would mean that it is difficult to define test criteria for the calculation scheme in Figure 4.24. Further investigation for this calculation scheme in order to accurately estimate the roll response motion for every sea state is therefore recommended.

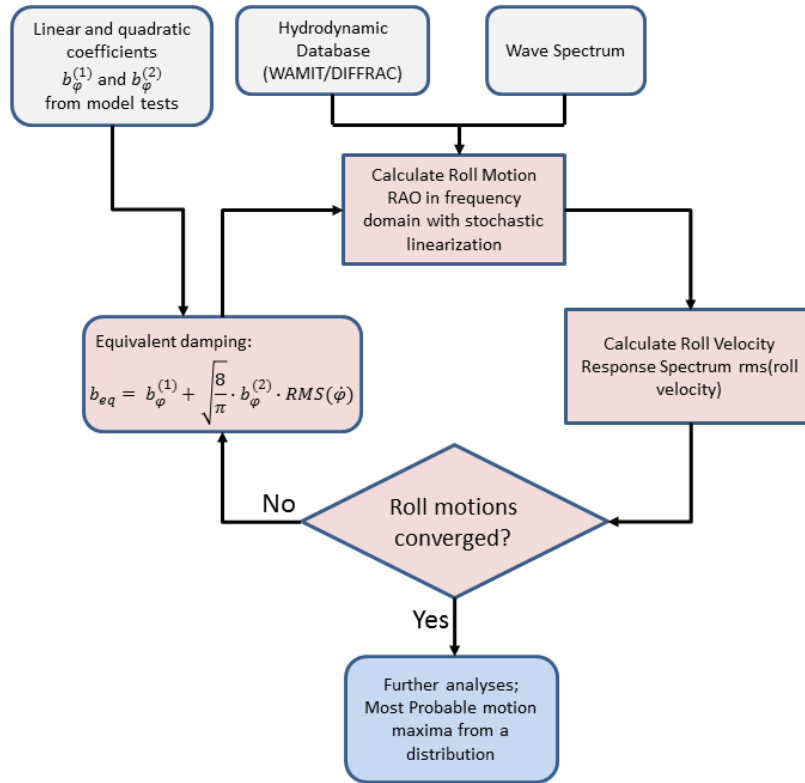


Figure 4.23: Global calculation scheme in order to calculate the roll response of a vessel suggested by [11].

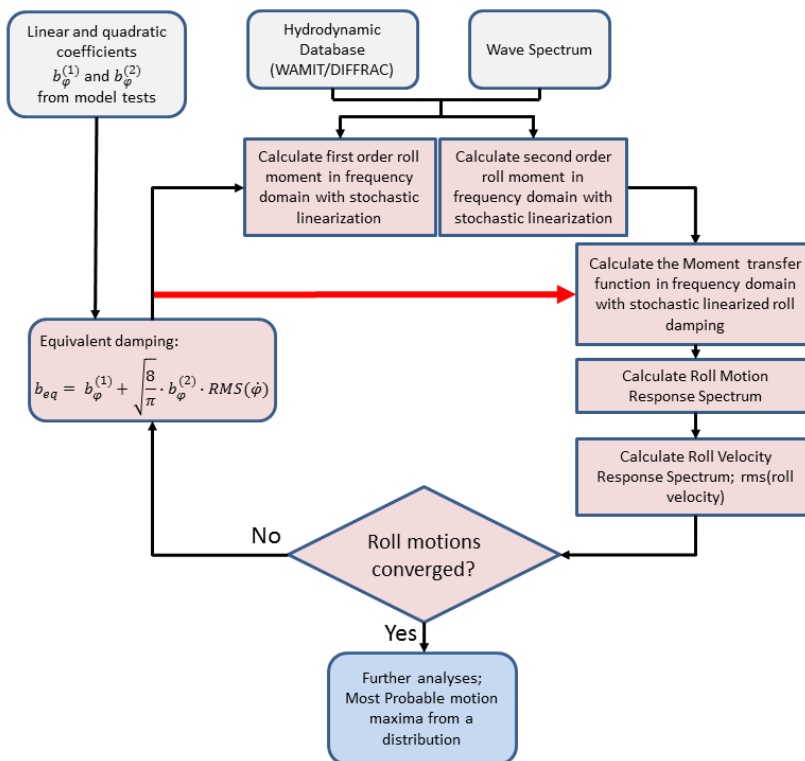


Figure 4.24: Global calculation scheme in order to calculate the total (including second order) roll response of a vessel.

4.6. COMPARISON OF WAMIT AND DIFFRAC CALCULATIONS

In this chapter the WAMIT and DIFFRAC results are compared. The WAMIT output is calculated around the hydrodynamic origin (CoH) but the DIFFRAC output is relative to the centre of gravity (CoG). The DIFFRAC output is transformed from the centre of gravity to the hydrodynamic origin as described in section B.1.2.

The presented results are obtained from calculations with the geometric model NSCVbase and frequency steps of $\Delta\omega = 0.01$ rad/s.

First the results of the first and second order calculations are presented. The results are discussed at the end of this chapter. The second order results are presented in figures in which the diagonal of the difference frequency (μ) is equal to the natural frequency of roll of the quadratic transfer function is plotted. As earlier discussed, this is the most important diagonal in order to calculate the roll response. First the total roll amplitude quadratic transfer function calculated with both software packages is compared in Figure 4.27. Then the amplitude quadratic transfer function of the first four contributions is compared in Figure 4.28. This quadratic transfer function is related to the quadratic terms of the second order moment and is calculated with first order quantities. Lastly the quadratic transfer function of the fifth contribution is compared in Figure 4.29. This quadratic transfer function is related to the moment contribution due to the second order potentials, related to the low frequent wave induced by wave groups. In Figure 4.30 and 4.31 the amplitude, in-phase and out-phase quadratic transfer function are presented for respectively the WAMIT and Diffrac calculations. The total, quadratic and the second order potential quadratic transfer function are indicated in each figure.

4.6.1. FIRST ORDER

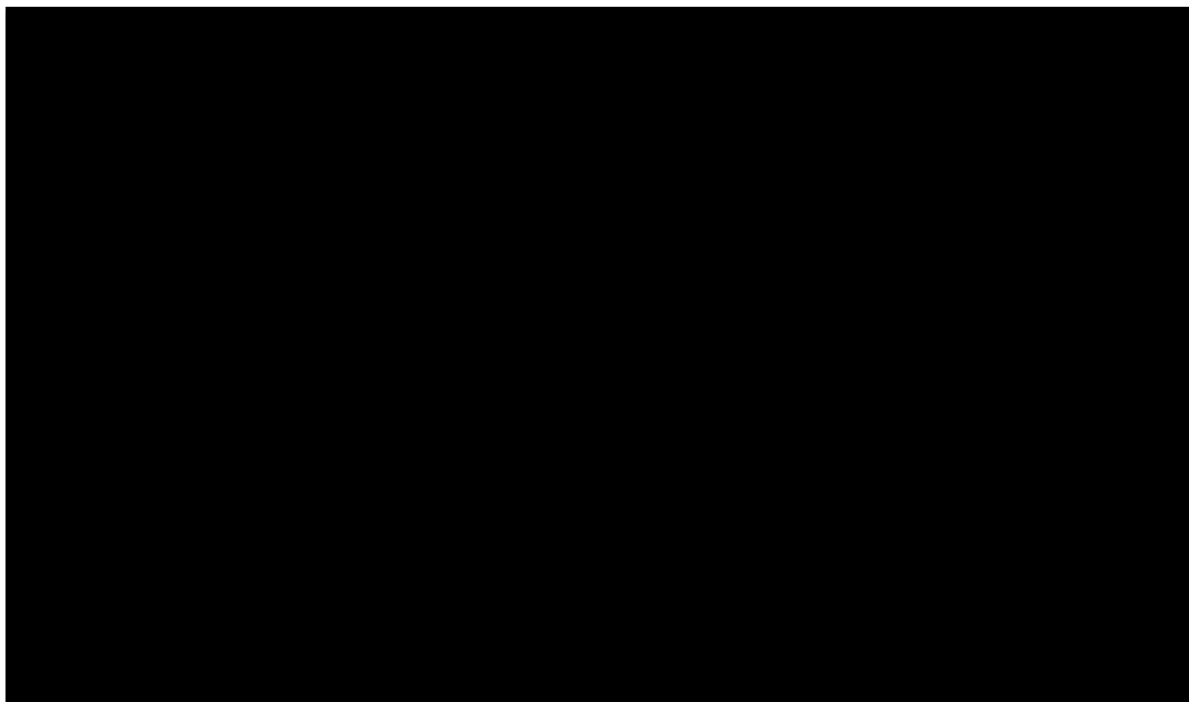


Figure 4.25: Added mass (A_{44}) and potential damping (B_{44}) for roll. The coefficients are compared in the hydrodynamic origin (CoH).

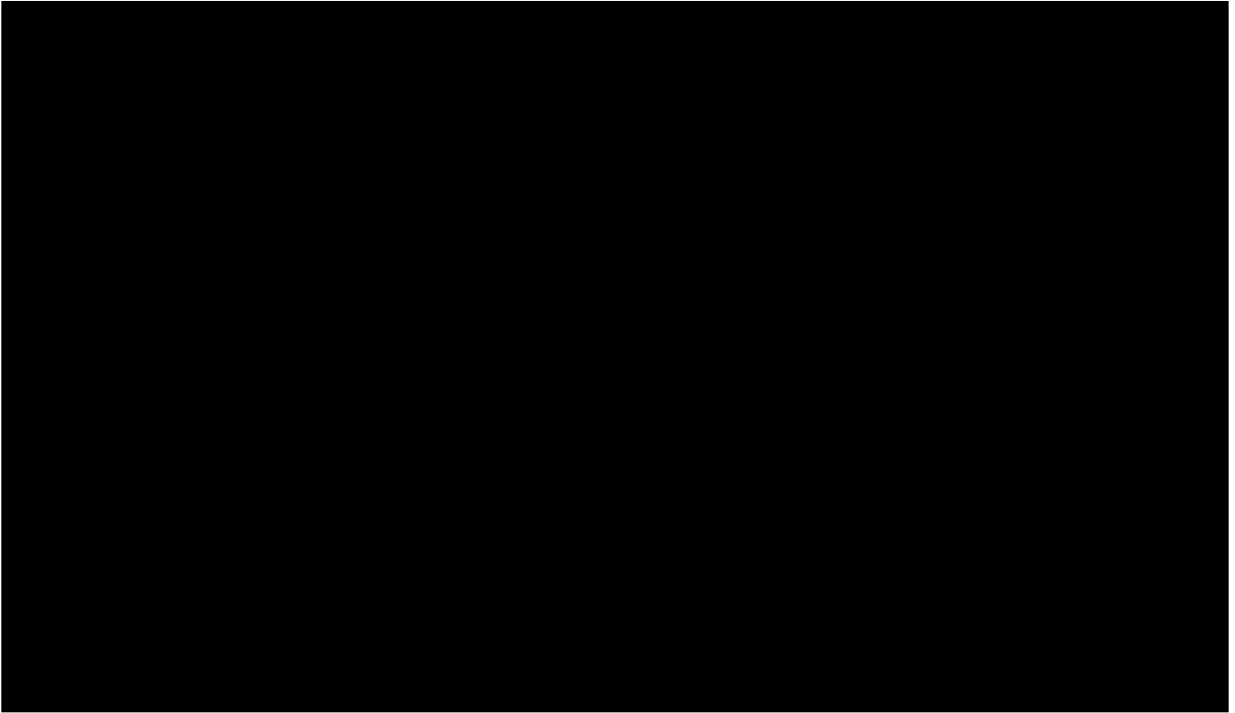


Figure 4.26: Roll moment (M_ϕ) for incoming waves of 270° and the corresponding phase ($\epsilon_{z_i, \phi}$) in hydrodynamic origin.

4.6.2. SECOND ORDER

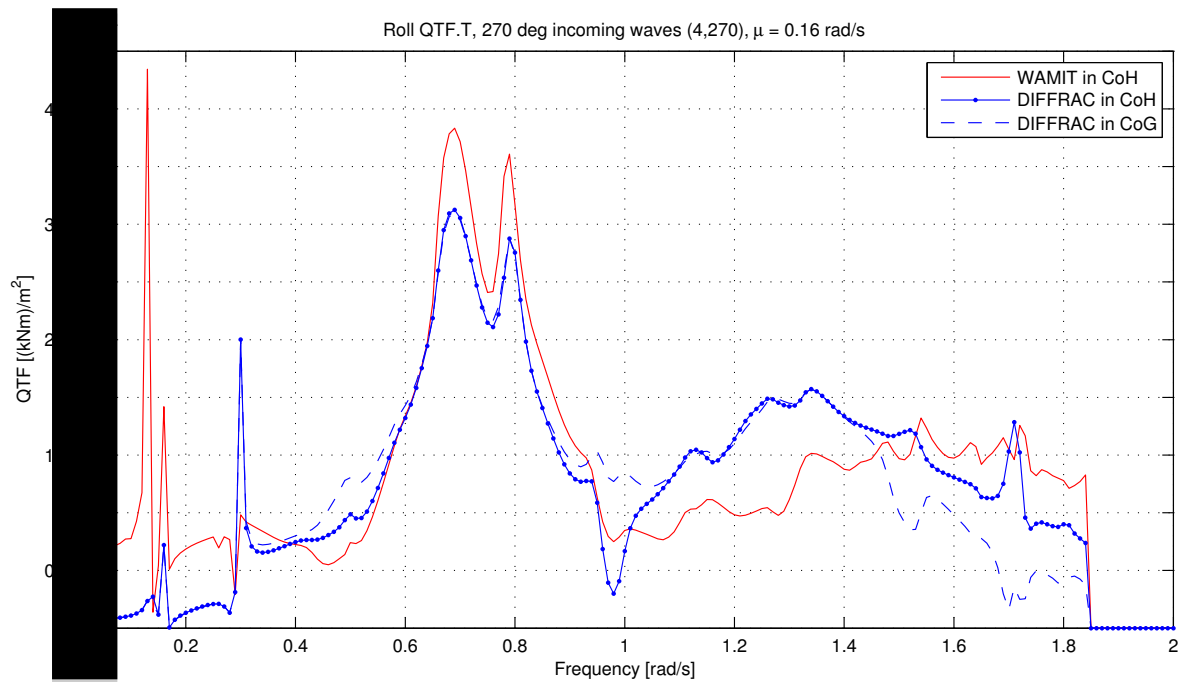


Figure 4.27: Amplitude (T) of the quadratic transfer function for roll with incoming waves of 270° in the hydrodynamic origin. The total QTF consisting of all five contributions is shown. Plotted is the diagonal with a difference frequency μ equal to the natural frequency of 0.16 rad/s .

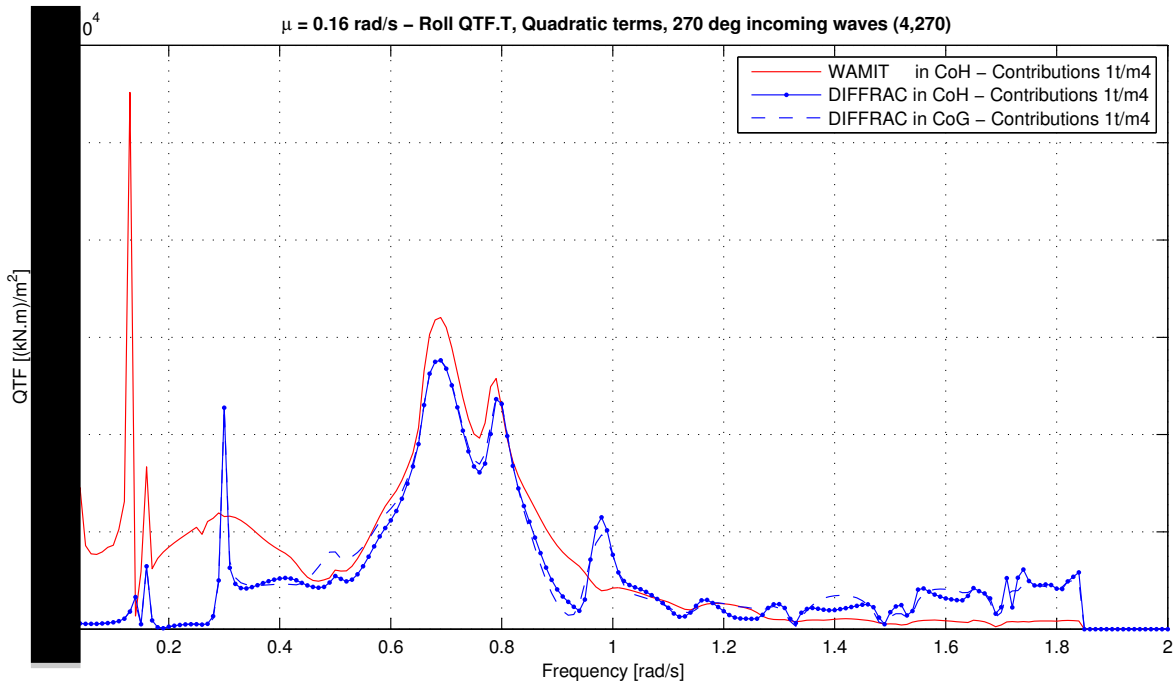


Figure 4.28: Amplitude (T) of the quadratic transfer function for roll with incoming waves of 270° . The quadratic terms (first four contributions) of the QTF are shown. Plotted is the diagonal with a difference frequency μ equal to the natural frequency of 0.16 rad/s .

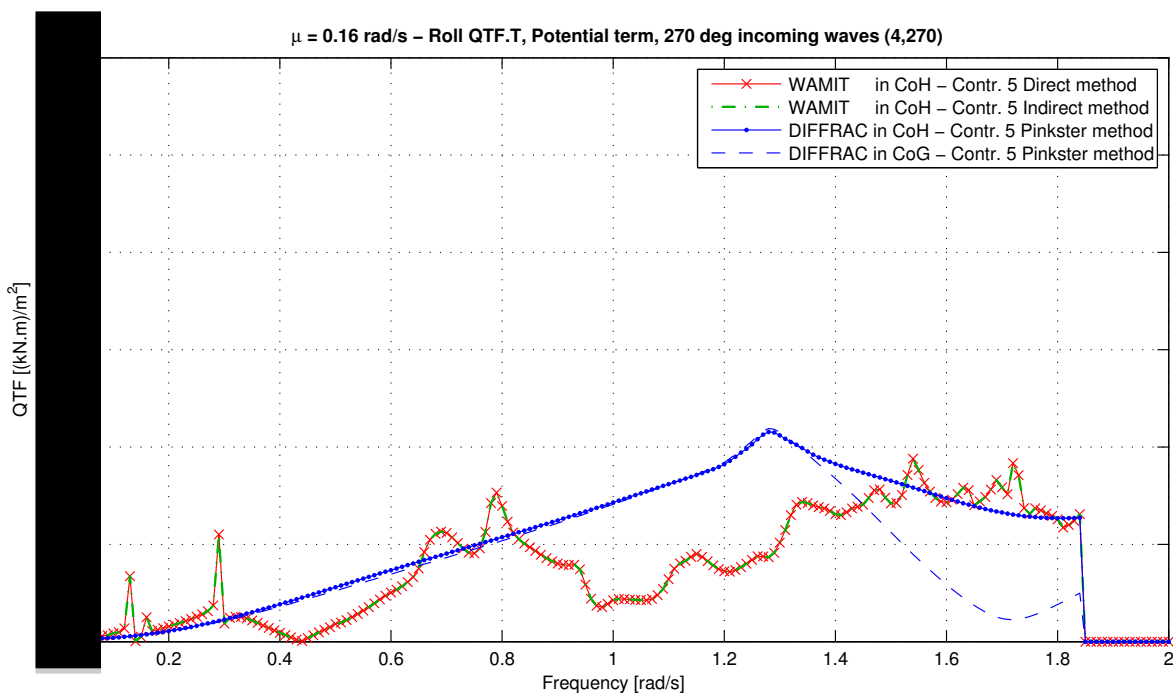


Figure 4.29: Amplitude (T) of the quadratic transfer function for roll with incoming waves of 270° . The potential term (fifth contribution) of the QTF is shown. Plotted is the diagonal with a difference frequency μ equal to the natural frequency of 0.16 rad/s .

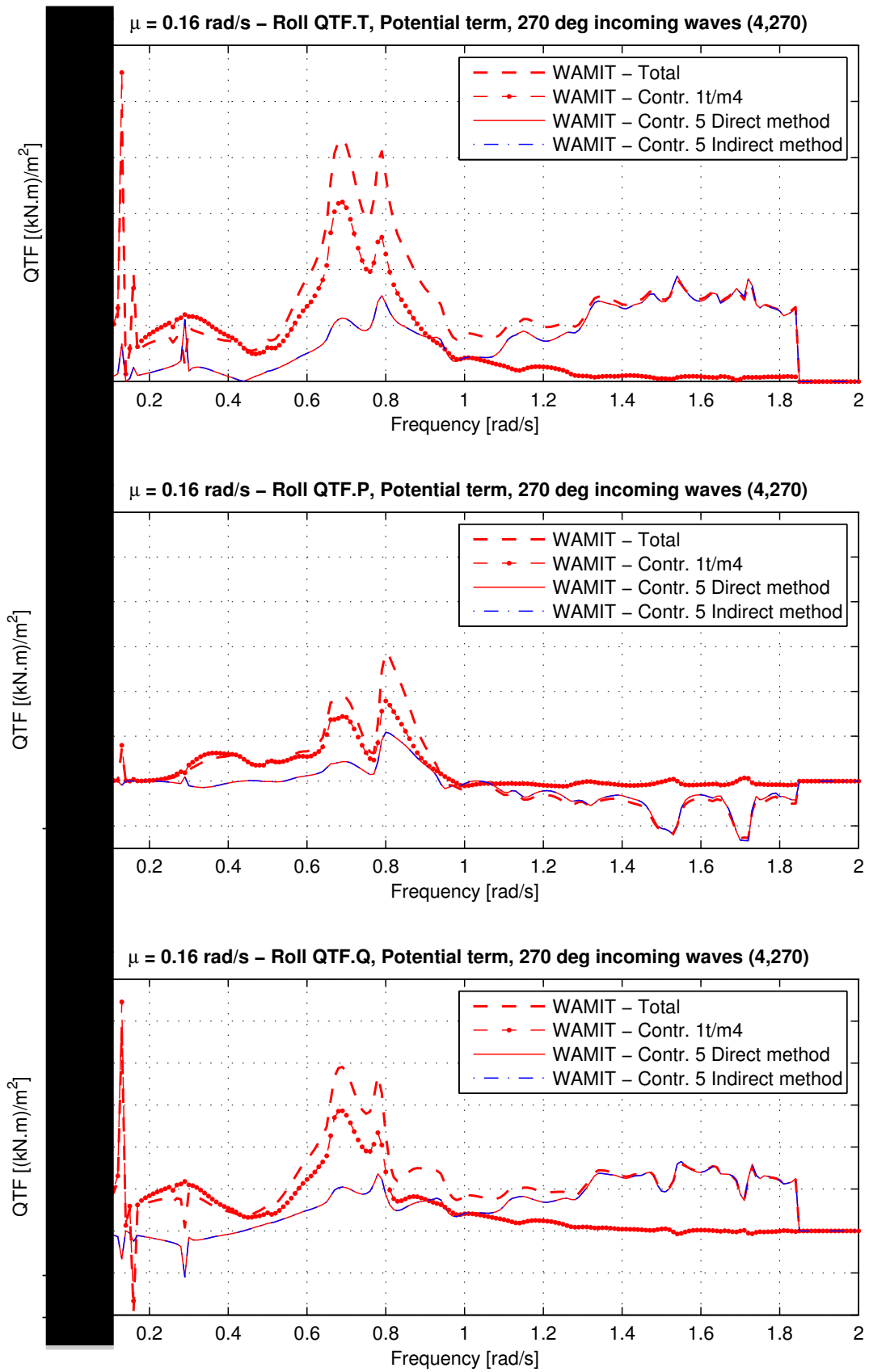


Figure 4.30: The total, quadratic terms and the potential term of the quadratic transfer function calculated by WAMIT for roll with incoming waves of 270° . From top to bottom the amplitude (T), the in-phase component (P) and the out-of-phase component (Q) of the quadratic transfer function are shown.

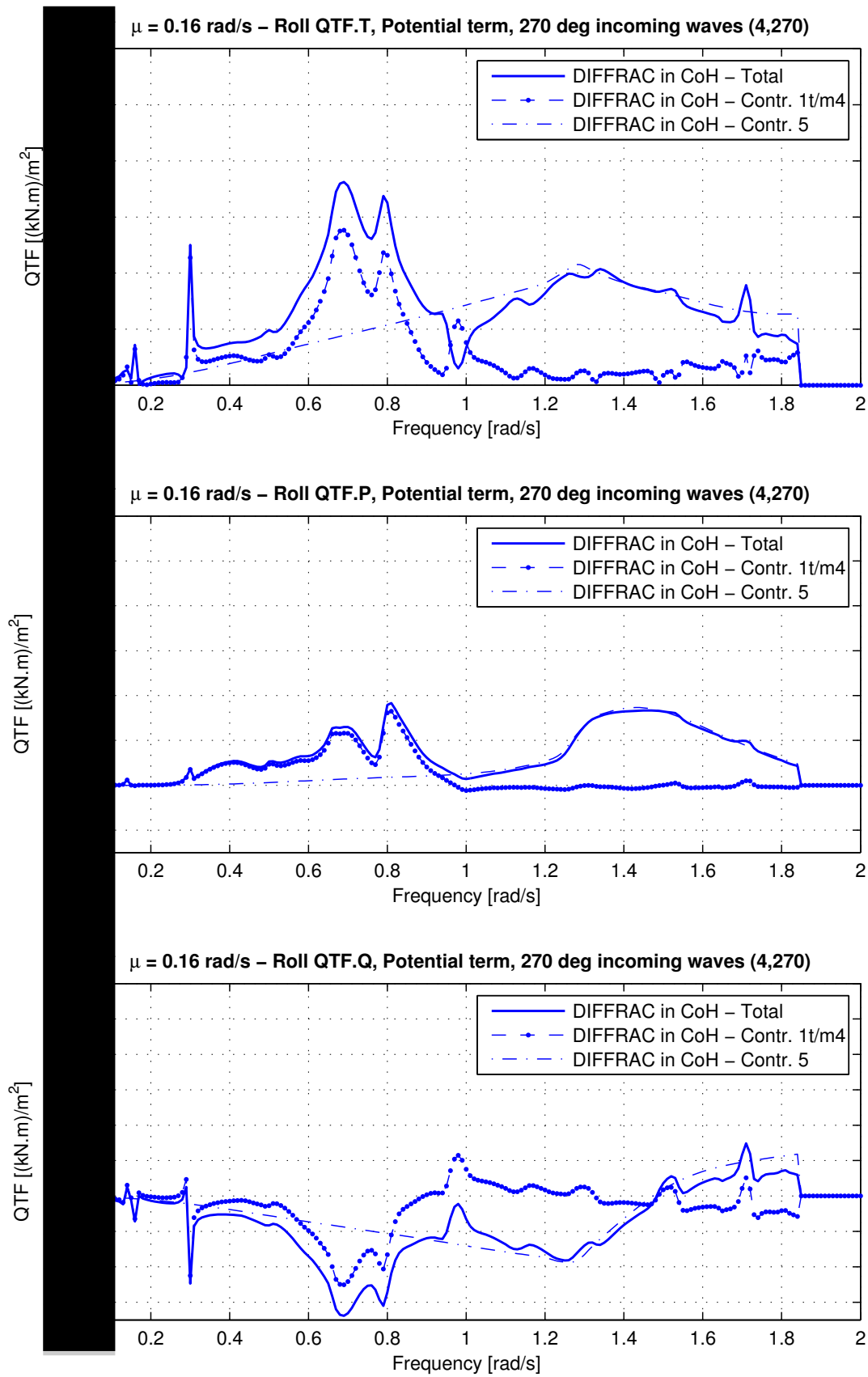


Figure 4.31: The total, quadratic terms and the potential term of the quadratic transfer function calculated by DIFFRAC for roll with incoming waves of 270° . From top to bottom the amplitude (T), the in-phase component (P) and the out-of-phase component (Q) of the quadratic transfer function are shown.

DISCUSSION

The first order forces, added mass and potential damping are expected to be equal, when calculated with an identical panel model with both software packages. Figure 4.25 shows that the added mass and potential damping do not totally match for the WAMIT and DIFFRAC calculation. The deviation could originate from the fact that DIFFRAC makes a PATRAN file from the defined discretized NSCVbase model. The PATRAN file differs slightly from the initial geometric hull shape because some quadrilateral panels are transformed in triangular panels. Consequently the added mass and potential damping will differ for calculations with a different panel model. Similar statements can be made for the first order exciting moment in Figure 4.26. This Figure shows that the phase related to the roll moment is, also after translation, not equal for the calculation with WAMIT and DIFFRAC. In the frequency range of the first moment 'peak', $0.3 \lesssim \omega \lesssim 0.82$ rad/s, the phase difference is approximately hundred-eighty degrees. The second first order moment peak, in $0.82 \lesssim \omega \lesssim 1.05$ rad/s, has equal a phase for the WAMIT and DIFFRAC calculations. In this research this phase difference has not been investigated. Based on the phase difference in the first order moment it can already be expected that the second order moment also will show differences in WAMIT and DIFFRAC calculations. This is due to the fact that the second order moment, but also the in- and out-of-phase components of the quadratic transfer function are related to the 'first order' phase of the motion. Therefore it would be interesting to investigate where the phase difference originates from and if the phase can be matched for both software packages.

In Figure 4.27 the total roll amplitude quadratic transfer function calculated with both software packages is compared. Before calculating the quadratic transfer function differences are expected because WAMIT uses the direct and indirect method to solve the second order potentials while DIFFRAC uses the Pinkster approximation. The different solving methods are described in Chapter 1. The results of the first order calculation should be equal for both software packages, using similar input variables. The four contributions of the quadratic transfer function, based on first order quantities, should therefore also be equal. However in the previous paragraph is concluded that based on the phase differences in the first order moment a mismatch in quadratic transfer functions is expected.

Figure 4.27 differences in the quadratic transfer functions can be observed. The comparison of both quadratic transfer functions can be done in roughly three frequency ranges. In the low frequency range of $0 \lesssim \omega \lesssim 0.5$ rad/s the quadratic transfer function do not match well. The WAMIT quadratic transfer function is larger than the one calculated with DIFFRAC. Also the peaks at $\omega \approx 0.05$ rad/s and $\omega = 0.13$ rad/s are visible in the WAMIT QTF while not or less visible in the results of DIFFRAC. In the mid frequency range of $0.5 \lesssim \omega \lesssim 1.0$ rad/s the transfer functions show similar behaviour with two characteristic peaks at $\omega \approx 0.65$ rad/s and $\omega \approx 0.8$ rad/s, although the WAMIT function is larger in magnitude. In the higher frequency range of $1.0 \lesssim \omega \lesssim 2.0$ rad/s the differences are again larger. The magnitude of the DIFFRAC transfer function is larger for the biggest part of this range.

Figure 4.28 shows that the origin of the differences in the low frequency range are the quadratic terms of quadratic transfer function. The peak in Figure 4.28 at $\omega \approx 0.3$ rad/s is notable in the DIFFRAC function in contrast to the WAMIT output. This is also the case in the mid frequency range at $\omega \approx 0.95$ rad/s. In the higher frequency range it is notable that the magnitude of the DIFFRAC transfer function increases until $\omega \approx 1.85$ rad/s.

In Figure 4.29 the second order potential contribution, calculated with the direct, indirect and Pinkster method, is plotted. The direct and indirect methods compute the same physical second order potential moment and it can be noticed that there is no significant difference in the resulting output (see Figure 4.29). This means that the moments computed by the different approaches are converged which is expected for finer discretization [19]. The Pinkster method uses a different approach in order to calculate the second order potential and is therefore expected to differ from the direct and indirect method.

Figure 4.29 shows that the second order potential contribution is dominant in the high frequency range $1.0 \lesssim \omega \lesssim 2.0$. The potential quadratic transfer function is different in 'shape', however the magnitude at $\omega = 0$ rad/s and at $\omega = 1.85$ rad/s is similar. In the second order potential term calculated with WAMIT two peaks are visible at $\omega \approx 0.13$ rad/s and $\omega \approx 0.3$ rad/s. These peaks are not present in the DIFFRAC calculations. The peaks could originate from the discretized free water surface as explained in section 4.4. It is shown in Figure 4.29 that the Pinkster approximation is larger in magnitude for $0.8 \lesssim \omega \lesssim 1.5$ which is also translates to the total quadratic transfer function in Figure 4.27.

In Figure 4.30 and 4.31 the amplitude, in- and out-of-phase quadratic transfer function for the total, quadratic and potential contribution per software package are shown. All transfer functions show that the quadratic

terms are dominant in the low and mid frequency range, while the potential contribution is dominant in the high frequency range.

Furthermore it is notable that the out-of-phase (Q) quadratic transfer function seems dominant in its contribution to the total quadratic transfer function in the low and mid frequency range in both software packages. The potential contribution in the high frequency range of the total quadratic transfer function seems to originate from equal contributions of the potential term in the in- and out-of-phase quadratic transfer functions. However the dominance of the potential contribution in the high frequency range in DIFFRAC is reduced due to the quadratic contributions in the out-of-phase quadratic transfer function in the range $1.5 \lesssim \omega \lesssim 1.85$.

In Figure 4.30 the second order potential contribution is shown calculated with the direct and indirect method. As also explained in Figure 4.29 the moments computed by the different approaches, are converged, which is expected for finer discretization [19].

In this section the differences in the quadratic transfer function calculated with two software packages are discussed. The influence of the dominance of specific contributions on the roll response spectrum is not discussed in this section, but will be incorporated in the discussion of the next section.

4.7. INFLUENCE SECOND ORDER CONTRIBUTIONS ON LOW FREQUENCY QUADRATIC TRANSFER FUNCTION

In DIFFRAC the option is available to plot the contributions of the quadratic transfer function separately. Consequently it is possible to determine which of the contributions is dominant in the quadratic terms of the quadratic transfer function in contrast to the previous section. In Figure 4.32 the amplitude transfer function is plotted. Secondly in Figure 4.33 the in-phase component (P) of the transfer function is shown. Lastly in Figure 4.34 the out-of-phase component (Q) of the transfer function is presented.

The quadratic transfer function presented in Figures 4.32, 4.33 and 4.34 are calculated relative to the hydrodynamic origin (CoH). The contributions are plotted separately and the total quadratic transfer function is indicated. First the quadratic transfer functions are presented, thereafter the results are discussed.

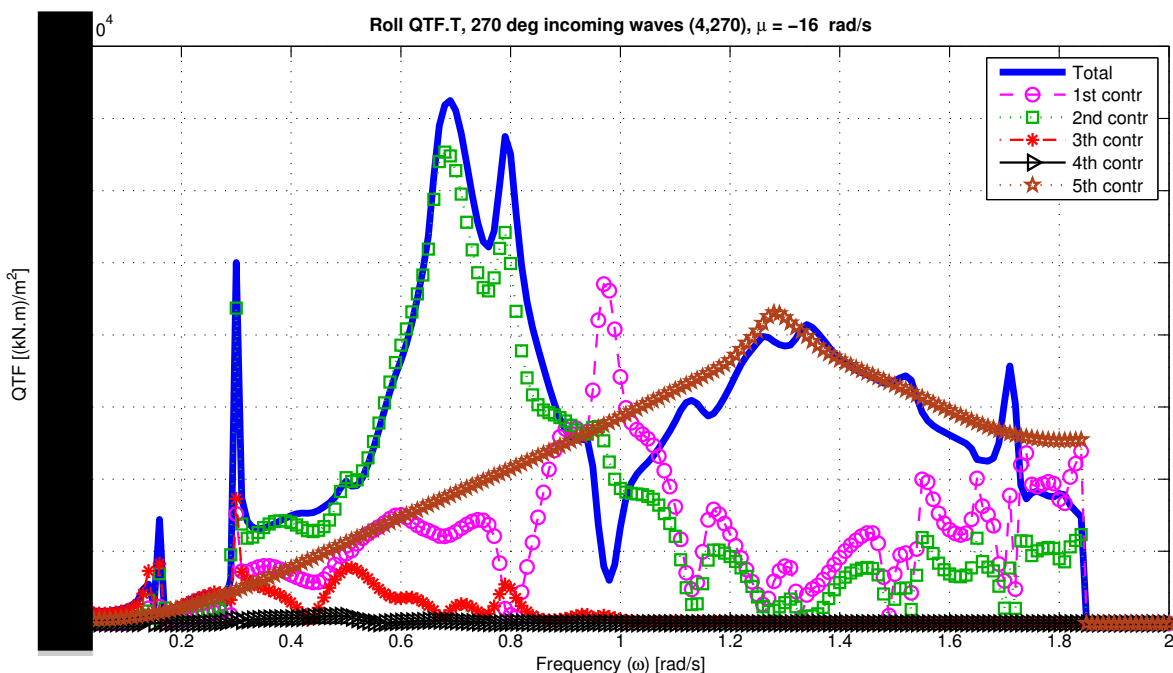


Figure 4.32: The amplitude of the quadratic transfer function calculated in CoH by DIFFRAC for roll with incoming waves of 270° . All contributions of the quadratic transfer function are shown.

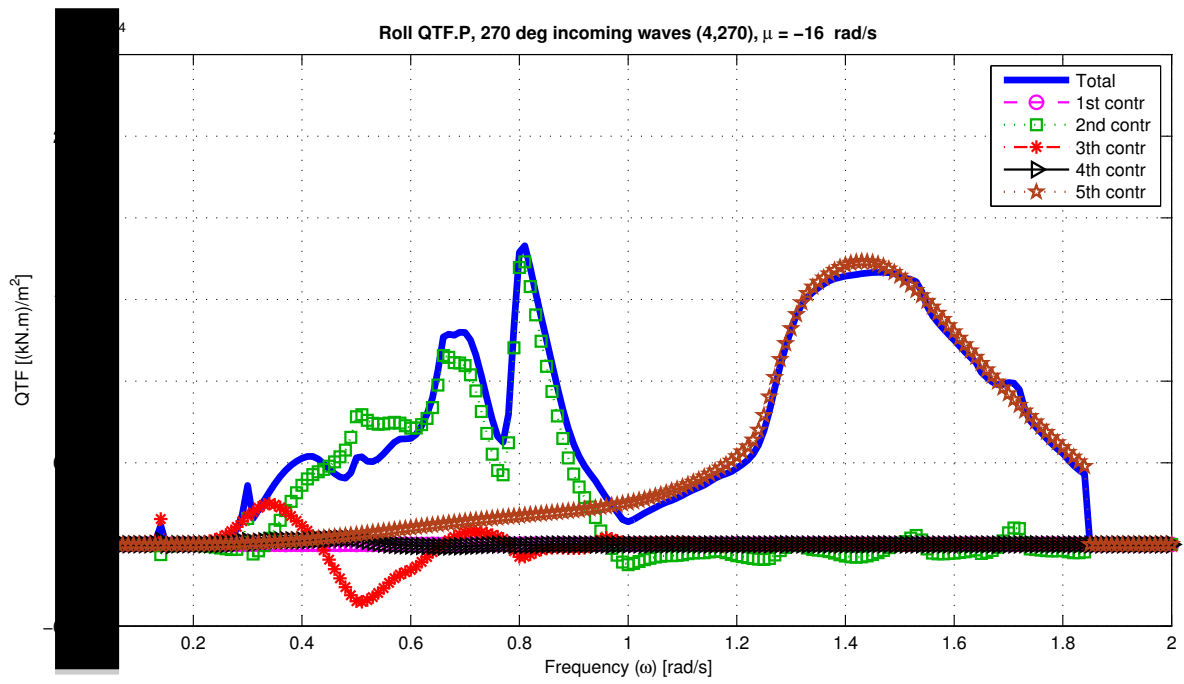


Figure 4.33: The in-phase component of the quadratic transfer function calculated in CoH by DIFFRAC for roll with incoming waves of 270° . All contributions of the quadratic transfer function are shown.

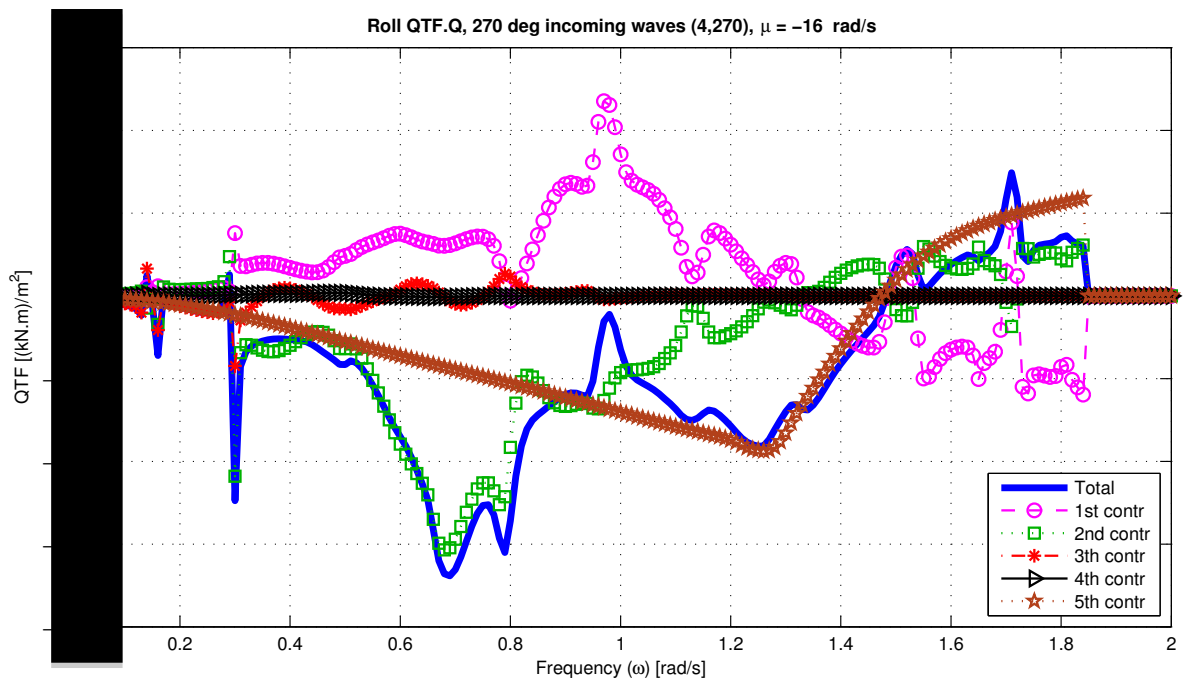


Figure 4.34: The out-of-phase component of the quadratic transfer function calculated in CoH by DIFFRAC for roll with incoming waves of 270° . All contributions of the quadratic transfer function are shown.

4.7.1. DISCUSSION

Figure 4.32 shows that the first, second and fifth contributions are the most important terms in the quadratic transfer function for roll in beam waves. In frequency range $0.3 \lesssim \omega \lesssim 0.9$ rad/s the second contribution is dominant. In the higher frequency range ($1.0 \lesssim \omega \lesssim 1.85$ rad/s) the fifth second order potential contribution is dominant. In between these ranges the first contribution is dominant in range $0.9 \lesssim \omega \lesssim 1.0$ rad/s. From Figure 4.33 and 4.34 it can be noted that the first contribution originated only from the out-of-phase quadratic transfer function. The reason that there is no influence of the first contribution in the in-phase transfer function is that the reference point is located in the waterline. The influence of the relative wave height contribution is zero in this situation. If the moments are calculated in the centre of gravity the quadratic transfer functions change. The transfer functions in the CoG for roll are presented in Appendix B.1.1 on page 98. Especially the in-phase component of the quadratic transfer function is more influenced by the first contribution of the second order moment as is shown in Figure B.6.

The second order motions in the vertical plane (heave, roll and pitch) have not been investigated by many research groups. Pinkster did calculate the influence of the separate contributions on the mean longitudinal drift force of a semi-submersible in head waves [12]. However the focus of this thesis is on the roll motion of a semi-submersible, it is interesting to compare the the two studies in order to see if Pinkster's findings also apply on the Sleipnir. In Figure 4.35 and 4.36 the contributions of the mean surge drift force in head waves, calculated by respectively Pinkster and by WAMIT, in this research, are presented. Pinkster concluded that the first contribution due to relative wave elevation is dominant in all cases. The second contribution, due to the pressure drop as a consequence of the fluid velocity, is in direction opposite to the first contribution. The third and fourth contribution are generally less important [12]. The fifth contribution is zero because the mean drift force is plotted. In the mean force there is no influence of energy in wave groups because $\mu = 0$, $\omega_1 = \omega_2$. Pinkster's conclusions stated above are also applicable on the findings in this research in Figure 4.36.

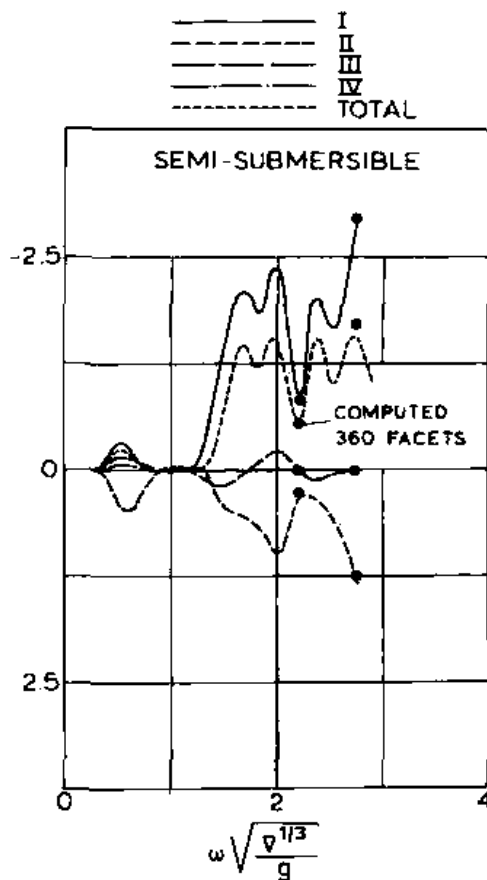


Figure 4.35: Different components of mean surge drift force in head waves [12].

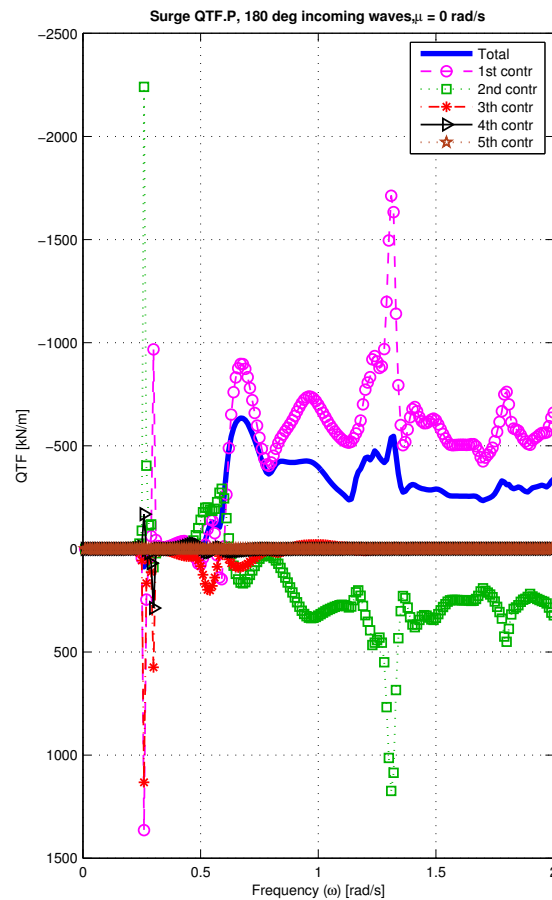


Figure 4.36: Different contributions of mean surge drift force in head waves calculated for the Sleipnir.

In Pinkster's work the influence of the five contributions of the second order drift forces on a semi-submersible in the horizontal plane are shown. In more recent work Matos et al discusses different options for modeling second order hydrodynamic forces and induced motions [7]. The methodology in this research is partly based on their work. Matos et al make distinction between the quadratic terms (first four contributions) and the second order potential term (fifth contribution) of the quadratic transfer function calculated by WAMIT. These contributions are discussed in the previous section for this research. The significant influence of the second order potential contribution in the higher frequency range on the transfer function of a semi-submersible, as shown in this research for roll, can also be found in their work for pitch.

The second order potential is related to the low frequent wave, with difference frequency μ , induced by the presence of wave groups. Voogt et al showed that a semi-submersible can take on a steady list angle caused by vertical drift forces in regular head waves [1]. However this phenomenon is not studied in this research. Voogt et al state that the roll response can be severely increased if the frequency of wave groups is close to the natural frequency of roll. In other words this means that although the natural roll frequency is far removed from the normal wave frequencies and therefore roll motions resulting from normal waves will be small, roll may be severely increased due to the natural frequency of wave groups. A quote from the last paragraph of the article of Voogt et al [1]:

" The challenge for the naval architect is to configure the hull so that the natural periods of the pitch and roll fall between the period of wave groups and the waves themselves and to ensure that the more obscure vertical wave drift forces are not creating other problems."

This research about the roll motions of the Sleipnir shows that the natural roll frequency of 0.16 rad/s is located in a frequency range in which the energy of wave groups may cause a substantial increase of roll motions. It must be noted that this effect depends on the specific sea state. In this research sea state one: $H_s = 1.5$ m, $T_p = 7$ s, sea state two: $H_s = 1.5$ m, $T_p = 12$ s and sea state three: $H_s = 3.0$ m, $T_p = 7$ s are tested. It is shown that especially in sea state three the roll motions are increased by second order effects.

In order to show the dependency of the roll response motion on the specific sea state the second order moment spectra for the tested sea states are presented in Figure 4.37 and 4.38. In Figure 4.37 the second order moment spectra are presented calculated with the total, quadratic and potential quadratic transfer functions. In Figure 4.38 the second order moment spectra are shown calculated with the total and all separate contributions of the quadratic transfer functions. In both figures it is clear that sea state two shows a different behaviour comparing with the other two sea states. The moment spectrum is more dependent on only the quadratic terms (Figure 4.37) of the transfer function than in the other sea states. In Figure 4.38 it is shown that especially contribution two, due to the pressure drop as a consequence of the fluid velocity, causes this different behavior in the low frequency range. It must be clear that dependent on the period of a sea state different contributions of the quadratic transfer function (see Figure 4.32) will be dominant in the second order moment spectrum and therefore also in the roll response motion. Contributions *I*, *II* and *V* are dominant in the tested sea states, as can be seen in Figure 4.38.

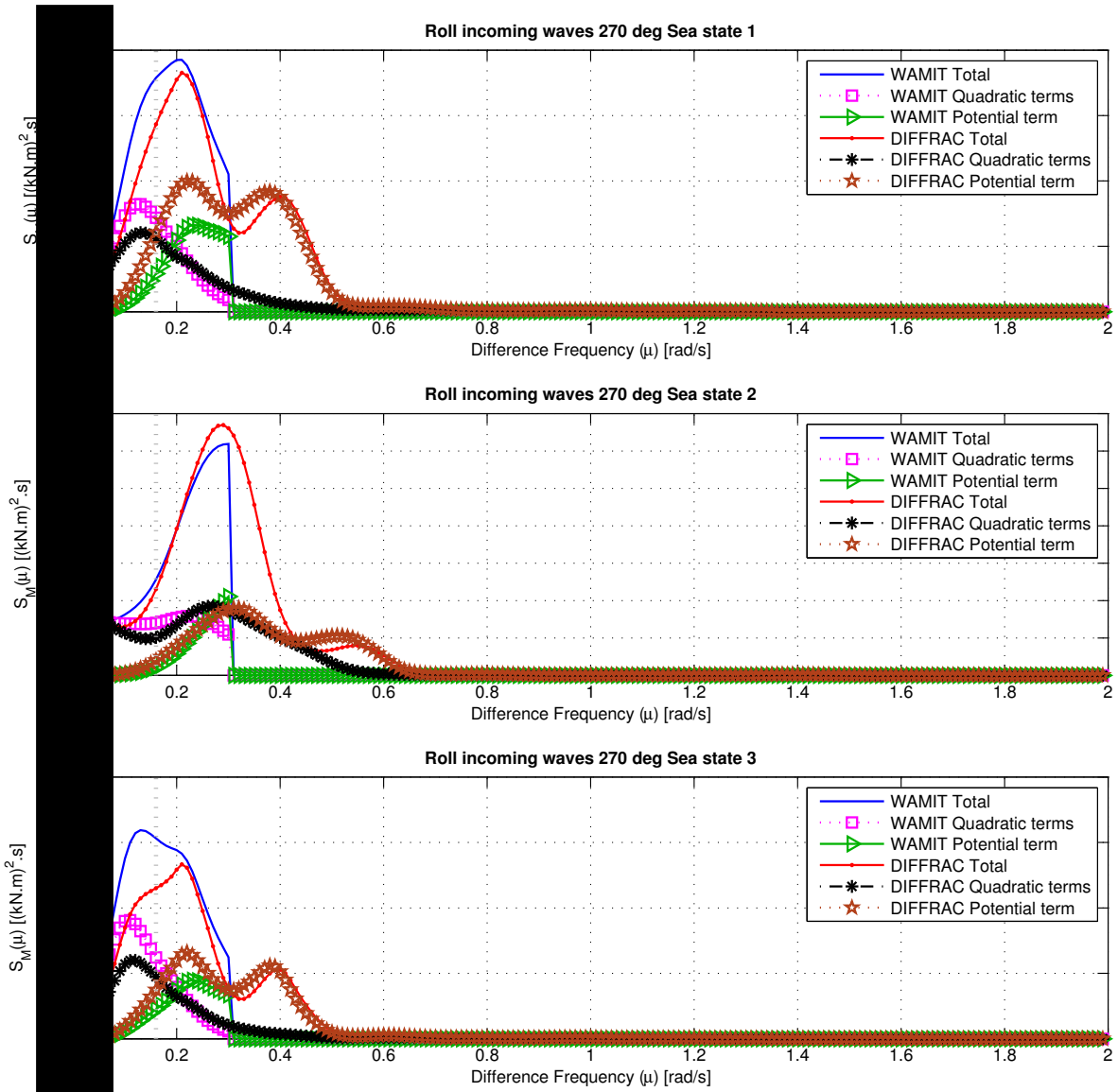


Figure 4.37: Second order moment spectra for the three tested sea states. The spectra are calculated with the total, quadratic and second order potential quadratic transfer function for roll with incoming waves of 270°. It can be seen that the influence of the contributions differ per sea state.

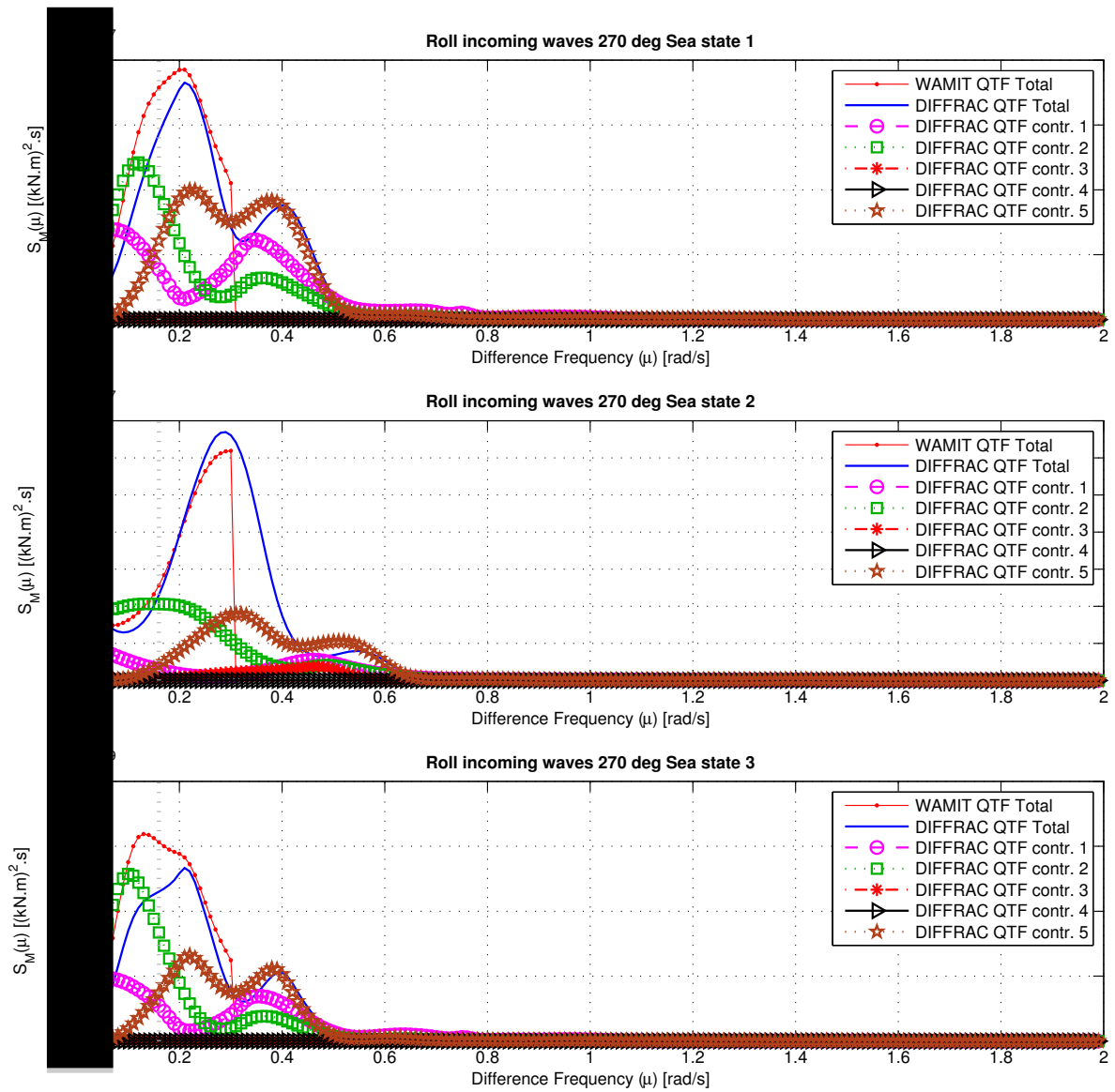


Figure 4.38: Second order moment spectra for the three tested sea states. The spectra are calculated for the total and all contributions of the quadratic transfer function for roll with incoming waves of 270° . It can be seen that the influence of the contributions differ per sea state.

4.8. TIME DOMAIN STUDY

The computer program aNySIM is used to simulate the motions of the Sleipnir in the time domain. In the time domain simulations with aNySIM a linear and quadratic damping term can be included. The linear and quadratic damping terms are calculated with the p and q values obtained from the still water decay test at MARIN (Figure 1.2).

First the decay test are simulated and validated with the measured still water decay test results. Secondly the model test with sea state $H_s = 3$ m, $T_p = 7$ s is simulated using the damping values found in the decay simulations. The model test is simulated with different wave trains as input. Wave trains measured at the wave probes WAVECL, WAVE180 and WAVE270 during the wave calibration tests and during model tests have been investigated. Furthermore time simulations using the JONSWAP with different wave seeds are performed. Lastly the the roll response spectrum is calculated from the time domain simulations and compared with the roll spectrum of the measured roll time traces. The chapter concludes with a discussion about the results.

4.8.1. DECAY TEST SIMULATION

In Figure 4.40 the results of the simulated decay tests are presented. For each mode the simulation is validated with the time trace of the measured roll decay tests. It can be noted that for all modes the damping is correctly simulated however the natural frequency of the simulations differ with de measured natural frequencies. In Figure 4.40 it can be seen that only the roll natural frequency is 'tuned' by changing the roll radius of gyration. The model tests have been simulated with the decay test results of Figure 4.40. The results of the model tests simulations are presented in the next section.

In an ideal situation all the decay tests should be tuned on damping and natural periods. However due to time limitations this has not been done in this research. The roll motion and sway motion are coupled. Therefore the period of the sway motion is also tuned for a second model test simulation. The sway period is tuned by chancing the spring stiffness of the four soft mooring lines using [18]:

$$C_{yy} = \sum_{i=1}^4 \frac{T_{0i}}{L_{0i}} \cdot \cos^2 \alpha_i + c_i \sin^2 \alpha_i \quad (4.1)$$

in which α_i the angle of the soft mooring line with respect to the centre line of the vessel [deg], c_i the stiffness of line i [kN/m], L_{0i} the stretched line i in equilibrium position [m], T_{0i} the pretension in line i [kN]. The initial sway stiffness of 535 kN/m is changed to 527 kN/m (-1.5%) in order to match the natural period of sway in the decay test. The natural period changed from ~ 175 s to ~ 180 s which is a -3 % change. The result is shown in Figure 4.39. The rest of the model test simulations have the same settings as the first simulation except for the matched sway period.

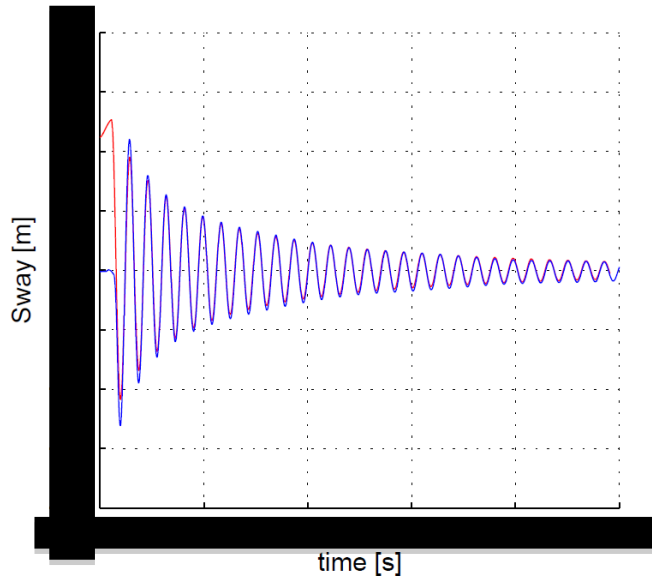


Figure 4.39: Still water decay test simulation for sway. The sway period is matched with the measured decay test by changing the sway stiffness.

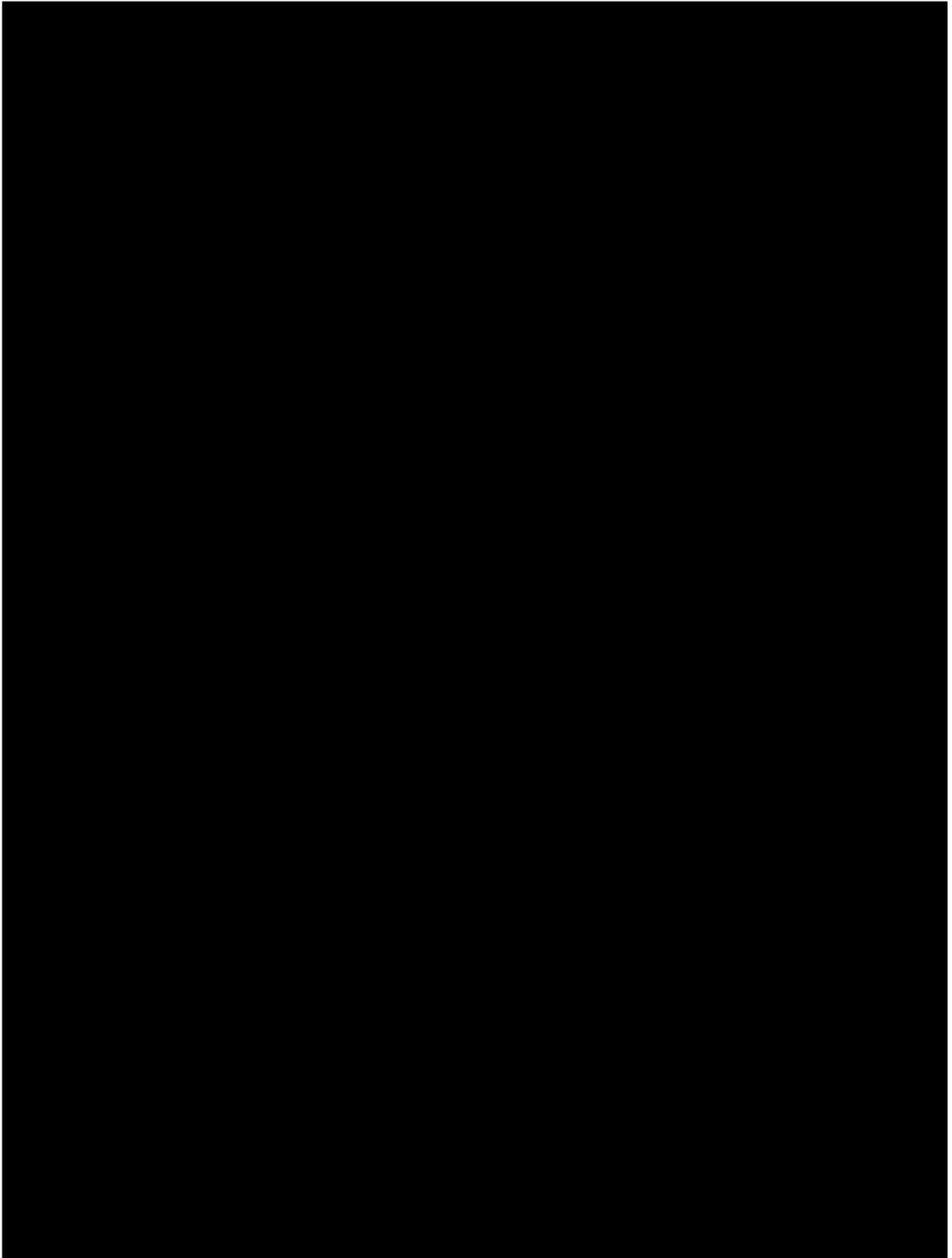


Figure 4.40: Still water decay test simulation validated with the measured decay results performed at MARIN. The simulations are the red line and the blue line indicates the measurements. All modes are simulated. The linear and quadratic damping term calculated from the p and q values obtained from the still water decay test at MARIN are used for the simulation. It must be noted that only the simulated natural period for roll is tuned (with the roll radius of gyration) and matches with the measurements. The natural periods of the simulated and the measured decay tests are indicated in the figures.

4.8.2. MODEL TEST SIMULATION

In this section the results of the model test simulations are presented. First the results of the model test simulation without a tuned still water sway decay simulation is presented followed by the simulation with the tuned sway period. These two simulations are performed using the wave time trace measured at wave probe WAVECL during the wave calibration tests (see Figure 2.3 in Chapter 2). Before the results are discussed it must be noted that based on the decay test simulations the damping seems to correspond well with the measurements.

In Figure B.21 the model test simulation for sea state three ($H_s = 3$ m, $T_p = 7$ s) is presented for the roll and sway motion response. Only the decay test of roll is tuned for this simulation. In Figure B.21 it is visible that the amplitude and phase of the simulated and measured time traces are more or less in agreement in a time range of $0 \leq t \leq 4500$ s. In Appendix B.2.1 a more extensive overview is given in which time ranges the roll simulations and measurements are in agreement.

In Figure B.21 also the sway motion is plotted versus time. It can be seen that the group behaviour of the sway motion of the simulation shows similarities with the group behaviour of the sway motion of the measurements. However the amplitude and phase do not match in many time ranges. Therefore it can be argued that if the decay test of sway is tuned in damping and period, the model test simulation would result in a better agreement with the measurements for sway.

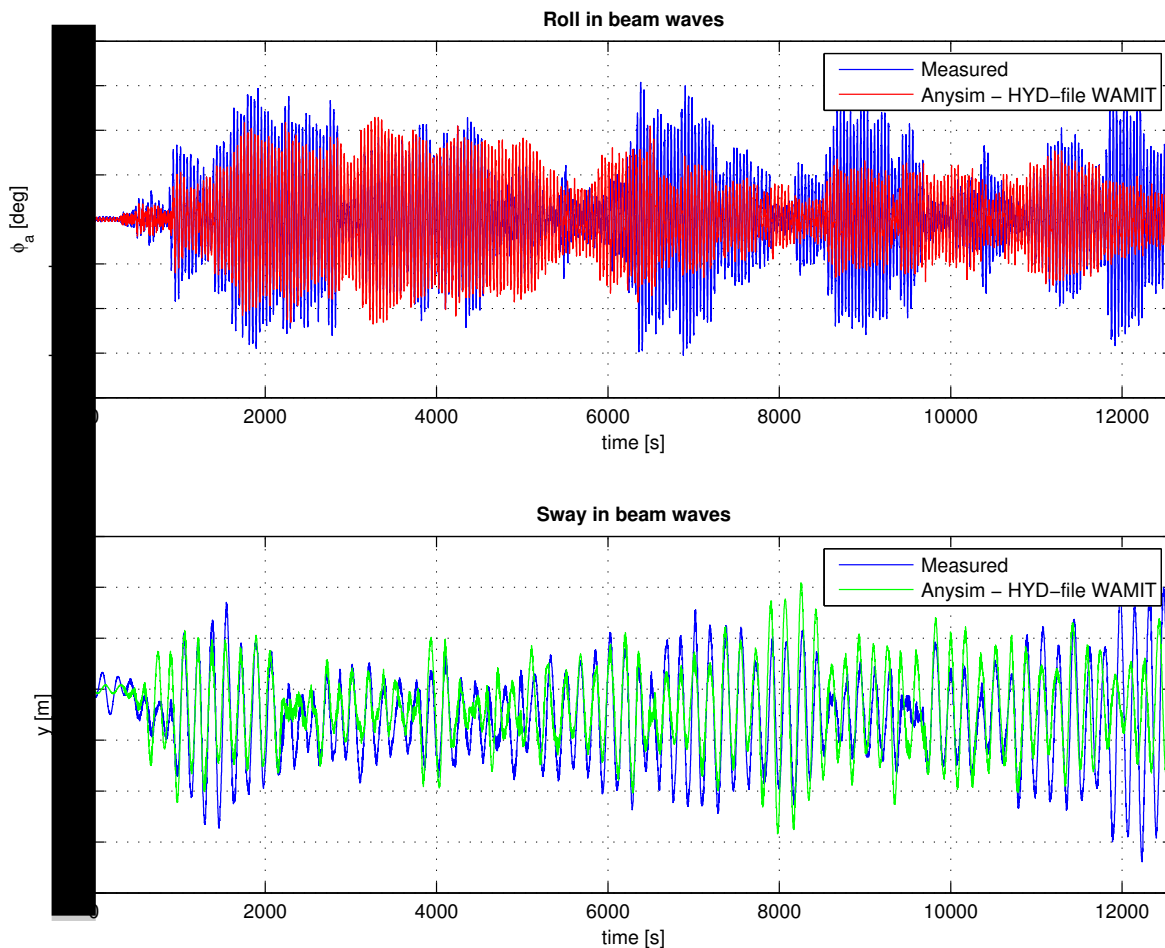


Figure 4.41: Time simulation for the roll and sway motion compared with MARIN model test 803004, sea state $H_s = 3$ m and $T_p = 7$ s, beam waves. Only the roll decay test is in agreement with the measurements in this simulation. Wave train of WAVECL has been used as input for the simulation.

In Figure 4.42 the results of the second model test simulation are presented for sway and roll. For this simulation first the sway and roll decay tests are simulated in agreement (tuned) with the measured decay tests as shown in Figure 4.39 and 4.40. Considering the roll motion in Figure 4.42 it can be seen that the simulation does match better in amplitude and group behaviour than the previous simulation in a time range of $0 \lesssim t \lesssim 3500$ s. However from 3500 s the amplitude and group behaviour of the roll simulation are in very poor agreement with the measurements. So in the largest part of the time range the simulation does not match with the measurements. In Appendix B.2.1 at page 123 a more extensive overview is given in which time ranges the roll simulations and measurements are in agreement.

The sway motion simulation in Figure 4.42 seems to be more or less in agreement with the measurements in the time range of $0 \lesssim t \lesssim 2100$ s. However after this time the amplitude, phase and group behaviour of the sway motion are in poor agreement with the measurements.

It can be concluded that a change of $\sim 3\%$ in sway period has a significant influence on the sway and roll simulation. This is more clearly in the motion response spectra, of the presented results, discussed in the next section.

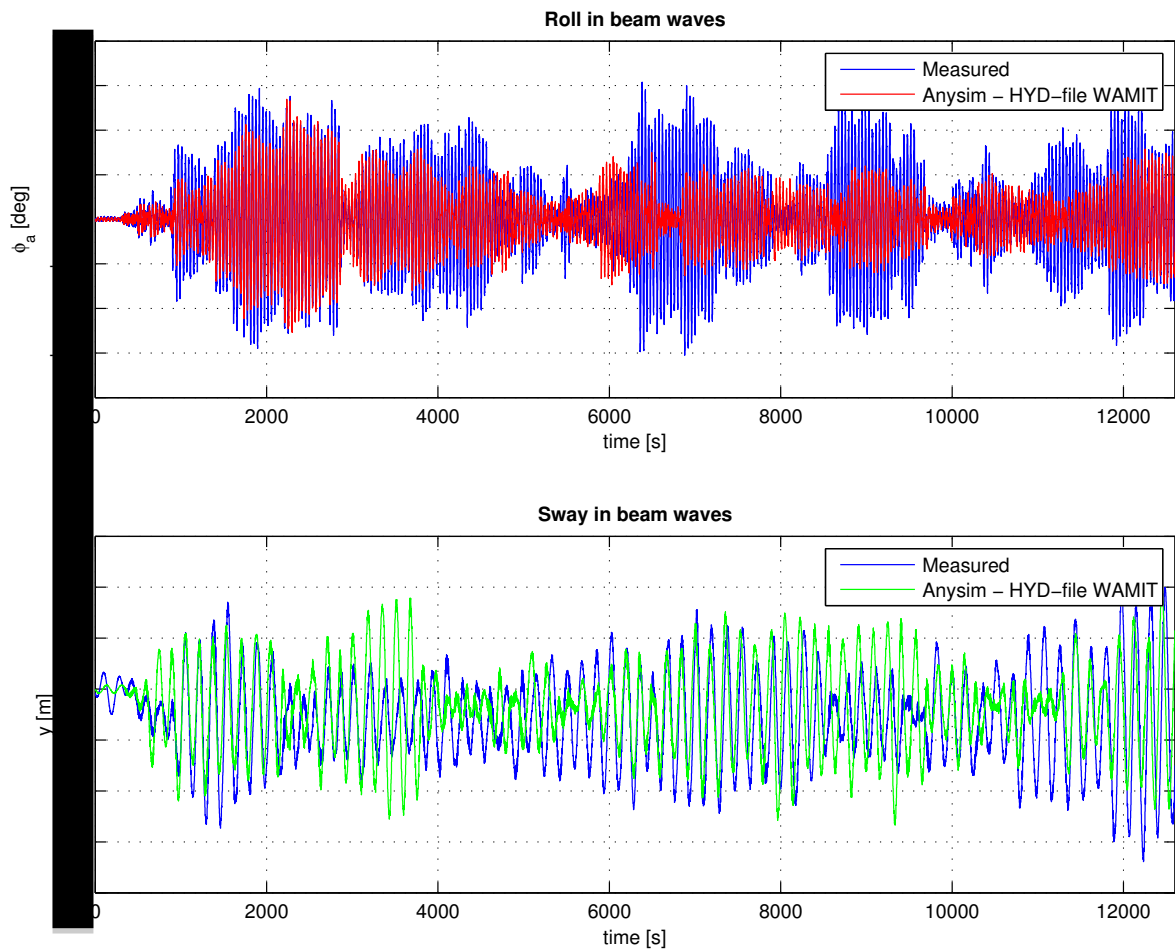


Figure 4.42: Time simulation for the roll and sway motion compared with MARIN model test 803004, sea state $H_s = 3$ m and $T_p = 7$ s, beam waves. The roll and sway decay tests are in agreement with the measurements in this simulation. Wave train of WAVECL has been used as input for the simulation.

ROLL AND SWAY MOTION SPECTRA

In Figure 4.43 the roll and sway spectra of the time domain simulations, presented in the previous section, are shown. The spectra of the measured motions, the model test simulations with and without sway 'tuning' are shown.

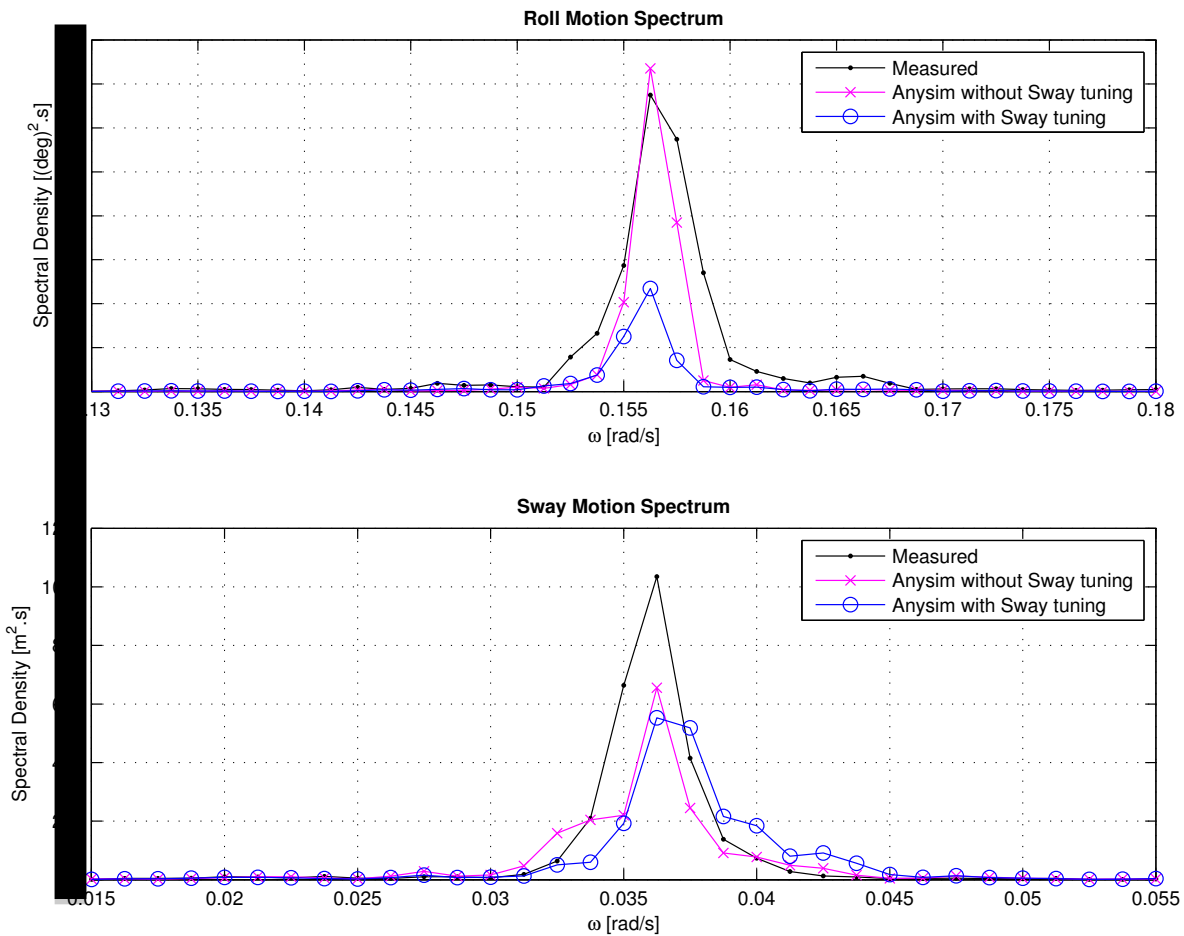


Figure 4.43: Spectral Density of low frequency roll and sway motion response. The spectra of the measured motion, the model test simulations with and without sway 'tuning' is shown. Model test 803004 is simulated with a sea state $H_s = 3$ m and $T_p = 7$ s in beam waves.

In Table 4.13 the zero order moment, the variance and the most probable maximum of the total response spectrum are presented for roll and sway. It can be concluded that a small change in sway period result in a significant change in roll response spectrum. It could be questioned if the phase has a influence on the roll response spectrum. In the next section the phase is subject of research.

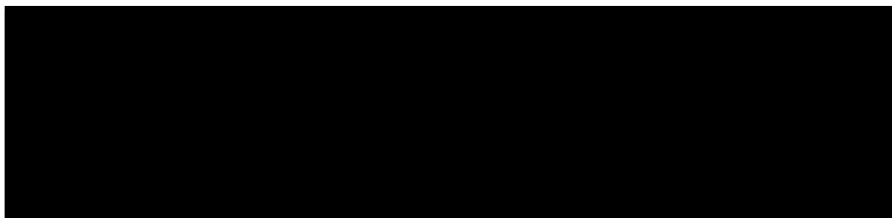


Table 4.13: aNySIM simulations compared with measured model test 803004. Wave train of the calibration tests at WAVECL is used for the simulations. The zero order moment, variance and most probable maximum are presented for roll and sway.

PHASE OF THE INCOMING WAVE WITH RESPECT TO THE PHASE OF THE MOTIONS OF THE MODEL

It must be noted that the wave train used for the model test simulations in the previous sections is not the wave train which was actually present in the basin during model tests. During the wave calibration tests the wave train is measured with three wave probes at WAVECL, WAVE180 and WAVE270 (see Figure 2.3 in Chapter 2). The wave probe WAVECL can not be used during model tests because the model is located at that position. However the waves are measured at the wave probes WAVE180 and WAVE270 during the wave calibration tests and during the model tests. Therefore the wave time traces measured during the model tests and during the calibration tests can be compared. The comparison of the time traces at WAVE180 and WAVE270 for all three tested sea states is presented in Appendix B.2.4. The WAVECL time trace which is used for the time domain simulations is shown in Figure B.31 on page 132. However, comparing the time traces from WAVE180 and WAVE270 in the same figure, it is seen that the phase of the measured waves differs from an early stage of the tests. Therefore it can be argued that it will be very complicated to simulate the responses exactly in agreement with the measurements while using the wave train at WAVECL. In order to investigate the influence of the other measured wave trains on the motion response also model test simulations are performed with the wave trains of WAVE180 and WAVE270. The results of the time simulations can be found in Appendix B.2.3 on page 128. The roll time traces are shown in Figure B.27. The sway motion time traces are presented in Figure B.28.

However it must be realized that there will be wave reflections due to the presence of the model. Therefore the measured wave trains at WAVE180 and WAVE270 not only consist of information about the wave height of the incoming exciting waves, but a combination of the incoming and reflected waves. Especially the wave at WAVE270 will consist of more energy because of the reflections due to the fact that the wave probe is located at port side (direction of incoming waves) of the vessel (see Figure 2.3 in Chapter 2). This phenomenon is visible in the wave spectra from WAVECL, WAVE180 and WAVE270 in Figure B.34 at page 135.

In Figure 4.44 the roll and sway spectra of all simulations described above are plotted. The zero order moment and variance are shown in Table 4.14. A distinction is made for the low frequency response and the high frequency (wave frequency) response. In Figure 4.44 only the low frequency response is shown. As expected the response calculated with the wave train from WAVE270 contains sufficient more energy than the other simulations. The roll response spectrum of the simulation using the model test WAVE180 wave train is in best agreement with the measurements. The wave spectrum of WAVE180 from the model tests as shown in Figure B.34 on page 135 shows a different phasing in comparing with WAVECL and WAVE180 from the calibration tests. The phase of the wave train measured at WAVE180 during model tests, the actual wave during model tests, is expected to be more accurate than the WAVECL wave train. However the zero order moment of the wave spectra of the model test WAVE180 is 1.6 deg^2 and for WAVECL 1.3 deg^2 . Thus the wave spectrum of the model test WAVE180 consists, apart from a different phasing, of more wave energy (probably due to partly reflected waves) in comparison with the spectra measured during calibration (Figure B.34). In other words the better agreement, in comparison with the measurements, of the simulation with wave train WAVE180 can not purely be assigned to the different phasing in comparison with the simulation with wave train WAVECL. In order to investigate the influence of the phase on the roll motion response the JONSWAP spectrum is used for time simulations.

In order to investigate the influence of phasing of input wave spectra on the roll motion response, ten time simulations are performed using a JONSWAP spectrum with different wave seeds. The results of this sensitivity study are presented in Appendix B.25 on page 125. In Figure B.25 the time traces of the roll response simulations can be found. The low frequency roll response spectra are presented in Figure B.26. Lastly the statistical analyses on these response spectra are shown in Table B.26 on page 127.

The ten simulations resulted in a mean zero order moment of 0.12 deg^2 with an error of $\pm 0.02 \text{ deg}^2$ and a mean variance of 0.34 deg with an error of $\pm 0.02 \text{ deg}$. The error analyses for small data sets is used as explained in Appendix F. It can be concluded that the phase of input sea state influences the motion response spectra. However, the difference in roll statistics of the simulation with the calibrated wave train and the measured roll response can not be blamed to only a phase difference, based on the performed sensitivity study.

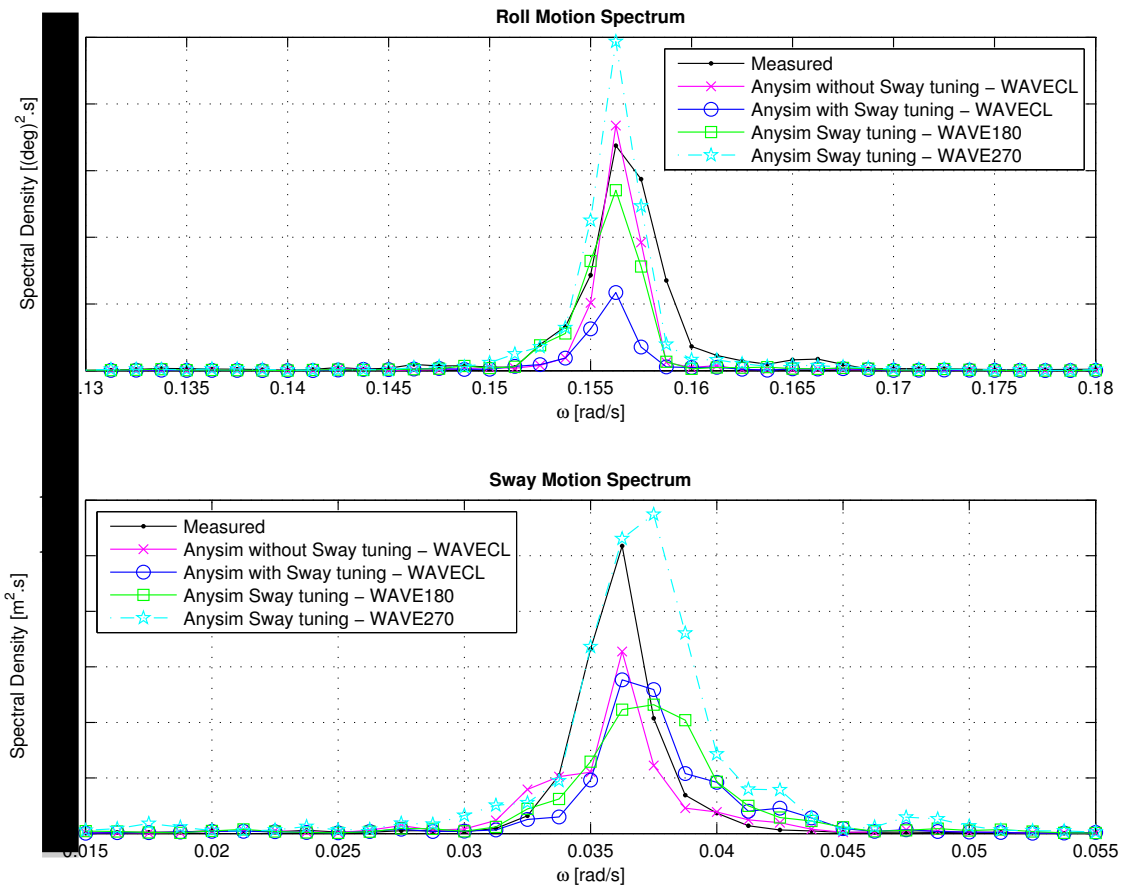


Figure 4.44: In this figure the roll and sway motion response spectra of model test simulations are compared with the measured motion response spectra. Simulations with different wave trains are performed. The wave train obtained during the calibration tests at WAVECL are used. Furthermore the wave trains measured during model tests at WAVE180 and WAVE270 are used for simulations.

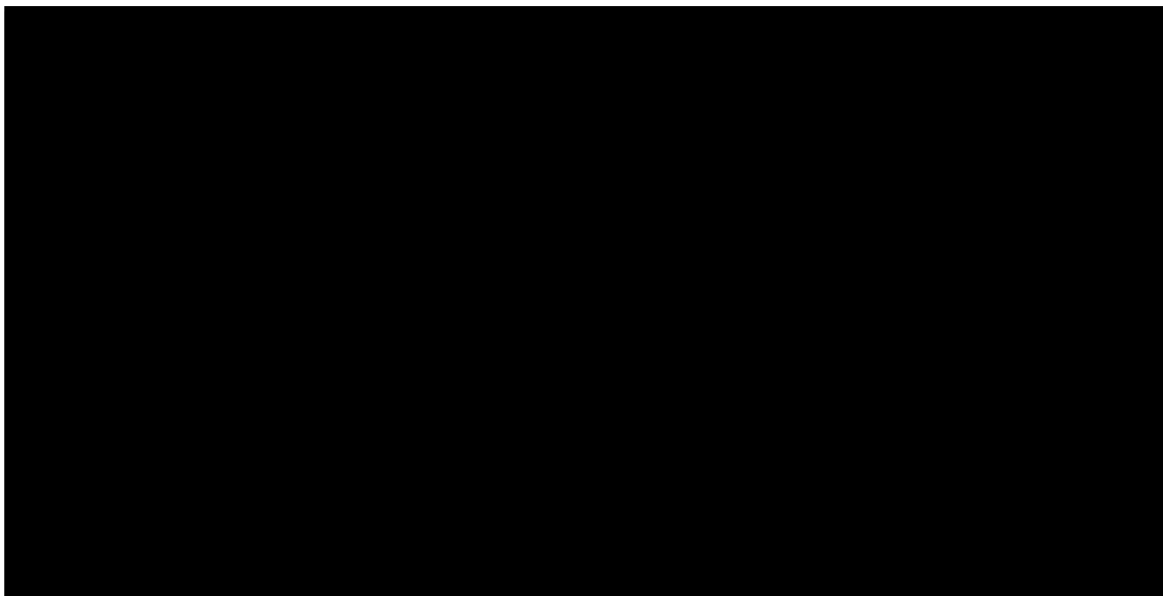


Table 4.14: Zero order moment, variance and most probable maximum (in a 3 hours storm) of the total, low frequency (LF) and high or wave frequency (HF) part of the response spectra. (Low frequency part for roll is calculated for range $0 < \omega < 0.4$ rad/s. Low frequency part for sway is calculated for range $0 < \omega < 0.5$ rad/s. High frequency part for roll and sway is respectively calculated for $0.4 < \omega < 2$ rad/s and $0.5 < \omega < 2$ rad/s.)

The M or C before WAVE indicates if the wave train is measured during model tests or calibration tests.

DISCUSSION

First the decay tests have been simulated using the linear $b^{(1)}$ and quadratic $b^{(2)}$ term obtained from the MARIN still water decay tests. The comparison between the decay test simulations and measurements gives confidence that the damping is in the correct order of magnitude as shown in Figure 4.40. Using the harmonic linearization technique the used damping terms correspond to a added equivalent viscous damping ratio of $\xi = 0.5\%$.

The above damping is used in the first model test simulation of model test 803004 with sea state $H_s = 3\text{m}$ and $T_p = 7\text{s}$ in beam waves, see Figure B.21. The model test simulation seems promising considering the roll amplitude. However the 'roll group' behaviour does not correspond with the measurements after $\approx 4500\text{ s}$. Similar statements can be made for the sway motion for this simulation. However the amplitude of the simulation is less in agreement with the measurement in comparing with the roll motion. This is also shown in Figure 4.43.

Comparing the measured and simulated (without sway tuning) roll spectra, shown in Figure 4.43 and Table 4.13, it can be noted that the peak is in the correct order of magnitude. This could mean that the used linear $b^{(1)}$ and quadratic $b^{(2)}$ damping values to predict the height of the peak are in agreement with the measured roll motion spectrum in the frequency domain. This would be very convenient for the reason that the estimation of the damping values, based on the p and q values obtained from still water decay tests, would be sufficient in order to simulate the model test roll motions in good agreement with measurements. However more sea states should be simulated and compared with the measurements in order to test if such statements hold. Furthermore it is noticed that the simulated spectrum 'misses' some energy comparing with the measured spectrum. This could be caused by the fact that not all natural frequencies are matching in the simulations of the decay tests as can be seen in Figure 4.40.

Based on the above statements and the fact that roll and sway are coupled motions another model test simulation is performed. First the sway decay test is 'tuned' in order to correspond with the measured sway decay test. This has been done by changing the soft mooring line stiffness as shown in Figure 4.39.

Although the 'matching' sway and roll decay tests settings have been used for the second model test simulation (see Figure 4.42), the roll and sway motion time traces do agree less with the measurements than the previous simulation. In the time range $0 \leq t \leq 3500\text{ s}$ the roll time trace is in good agreement with the amplitude but especially with the roll 'group behaviour' comparing with the measurements. However considering the whole time range the amplitude of the roll time trace is less in agreement with the measurements as the previous model test simulation. This is clearly visible in Figure 4.43.

The sway motion of the simulation is not in good agreement with the measurements. Not only the sway amplitudes but also the group behaviour of the sway motion is not corresponding with the measured sway motion.

It can be stated that the energy in the roll motion in the time domain is sensitive to changes in the natural period of the coupled sway motion (see Figure 4.43). Besides sway also heave is coupled with the roll motion. Tuning the heave decay test could therefore result in a better agreement in the model test simulations comparing with the measurements. However in Figure 4.40 it can be seen that the period of the heave decay test simulations are in better agreement with the measurements than the initial sway decay simulations.

In general it can be noted that further investigation on the time domain simulations of the model is needed. It can be stated that the energy in the roll motion in the time domain is sensitive to changes in the natural period of the coupled sway motion (see Figure 4.43). Therefore it is recommended to exactly 'tune' the decay test simulations for every mode on period and damping comparing with the measurements. The sway period is tuned in the decay tests before performing a second model test simulation (see figure Figure 4.39 and 4.42). In order to conclude the discussion about the performed time domain simulation two main statements need to be considered for further research. First it must be clear that time domain simulations provide information about phasing of the response motions in contrast to the frequency domain study performed in this research. So not only the calculated force and added viscous damping but also the phasing of the motions must be part of the discussion. In this study the force or moment calculated with WAMIT and DIFFRAC is assumed to be correct for a fine discretized hull model and is not investigated nor validated in this report. The linear and quadratic damping terms are considered to be validated during the simulations of the still water decay tests, see Figure 4.39 and 4.40. Therefore it can be argued that missing energy in the best simulated roll response spectrum (with sway tuning) compared with the measured roll response spectrum (Figure 4.43) is caused by

the phasing of the motions with respect to the phase of the waves. In other words the location of the model in the wave field is important regarding the wave excitation.

Moreover roll is a coupled motion with heave and sway. Therefore considering roll the phase of all these three motions regarding the phase of the exiting waves must be correctly simulated in order to match with the measurements. This seems not to be the case in the performed time simulations in Figure B.21 and 4.42.

Lastly, Figure 4.45 is presented. In this figure all performed simulations, in the frequency and time domain, of sea state three have been plotted. The error in zero order moment caused by solely a phase difference is indicated. Note that all time domain simulations are performed with one damping level, the damping level found in the decay simulations tests. It must be concluded that the error, caused by the phase, is probably not responsible for the big difference in zero order moment between the measurements and the WAVECL time simulations. In order to investigate if the roll statistics can be improved, model tests with different seeds can be performed.

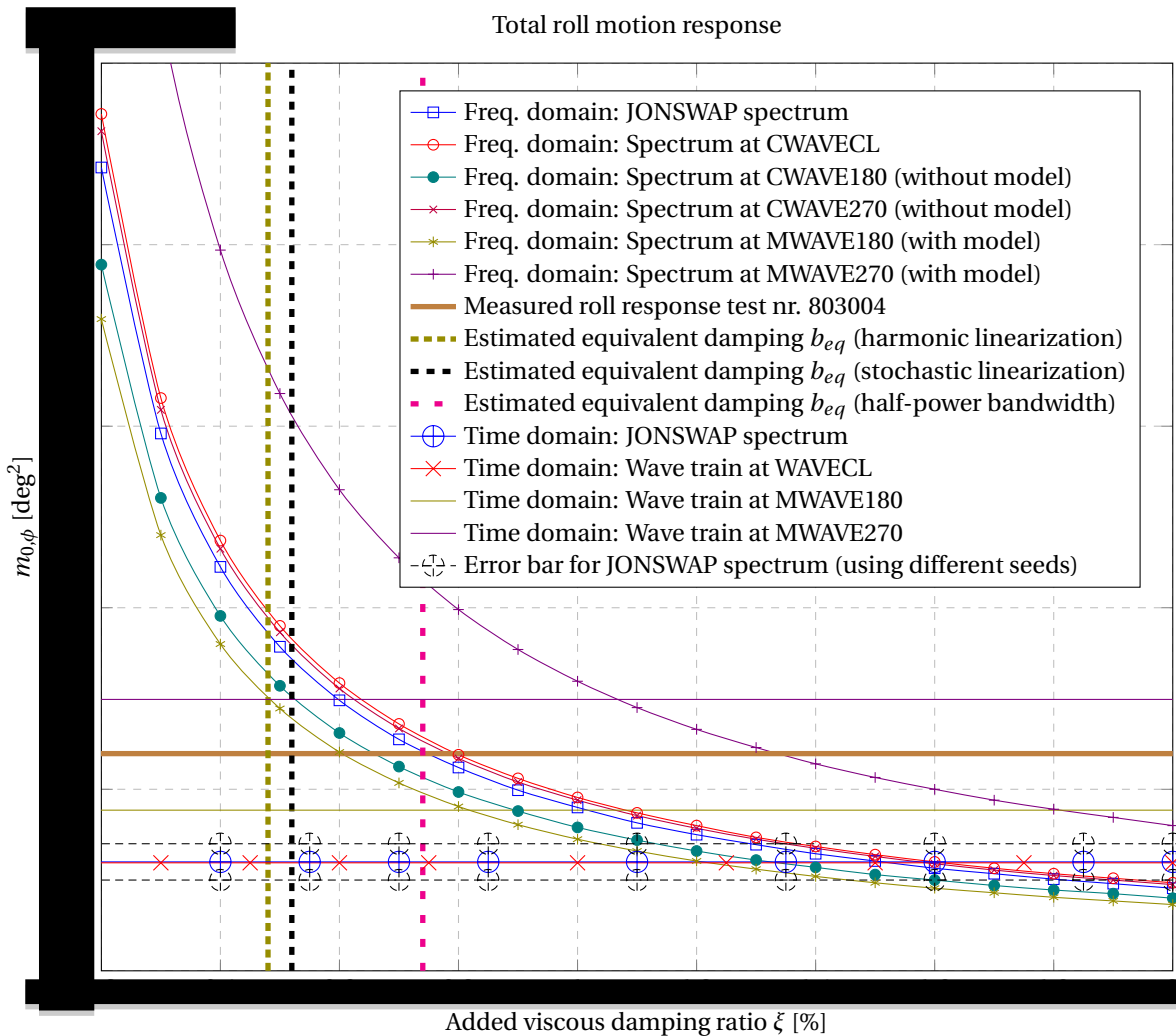


Figure 4.45: Sea state $H_s = 3\text{m}$, $T_p = 7\text{s}$. The influence of the added viscous damping ratio ($\xi = b/b_{crit}$) on the zero order moment of the roll motion response spectrum is plotted. The results of the frequency domain are shown and compared with the time domain results. Frequency domain: The roll response spectrum is calculated making use of the theoretical JONSWAP wave spectrum and all the measured wave spectra during calibration tests and model tests.

Time domain: The zero order moment of the simulations using wave trains from measured at CWAVECL, MWAVE180 and MWAVE270 roll response are plotted. The time simulations using the JONSWAP spectrum with different seeds is also plotted. The spreading in the JONSWAP simulations is indicated.

The zero order moment of the measured roll response spectrum of MARIN test 803004 is indicated. As well the predicted equivalent damping using stochastic linearization.

5

CONCLUSIONS AND RECOMMENDATIONS

In this chapter the conclusions of this master research about the low frequency second order roll of the Sleipnir are presented. First the conclusions (•) and recommendations (r) are presented for the complete study. Thereafter the answers to the research question are described. The second order roll problem is put in perspective. Lastly the conclusions and recommendations are repeated in the last two sections.

During model tests at MARIN roll motions, excited by second order wave forces, have been measured for three tested sea states. The aim of this research is to predict this second order roll response motion with the use of a frequency domain simulation method and a time domain simulation method. In order to set up both simulation methods the first and second order forces are approximated with the use of potential theory. The software packages WAMIT and DIFFRAC, based on potential theory, are used for the calculations.

The calculated first order forces, hydrodynamic coefficients and second order forces are used to define a first order roll moment spectrum, a second order roll moment spectrum and a moment transfer function. These are the requisite 'ingredients' in order to calculate the roll response spectrum in the frequency domain. First refinement studies have been performed on variables which influence mainly the calculation of the first and second order forces, which therefore influence the calculation of the roll response spectrum. The investigated variables are the panel size of the discretized geometric hull shape of the Sleipnir, the frequency resolution in the force calculation and the additional viscous damping terms.

5.1. REFINEMENT STUDIES

The panel size of the discretized geometric hull shape of the Sleipnir influences the results of the calculation of the first and second order forces. First is investigated for which panel size the calculated forces are converged (see Section 4.2).

- It is concluded that the calculated forces and moments are converged for a discretized hull model with 9892 panels. The panels at the columns of the model consist of stretched panels to the waterline (see Figure 3.2). The panels at the waterline are 3.44 m in length and 0.64 m in height.

It must be noted that the calculated forces and moments using potential theory are not validated with measurements. The calculation of the forces are compared with a calculation using a very fine panel grid size (NSCVfine model with 22338 panels). It is assumed that this calculation approximates the first and second order forces and moments in best agreement with reality. The validation of the calculated forces and moments is not investigated further in this research. Though the drift forces in the vertical plane have not been researched extensively in the past, therefore it would be very interesting to validate the calculated vertical drift forces with measurements.

- r) Perform a validation study on the vertical drift forces, calculated with potential theory, compared with measurements.

Secondly in Section 4.3 the influence of the frequency resolution on the calculation of the roll response spectrum is investigated.

- It is concluded that the roll moment spectrum is converged for a frequency resolution of 0.025 rad/s.

The potential flow method assumes the fluid to be ideal, irrotational and viscous effects are neglected. In potential flow calculations (using WAMIT and DIFFRAC) viscous effects can be accounted for by additional (viscous) damping terms. The influence of the additional viscous damping terms on the calculation of the roll response spectrum is investigated in Section 4.4. The added viscous damping terms can be incorporated in the calculation of the second order forces and in the calculation of the moment transfer function.

- The potential damping is a fraction of 0.001% of the critical damping.
- Although the added viscous roll damping term effects the calculated quadratic roll transfer function, the second order roll moment spectrum is not significantly influenced by the added viscous damping.
- Due to the small amount of potential damping, the viscous damping is dominant in the calculation of the moment transfer function.
- The roll motion response spectrum is dominated by the amount of viscous damping added in the calculation of the moment transfer function.

The refinement studies are closed with a recommendation. It must be realized that the second order drift moment spectrum and the moment transfer function are calculated with uncoupled first and second order variables. The uncoupled second order response amplitude operator (RAO) is used in order to determine the second order drift force spectrum. The WAMIT output consist of a coupled second order response amplitude operator (.16d-file). Matos et al showed that the second order response amplitude operator, decreases in amplitude for heave and pitch, when calculated for coupled motions [7]. The moment transfer function is calculated, making use of the uncoupled added mass and uncoupled potential damping matrices.

- r) It is recommended to use the coupled second order response amplitude operator and coupled added mass and potential damping matrices in order to define respectively the moment drift spectrum and moment transfer function.

5.2. FREQUENCY DOMAIN SIMULATION STUDY

The results of the refinements studies have been used in order to investigate the roll response spectra calculated for the three tested sea states. The roll response spectra for every tested sea state are calculated for different added viscous damping ratios as presented in Section 4.5. The zero order moment of the calculated roll response spectra is compared with the zero order moment of the measured roll response spectrum. Empirical values for the (linear) equivalent added viscous damping are obtained from this comparison in Figure 4.20, 4.21 and 4.22.

- In order to obtain a roll response spectrum with similar roll energy as measured for sea state one ($H_s = 1.5$ m, $T_p = 7$ s), a linear equivalent damping ratio of $\xi = 0.39$ % is needed in the frequency domain calculation.
- In order to obtain a roll response spectrum with similar roll energy as measured for sea state two ($H_s = 1.5$ m, $T_p = 12$ s), a linear equivalent damping ratio of $\xi = 0.95$ % is needed in the frequency domain calculation.
- In order to obtain a roll response spectrum with similar roll energy as measured for sea state three ($H_s = 3.0$ m, $T_p = 7$ s), a linear equivalent damping ratio of $\xi = 0.75$ % is needed in the frequency domain calculation.

In the figures in this Section also predicted equivalent damping values are indicated. In the frequency domain roll motion simulation method, the viscous damping is incorporated with a linearized equivalent damping term. In Section 4.1 three (partly mathematical) methods in order to predict a linearized viscous damping term are presented. The harmonic and stochastic linearization method use the p and q values obtained from the still water decay tests performed at MARIN. Furthermore the linearized roll damping is predicted from the measured roll response spectra using the half-power bandwidth method. From Figure 4.20, 4.21 and 4.22 can be concluded that:

- The harmonic and stochastic linearization techniques under predict the damping of the roll response in comparison with the measurements for sea state two and three. In sea state one the linearization methods predict the damping of the roll response in agreement with the measurements.

- The half-power bandwidth method over predicts the damping in sea state one and under predicts the damping in sea state two. In sea state three the method predicts the damping of the roll response in agreement with the measurements.

It must be mentioned that the harmonic and stochastic prediction methods use the p and q values obtained from still water decay test results. In still water there are no orbital velocities due to the absence of waves. The damping is related to the fluid velocity and therefore the orbital velocities could cause for additional damping of the global motion of the vessel. In the model test simulations, the still water decay p and q values are used, therefore the damping is expected to be underestimated. This underestimation due to the still water p and q values is not been investigated in this research.

The half-power bandwidth method is a rough damping estimation method which is highly sensitive for spectral resolution. Furthermore the results of this estimation technique provide strictly speaking not purely information about the damping but about the damping and excitation combined. Therefore the damping is expected to be overestimated (see Section B.1.4). The half-power bandwidth results are not used for further analyses.

An advantage of the frequency domain simulation method is the simplicity in application. Using the frequency method it is 'relatively' simple to calculate the roll motion responses. van 't Veer showed that implementing the stochastic linearization technique, which is dependent on the variance of the roll velocity spectrum, is applicable for every (user specified) sea state [11]. The calculation scheme of this process, which is applicable on the calculation of first order motions, is presented in Figure 4.23. In Figure 4.24 a calculation scheme applicable for the calculation of second order motions is proposed.

- r) The validation of the second order calculation scheme, including the stochastic linearization technique, has not been performed and is therefore recommended.

There are two main disadvantages of the frequency domain simulation method. Firstly the viscous damping can only be incorporated with a linearized equivalent damping term. Secondly the frequency domain simulation method provides no information about the phase of the calculated motions. In this research it is shown that the linearization of the viscous damping causes an over estimation of the simulated roll response spectra compared with the measured roll response spectrum, for two of the tested sea states. In other words the linearization techniques, which are used in order to determine an equivalent damping term, underestimate the actual viscous damping term for two of the three tested sea states. The underestimation of the damping, using the stochastic linearization technique proposed by Borgman, is also found in other research (see Section 4.1, [24]). In this research correction measures on the linearization method are applied.

- r) An interesting future research topic would be to investigate if the correction measures, suggested in earlier research, also apply on the linearization of the viscous damping of the Sleipnir.

Because the Sleipnir is a very low (potential or wave) damped system it is important to accurately predict the viscous damping term. The linearization of the viscous damping is concluded to be a big source of inaccuracy in the roll motion simulations. However the linearization of damping is not necessary in time domain simulations. Furthermore the time domain simulation method provides information about the phase of the motions.

5.3. TIME DOMAIN SIMULATION STUDY

In the time domain simulation method the non linear viscous damping can be incorporated making use of a linear and quadratic viscous damping coefficient. The still water decay tests, performed at MARIN, are simulated and compared with the measurements. From Figure 4.39 and 4.40 it can be concluded that:

- The damping in still water decay test simulations is in very good agreement with the measurements.

The damping coefficients, found in the decay test study, are used for the model test simulations. First the model test is simulated using the wave train measured during wave calibration tests of sea state three ($H_s = 3$ m, $T_p = 7$ s).

- It is found that, without changing the wave input, a ~3% change in sway period causes a ~25% change in zero order moment of the roll response (Figure 4.44 and Table 4.13).

This indicates that the amount of roll energy is (very) sensitive to the phase of the motion with respect to the phase of the incoming wave. In other words, the change in sway period causes a different location in the wave field, which effects the phase of the (coupled) roll motion with respect to the incoming waves. Therefore,

- r) it is recommended to also 'tune' the heave decay test simulation in Figure 4.40.

Due to the sensitivity for the location of the model in the wave field, it should be noted that the above time simulations have been performed with the wave train measured during wave calibration tests. Ideally, the generated waves during calibration tests and during model tests would be exactly equal. The measured wave time traces and wave spectra are compared in Section B.2.4. Between the wave time traces, measured at the same wave probe during model tests and calibration tests, exist differences. In order to investigate the influence of these different wave trains, simulations are performed using the wave trains measured during model tests. It must be realized that these wave trains are measured at a location in the basin next to the model (see Figure 2.3). Therefore the measured wave trains during model tests (especially at WAVE270) are 'contaminated' with wave reflections caused by the presence of the model. However the model tests have been performed with long crested waves. Therefore the wave train at WAVE180 should consist of more accurate phase information about the actual wave during model tests than the calibrated wave train. As a possible result of the statement in the previous sentence, it is shown, in Figure 4.44 and Table 4.14, that:

- The model test simulation with the wave train measured at WAVE180 during model tests is in best agreement with the measurements.

It must be noted that this better agreement could on one hand, originate from more accurate phase information of the wave train. On the other hand the better agreement could originate from the increased measured wave amplitude due to reflections, which is more plausible. This increase in measured wave amplitude will cause an increase in motion responses. There is not enough information, from the measurements performed at MARIN, to investigate the wave energy propagation or in other words the wave reflections.

- r) In order to study the wave energy propagation, the wave height could be measured on more specified locations during future model tests.

In order to investigate the influence of the phase on the roll response, a phase sensitivity study is performed. Ten model test simulations are performed using a JONSWAP spectrum with different wave seeds. The wave seeds provide a random phase to the waves in the spectrum. This study resulted in a mean zero order roll moment of 0.12 deg^2 with an error of $\pm 13\%$. These zero order values correspond with a mean maximal probable roll angle (in a 3 hours storm) of $1.28 (\pm 7\%) \text{ deg}$. It can be concluded that the phase does have a significant influence on the roll motion response. However, the better agreement, of the model test simulation with wave train MWAVE180 compared with the measurements, is more likely to originate from the added wave energy due to reflections. It would be very interesting to validate the aNySIM simulation with different wave seeds with model tests.

In the time domain simulations, as also in the frequency domain simulation method, the still water p and q values have been used. The still water decay test simulations are in good agreement with the measurements (Figure 4.40). The model test simulations have been performed with the still water damping constants. In Figure 4.44 the mismatch in roll response between the simulations and measurements can still be assigned to the lack of damping information of the orbital velocities of waves. However this would mean, in the case of the time simulations, that the still water p and q values do over predict the viscous damping in waves. This seems unrealistic, but therefore:

- r) It is recommended to investigate the influence of orbital velocities on the viscous damping terms of the Sleipnir.

INFLUENCE OF SECOND ORDER CONTRIBUTIONS ON THE QUADATIC TRANSFER FUNCTION

In Section 4.6 the first and second order calculations performed with WAMIT and DIFFRAC are compared. Although the calculated first and second order forces show similar behaviour, it is concluded that:

- The first and second order output of WAMIT and DIFFRAC, while using identical input variables, do not correspond.

The differences in second order results are expected due to different solving methods of the second order potential contribution. The direct, indirect and Pinkster method are compared in Figure 4.29. However the differences in the first order output and the second order contributions, based on first order quantities, are not expected (Figure 4.25, 4.26, 4.27). The differences can partly be assigned to the differences in the geometric input files (GDF- and PATRAN- file) and the differences in phase of the first order moment (see Figure 4.26).

- r) The differences between WAMIT and DIFFRAC output are not investigated but would be an interesting research topic for future research.

DIFFRAC is used in order to plot the five different contributions of the quadratic transfer function. In Figure 4.29 it can be seen that contribution one, the contribution due to the relative wave elevation, contribution two, the contribution due to the pressure drop as a consequence of the fluid velocity and contribution five, contribution related to the long wave induced by the presence of regular wave groups are dominant in the quadratic transfer function. The quadratic transfer function for the surge motion is validated with the findings of Pinkster in Section 4.7. Both results show similar behaviour (Figure 4.35, 4.36). In the low frequency range, of the roll quadratic transfer function (Figure 4.29), contribution two is dominant. Contribution five is dominant in the high frequency range. Because different contributions are dominant for different frequency ranges of the quadratic transfer function, it means that the dominant contribution for the roll response motions differ per specific sea state. This is shown by means of the second order moment spectrum for the three tested sea states in Figure 4.38. It can be concluded that:

- In sea state one and three, contributions two and five are dominant in the roll motion response spectrum at the natural frequency.
- In sea state two, contribution two is dominant in the roll motion response spectrum at the natural frequency.

In the frequency domain method the first and second order roll motions are calculated separately, see section 3.4. As a consequence it can be calculated which percentage of the second order or first order forces excite the low frequency response. In Section B.1.5 the roll response spectrum is calculated with all the wave spectra measured during model tests. The resulting roll motion spectra are compared for the total range, the low frequency range ($0 < \omega < 0.4$ rad/s) and the high (wave) frequency range ($0.4 < \omega < 2$ rad/s). It can be concluded that:

- In sea state one the low frequency roll response motion originates for 87 % from second order moments (average from all calculated roll response spectra using measured wave spectra).
- In sea state two the low frequency roll response motion originates for 98 % from second order moments (average from all calculated roll response spectra using measured wave spectra).
- In sea state three the low frequency roll response motion originates for 98 % from second order moments (average from all calculated roll response spectra using measured wave spectra).

In order to conclude a last recommendation for further research is suggested. Based on the conclusions that:

1. the Sleipnir is a very low damped system.
2. the roll response spectra are not in agreement with the measurements in the time domain
3. the contribution related to the long wave, induced by the presence of regular wave groups, is dominant in the quadratic transfer function

It could be argued that the duration of the model tests have been too short. The wave elevation of the long wave, induced by the presence of regular wave groups, seems important in the second order roll of the Sleipnir. The amount of wave groups, e.g. in Figure B.27, of the measured wave and the amount of 'roll motion groups' are in the order of ten. Using the rule of thumb that hundred relevant oscillations are needed for proper statistical analyses, the duration of the model test should be ten times longer. Theoretically a model test with a duration of 35 hours would give a better results regarding the statistics in this case. Practically it will be very difficult to obtain good results from such a model test. However this could be an interesting future research topic.

- r) It is recommended to investigate if performing model tests with a larger duration (or performing several model test with a different wave seed) result in a roll response spectrum in better agreement with the measurements.

5.4. ANSWER TO RESEARCH QUESTION

The main research question, as presented in the introduction, is defined:

Is it possible to predict the low frequency second order roll motions of the Sleipnir, in good agreement with the model tests, in the frequency and time domain?

The subquestions are considered to be extensively answered in the previous section. The answer to the main question is presented in two sections.

1. For the frequency domain, it is possible to simulate, using empirical obtained linear damping values, a roll response spectrum with a zero order moment in exact agreement with the measurements for three tested sea states. However it is in the interest of Heerema in order to predict the second order motions in every specified sea state.

Therefore a second order roll motion simulation method is presented in which, a prediction method for the linearized viscous damping, is incorporated. It still needs to be investigated if the second order calculation method does converge to the measured motion response.

2. In the time domain, the best simulation, using a wave train from the calibration tests, results in a most probable maximum roll angle of 1.57 deg comparing to 1.85 deg of the measured roll response (deviation of ~ 30 %).

In a phase sensitivity study it is concluded, based on ten simulations with a JONSWAP spectrum with different wave seeds, that solely a different phase can cause for a spread of ~ 13 % in the most probable maximum roll angle. It is recommended to perform more model tests in order to investigate if the probable phase difference, between the calibrated wave and the wave generated during model tests, influences the second order roll statistics.

Secondly it is recommended to perform model test with a larger duration. By performing longer model tests, more roll groups can be measured, which could influence the low frequency second order roll statistics.

5.5. SECOND ORDER ROLL PROBLEM IN PERSPECTIVE

Second order wave forces are generally significantly smaller with respect to first order wave forces. However due to the long roll period, the very low initial stability, the Sleipnir is sensitive for the energy in the energy of low frequency wave groups. Depending on the sea state the Sleipnir could start to resonate in the natural roll frequency excited by the low frequent second order wave forces, which is undesirable for performing a heavy lift.

Firstly, it must be noted that the sea states, used during model tests, exceed Heerema's typical operability limit for performing a heavy lift as shown in Figure 5.1. Secondly, note that the model tests have been performed with long crested beam waves. On open sea such conditions are very rare. Directional wave spectra may play an important role in the second order dynamics, as is also suggested by other research, e.g. [6]. Therefore investigation to the influence of directional quadratic transfer functions, on the low frequency roll motion simulation methods, presented in this research, is recommended.

Furthermore, it must be realized that the model tests have been performed with a low initial stability (small GM value). This low initial stability will only be reached when performing an extreme heavy lift. It would probably be commercially attractive for Heerema to perform only extreme heavy lifts in the future, however this is not expected to happen for practical reasons. This section will be concluded with an question and an answer.

Will the second order roll behaviour decrease the operability in future lift operations?

Yes, occasionally. Based on the performed master research, it is argued that second order roll behaviour will be a limiting factor for operability if:

- 1 The Sleipnir will have a low initial stability, e.g. in order to perform a very heavy lift.
- 2 The operation will be performed at an offshore location with long crested waves,
- 3 with (enough) low frequent wave energy in the order of magnitude of the long roll period.
- 4 The lift operation will be executed in beam waves.

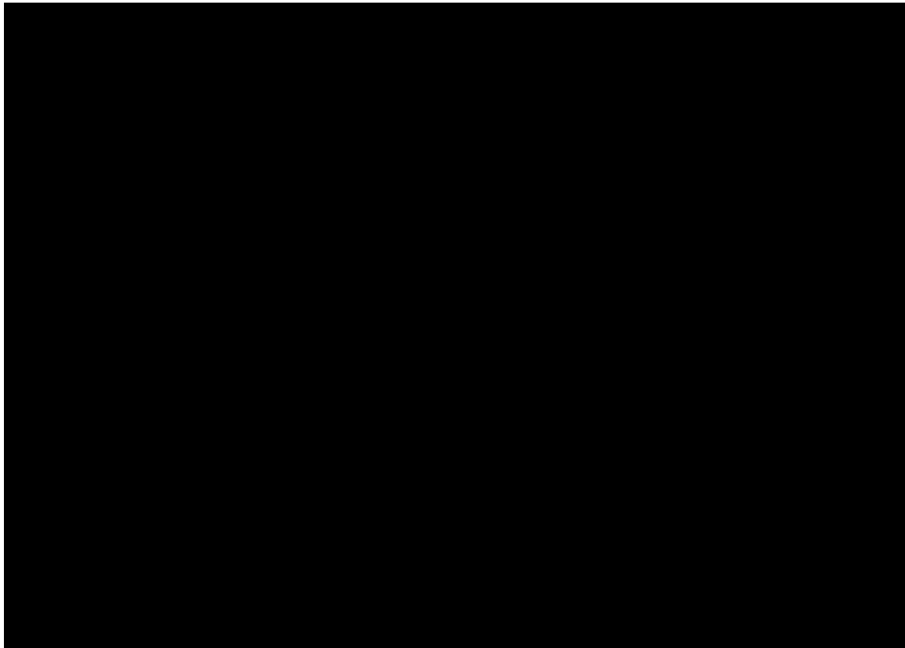


Figure 5.1: Typical heavy lift operability limit, used by Heerema. The sea conditions under the blue line are considered to be operable for performing a heavy lift. The sea states, used during model tests, exceed the operability limit.

5.6. ENUMERATION OF CONCLUSIONS

- It is concluded that the calculated forces and moments are converged for a discretized hull model with 9892 panels. The panels at the columns of the model consist of stretched panels to the waterline (see Figure 3.2). The panels at the waterline are 3.44 m in length and 0.64 m in height.
- It is concluded that the roll moment spectrum is converged for a frequency resolution of 0.025 rad/s.
- The potential damping is a fraction of 0.001% of the critical damping.
- Although the added viscous roll damping term effects the calculated quadratic roll transfer function, the second order roll moment spectrum is not significantly influenced by the added viscous damping.
- Due to the small amount of potential damping, the viscous damping is dominant in the calculation of the moment transfer function.
- The roll motion response spectrum is dominated by the amount of viscous damping added in the calculation of the moment transfer function.
- In order to obtain a roll response spectrum with similar roll energy as measured for sea state one ($H_s = 1.5$ m, $T_p = 7$ s), a linear equivalent damping ratio of $\xi = 0.39$ % is needed in the frequency domain calculation.
- In order to obtain a roll response spectrum with similar roll energy as measured for sea state two ($H_s = 1.5$ m, $T_p = 12$ s), a linear equivalent damping ratio of $\xi = 0.95$ % is needed in the frequency domain calculation.
- In order to obtain a roll response spectrum with similar roll energy as measured for sea state three ($H_s = 3.0$ m, $T_p = 7$ s), a linear equivalent damping ratio of $\xi = 0.75$ % is needed in the frequency domain calculation.
- The harmonic and stochastic linearization techniques under predict the damping of the roll response in comparison with the measurements for sea state two and three. In sea state one the linearization methods predict the damping of the roll response in agreement with the measurements.
- The half-power bandwidth method over predicts the damping in sea state one and under predicts the damping in sea state two. In sea state three the method predicts the damping of the roll response in

agreement with the measurements.

- The damping in still water decay test simulations is in very good agreement with the measurements.
- It is found that, without changing the wave input, a ~3% change in sway period causes a ~25% change in zero order moment of the roll response (Figure 4.44 and Table 4.13).
- The model test simulation with the wave train measured at WAVE180 during model tests is in best agreement with the measurements.
- The first and second order output of WAMIT and DIFFRAC, while using identical input variables, do not correspond.
- In sea state one and three, quadratic transfer function contributions two and five are dominant in the roll motion response spectrum at the natural frequency.
- In sea state two, quadratic transfer function contribution two is dominant in the roll motion response spectrum at the natural frequency.
- In sea state one the low frequency roll response motion originates for 87 % from second order moments (average from all calculated roll response spectra using measured wave spectra).
- In sea state two the low frequency roll response motion originates for 98 % from second order moments (average from all calculated roll response spectra using measured wave spectra).
- In sea state three the low frequency roll response motion originates for 98 % from second order moments (average from all calculated roll response spectra using measured wave spectra).

5.7. ENUMERATION OF RECOMMENDATIONS

- r) Perform a validation study on the vertical drift forces, calculated with potential theory, compared with measurements.
- r) It is recommended to use the coupled second order response amplitude operator and coupled added mass and potential damping matrices in order to define respectively the moment drift spectrum and moment transfer function.
- r) The validation of the second order calculation scheme, including the stochastic linearization technique, has not been performed and is therefore recommended.
- r) An interesting future research topic would be to investigate if correction measures, suggested in earlier research, also apply on the linearization of the viscous damping of the Sleipnir.
- r) It is recommended to also 'tune' the heave decay test simulation in Figure 4.40.
- r) In order to study the wave energy propagation, the wave height could be measured on more specified locations during future model tests.
- r) It is recommended to investigate the influence of orbital velocities on the viscous damping terms of the Sleipnir.
- r) The differences between WAMIT and DIFFRAC output are not investigated but would be an interesting research topic for future research.
- r) It is recommended to investigate if performing model tests with a larger duration (or performing several model test with a different wave seed) result in a roll response spectrum in better agreement with the measurements.

BIBLIOGRAPHY

- [1] A. J. Voogt, J. J. Soles, and R. V. Dijk, *Mean and low frequency roll for semi-submersibles in waves*, 12th ISOPE (2002).
- [2] M. Takagi, S.-I. Arai, S. Takezawa, K. Tanaka, and N. Takarada, *A comparison of methods for calculating the motion of a semi-submersible*, *Ocean Engineering* **12**, 45 (1985).
- [3] J. Wichers, *Low frequency motions of moored vessels*, SWZ 11-91, 625 (1991).
- [4] R. Dallinga, R. Huijsmans, and J. Pinkster, *Combined statistics of first and second order motions of semi-submersibles*, BOSS Conference, Trondheim **2: Hydrodynamics**, 737 (1988).
- [5] J. A. Pinkster, *Mean and low frequency wave drifting forces on floating structures*, *Ocean Engineering* **6**, 593 (1979).
- [6] V. L. F. Matos, E. O. Ribeiro, A. N. Simos, and S. H. Sphaier, *2nd order pitch and roll slow motions of a semi-submersible platform: Full scale measurements and theoretical predictions comparative study*, OMAE2010-20898 **1**, 581 (2010).
- [7] V. L. F. Matos, A. N. Simos, and S. H. Sphaier, *Second-order resonant heave, roll and pitch motions of a deep-draft semi-submersible: Theoretical and experimental results*, *Ocean Engineering* **38**, 2227 (2011).
- [8] F. T. Matsumoto and A. N. Simos, *Predicting the second-order resonant roll motions of an FPSO*, OMAE2014-24530 **8B** (2014).
- [9] F. Tasai, *Ship Motions in Beam Seas*, Tech. Rep. 45 (Reports of Research Institute for Applied Mechanics, Kyushu University, 1965).
- [10] L. E. Borgman, *Ocean wave simulation for engineering design*, (1967).
- [11] J. K. R. van 't Veer, F. Fathi, ed., *On Roll Hydrodynamics of FPSO's Fitted with Bilge Keels and Riser Balcony*, Vol. 30 (OMAE2011, 2011).
- [12] J. Pinkster, *Low frequency second order wave exciting forces on floating structures*, Ph.D. thesis, Delft University of Technology (1980).
- [13] J. Journée and W. Massie, *Offshore Hydromechanics*, 1st ed. (Delft University of Technology, 2001).
- [14] C. Lee, *WAMIT Theory Manual*, Massachusetts Institute of Technology, report no. 95-2 ed. (1995).
- [15] G. de Hauteclocque, F. Rezende, O. Waals, and X. B. Chen, *Review of approximations to evaluate second-order low-frequency load*, OMAE2012-83407 **1**, 363 (2012).
- [16] Y. Himeno, *Prediction of ship roll damping*, , 86 (1981).
- [17] *Operational wave tests of the NSCV*, DATA Report 27311-3-SMB Volume II (MARIN (Maritime Research Institute Netherlands), 2014).
- [18] E. de Ridder and R. van Engelenburg, *Operational Wave Tests of the NSCV*, Final Report 27311-3-SMB (MARIN (Maritime Research Institute Netherlands), 2014).
- [19] WAMIT, *WAMIT User Manual Versions 6.1, 6.4, 6.4S, 7.0*, WAMIT, Inc. (2014).
- [20] C. L. X. Zhu, *Removing the irregular frequencies in wave body interactions*, (1994).
- [21] Y. H. Y. Ikeda, K. Komatsu and N. Tanaka, *On roll damping force of ship*, The Kansai Society of Naval Architects (1977).

- [22] M. Hajiarab, *Roll Damping Prediction of a Free Floating Barge*, Ph.D. thesis, School of Marine Science and Technology, Newcastle University (2013).
- [23] R. S. J. Falzarano, A. Somayajula, *An overview of the prediction methods for roll damping of ships*, *Ocean Systems Engineering* **5**, 55 (2015).
- [24] J. Wolfram, ed., *On Alternative Approaches to linearization and Morison's equation for wave forces*, 455, Royal Society Mathematical, Physical and Engineering Sciences (The Royal Society, 1998).
- [25] G. H. G.A. Papagiannopoulos, *On the use of the half-power bandwidth method to estimate damping in building structures*, *Soil Dynamics and Earthquake Engineering* **31**, 1075 (2011).
- [26] O. F. N. Salvesen, E.O. Tuck, *Ship motions and sea loads*, The Society of Naval Architects and Marine Engineers **78**, 250 (1970).
- [27] A. F. Seybert, *Estimation of damping from response spectra*, *Journal of Sound and Vibration* **75**, 199 (1981).
- [28] T. D. S. Gueydon, *Comparison of second-order loads on a semisubmersible floating wind turbine*, *OMAE* **OMA2014-23398** (2014).
- [29] *DIFFRAC User guide*, MARIN, version 2.4.4 ed. (2014).
- [30] *Averaging, Errors and Uncertainty*, Department of Physics & Astronomy, University of Pennsylvania.

A

VESSEL SPECIFICATIONS OF SLEIPNIR

Ship name:	Sleipnir
Ship type:	Semi-Submersible Crane Vessel
Lift capacity:	2 × 10,000 tonnes
Classification Society:	Lloyd's Register
Expected date of delivery:	end of 2018

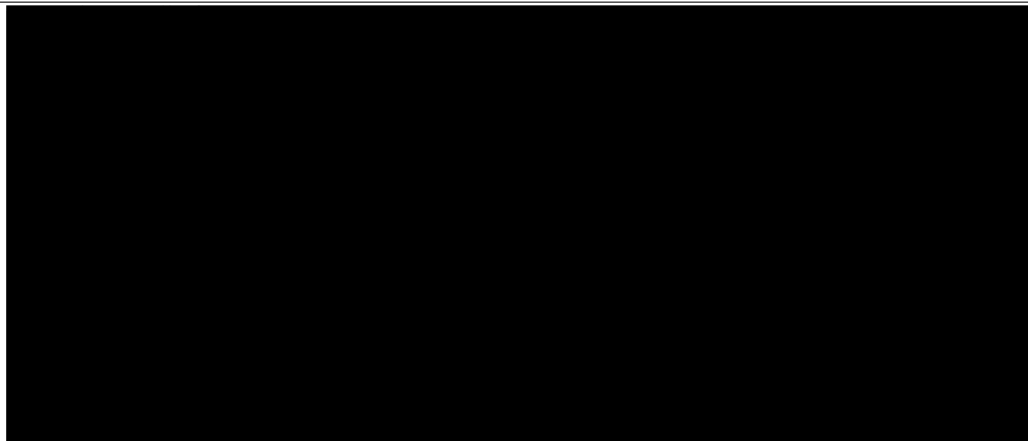
Description	Unit	Magnitude <i>Specified</i>
		

Table A.1: Main specifications of the Sleipnir.

B

RESULTS

C

THEORETICAL BACKGROUND

C.1. STATISTICAL ANALYSIS

C.1.1. STATISTICAL DESCRIPTION OF WAVES

In order to do predictions about how a floating structure will behave in a certain sea state it is necessary to first understand the basic principles of ocean waves. In this chapter the basic theory about this subject is given and explained.

WAVES

The sea surface consists of a pattern of waves with various periods, heights and phase angles. The water surface elevation $\zeta(t)$ at a fixed location in the sea is a random process that can be modeled as a long-term non-stationary process over a period of years [2]. However, for short-term intervals, of the order of some hours, the surface elevation can be approximated as a stationary process. That is a sea state in which the significant wave height and mean wave period are assumed constant during the time considered.

The long-term variation of a wave climate can be described in terms of generic distributions or in terms of governing sea state parameters. Long-term statistics are associated with non-stationary processes occurring over a period of months and years, and long-term data for wave conditions are commonly given in the form of a scatter diagram.

In this study $\zeta(t)$ is considered to be a zero mean, Gaussian, stationary process and is represented by a linear summation of an infinite number of sinusoids with phase angles randomly distributed between 0 and 2π . Since the wave profile is assumed to be the sum of sine and cosine functions, a Fourier series can describe the wave process. Neglecting the non-linear effects and making use of linear superposition. To do this, one selects a time record segment containing many waves. Indeed, one assumption implicit in this analysis is that the signal being studied repeats itself after each (long) interval. A wave record does not do this exactly, but that little detail is neglected in this case.

WAVE SPECTRA

The wave elevation (in the time domain) of a long-crested irregular sea, propagating along the positive x axis, can be written as the sum of a large number of regular wave components (in the frequency domain):

$$\zeta(t) = \sum_{n=1}^N \zeta_{an} \cos(k_n x - \omega_n t + \epsilon_n) \quad (\text{C.1})$$

In which each component n represents random wave characteristics. The Fourier series will thus yield a set of values for ζ_{an} and ϵ_n , each associated with its own ω_n . If enough Fourier series terms are included, the entire time record at that point can be reproduced using this set of values. In practice, however, one is not really interested in the exact water level at some time t. It is sufficient to know only the statistical properties - now in terms of both frequency and amplitude - of the signal. This means that the ϵ_n can be discarded [13].

In equation C.1 the wave amplitude for each component ζ_{an} can be expressed in a wave spectrum:

$$S(\omega_n) \cdot \Delta\omega = \sum_{\omega_n}^{\omega_n + \Delta\omega} \frac{1}{2} \zeta_{an}^2(\omega) \quad (\text{C.2})$$

Where $\Delta\omega$ is a difference between two successive frequencies. Multiplied with $\rho \cdot g$, this expression is the energy per unit area of the waves in the frequency interval $\Delta\omega$, see Figure C.1.

JONSWAP SPECTRUM

Under the design stage of an offshore structure, spectra describing the actual sea state in the relevant area of operation are not always available. However for design purposes often standardized analytical wave spectra are being used. In this study the JONSWAP (Joint North Sea Wave Project) spectrum is used. The JONSWAP spectrum is defined as follows [13]:

$$S_{\zeta}(\omega) = \frac{320 \cdot H_{1/3}^2}{T_p^4} \cdot \omega^{-5} \cdot \exp \left\{ \frac{-1950}{T_p^4} \cdot \omega^{-4} \right\} \cdot \gamma^A \quad (\text{C.3})$$

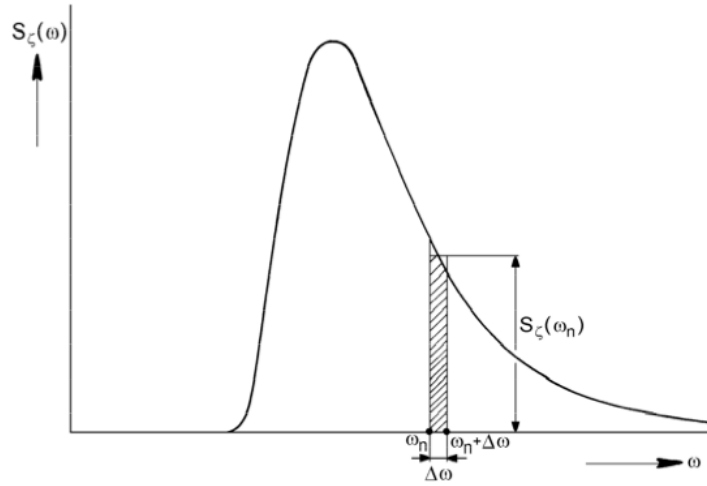


Figure C.1: Illustration of a spectral density spectrum plotted against frequency.

in which: γ = peakness factor (3.3).
 $A = \exp \left\{ - \left(\frac{\omega}{\omega_p} - 1 \right)^2 \right\}$.
 ω_p = frequency at spectral peak.
 σ = step function if $\omega < \omega_p$ then: $\sigma = 0.07$.
if $\omega > \omega_p$ then: $\sigma = 0.09$.

ZERO ORDER MOMENT AND RMS

Important characteristics of a spectrum are the moments of area. The moments of area under the spectrum are with respect to the vertical axis at $\omega = 0$. If m denotes a moment, then $m_{n\zeta}$ denotes the n^{th} order moment given in this case by:

$$m_{n\zeta} = \int_0^{\infty} \omega^n \cdot S_{\zeta} d\omega \quad (C.4)$$

From Equation C.4 it can be seen that, $m_{0\zeta}$ is the area under the spectral curve, $m_{1\zeta}$ is the first order moment (static moment) of this area and $m_{2\zeta}$ is the second order moment (moment of inertia) of this area and so on. The value of $m_{0\zeta}$ is equal to the variance squared σ_{ζ}^2 of the water surface elevation, since it is the area under the (in this case JONSWAP) spectrum. The root mean square of the water surface elevation is defined as:

$$\sigma_{\zeta} = RMS = \sqrt{m_{0\zeta}} \quad (C.5)$$

In order to calculate the RMS of a spectrum, the corresponding zero order moment m_{0k} has to be calculated in which k is the related motion, velocity or acceleration. If the wave spectrum S_{ζ} and the RAO's of specific motion are known, it is possible to calculate the corresponding spectrum of the specific motion. To obtain this spectrum, the wave elevation spectrum has to be multiplied with the related transfer function squared:

$$S_m = \left| \frac{m}{\zeta_a} \right|^2 \cdot S_{\zeta} \quad (C.6)$$

In this equation m represents the related motion or acceleration. [13]

D

SOFTWARE

MULTISURF

MultiSurf is a software package for parametric design of 3D geometric objects. Multisurf is used to make a discretized geometric model of the Sleipnir. Three different panel distributions have been created in order to perform hydrodynamic analyses. The models are exported in Geometric Data File (GDF) format. The geometric panel models are presented in Appendix E.1. MultiSurf is furthermore used in order to create a Free surface Data File (FDF-format) shown in Appendix E.2.

WAMIT

WAMIT (Wave Analysis Massachusetts Institute of Technology) is a program for computing the wave loads and the motion behaviour of floating bodies with zero forward speed in deep and shallow water. The program uses linear and second order potential theory in order to solve the velocity potential around a floating body. WAMIT uses the 3D panel method in order to solve the velocity potential.

In this research WAMIT version 6.1 has been used to calculate the first and second order wave loads and motion behaviour [19]. In this version the second order module requires a low order panel model of the floating body. In the low order method the geometry is represented by quadrilateral panels and the velocity potential is assumed constant on each panel. The low order panel model for this research is presented in Appendix E. The velocity potential is calculated on the body with the radiation and diffraction analysis. In linear potential theory the fluid pressure and the velocity potential is solved using the boundary element method (BEM). Separate solutions are carried out simultaneously for the diffraction and the radiation problem [28]. The pressure distribution on the panels is calculated using the velocity potentials. Finally the pressure distribution is used to determine the hydrodynamic added mass and damping coefficients and the first and second order wave forces. The first-order solution consist of contributions which can be calculated distinctly and independently. WAMIT consists of the two subprograms POTEN and FORCE. POTEN solves the radiation and diffraction velocity potentials on the body surface for specified modes, frequencies and wave headings. FORCE computes global quantities including the hydrodynamic coefficients, motions and first and second order forces.

In order to solve the second order velocity potential, the diffraction and the radiation problem can no longer be considered separately. The second order velocity potential can be calculated completely by WAMIT using a discretized free water surface, which is shown in Appendix E.

In Figure D.1 a flow chart is shown of the analyses in this research by WAMIT.

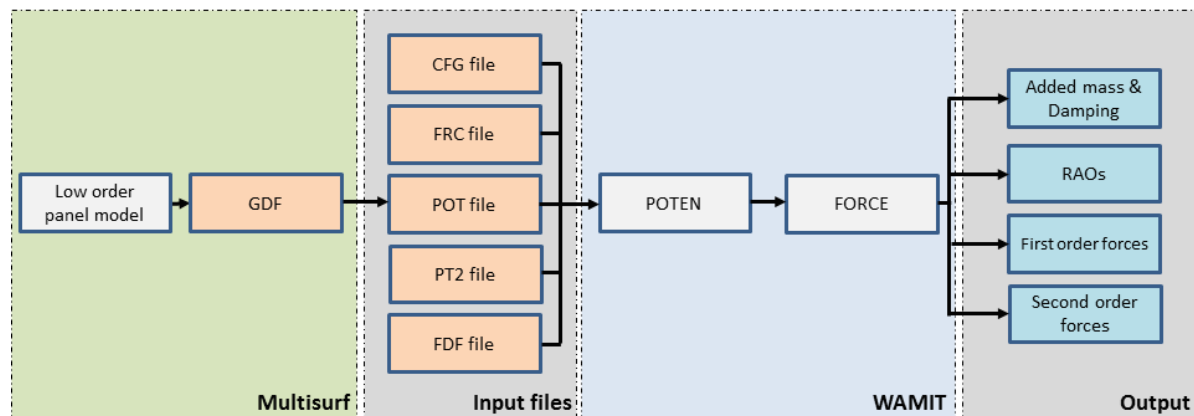


Figure D.1: Flowchart of the WAMIT analysis.

INPUT FILES

The input files needed for WAMIT to evaluate the velocity potentials on a body are the following [19]:

1. **Geometric Data File (GDF):**

The basic geometry of the submerged body surface is specified in the GDF file. The GDF file provides the coordinates of all panel vertices. For this research the low order GDF file of the Sleipnir has been designed with Multisurf (See Appendix E.1).

2. **Force Control File (FRC):**

The FRC file is used to set which hydrodynamic parameters must be computed by the FORCE program.

In this research the *Alternative form 2* of the FRC file is used to define the water density, center of gravity, the mass matrix, an external damping matrix and an external stiffness matrix. This permits analysis of bodies which are not freely floating in waves.

3. Potential Control File (POT):

The potential control file specifies various input parameters to the POTEN subprogram. The potential control file defines the water depth, range of frequencies, frequency step and the position of the body in the global coordinate system.

4. Configuration File (CFG):

The configuration file is used to specify various parameters and options in WAMIT. The CFG file defines if the FORCE subprogram must perform second order force calculations. Furthermore the option in order to remove irregular frequencies can be set.

Additional input files for second order calculations:

5. Potential Control File 2 (PT2):

The potential control file 2 specifies which modes and for which period and heading combination the second order output must be calculated. The option in order to calculate the sum or/and difference frequencies is also set in the PT2 file.

6. Free Surface Data File (FDF):

The FDF file contains all requisite data to perform a free surface integration exterior to the body. The free surface is discretized with quadrilateral panels in order to solve the free surface integral numerically. In this research the FDF file have been designed with Multisurf (See Appendix E.2).

OUTPUT FILES

The results of the WAMIT calculations consists of separate output files which have been specified in the FRC files. In this study the following output files have been used:

1. **Added mass and damping coefficients (.1 file)**
2. **Exciting forces from diffraction potential (.3 file)**
3. **Response Amplitude Operators (.4 file)**
4. **Mean drift force and moment from pressure (.9 file)**

The output files from second order calculations are presented below. In this research only the difference frequencies have been used for analysis. The added -d in the file names signifies the output of difference frequencies.

5. Quadratic second order forces and moments by pressure integration (.10d file):

The .10d file consists of the quadratic second order forces and moments which are build up by the summation of the four first contributions. The potential contribution is excluded in this output. The forces and moments in this output file can be calculated without the FDF file.

6. Total second order forces by indirect method (.11d file):

The .11d file consists of the the total second order potential forces and moments not evaluated from the scattering solution but from the appropriate component of the radiation solution. The FDF file is needed in order to calculate the total forces and moments.

7. Total second order forces by direct method (.12d file):

The .12d file consists of the the total second order potential forces and moments evaluated from the scattering solution. The FDF file is needed in order to calculate the total forces and moments.

DIFFRAC

DIFFRAC is a program package which calculates the hydrodynamic properties of floating bodies in regular waves or wave groups. This program is based on the same 3D potential theory as WAMIT uses. In DIFFRAC the panels which describe the submerged part of a floating body are flat and the value of the velocity potential is assumed constant over each panel area. This method is similar with the low order method used in WAMIT. DIFFRAC uses different subprograms in order to calculate the hydrodynamic properties of a specified floating body. The subprograms which calculate the added mass, damping, wave induced motions (RAO's), first order wave forces and second order wave forces are described below [29].

INPUT AND OUTPUT FILES

1. **PATDIF:**

Converts a 'neutral system file' with geometric data to files suitable as input for the subprogram INIDIF of the DIFFRAC software package.

- (a) Input:
PATRAN.OUT file.
- (b) Output:
PATDIF.OUT - printer output file
GEOM.DAT - a file with the geometric data.
CORNER.DAT - file with panel vertices.

In this research the geometric data file of the sleipnir is created with Multisurf. This geometric data file is converted to a PATRAN file, suitable for the DIFFRAC program, with Rhino 3D, a 3D computer graphics and computer aided design program.

2. **INIDIF:**

This subprogram creates and initializes a DIFFRAC database and checks correctness of geometric data.

- (a) Input:
INIDIF.INP
GEOM.DAT
CORNER.DAT
- (b) Output:
INIDIF.OUT
DIFFRAC database

3. **DIFFRAC:**

Subprogram which computes the added mass, damping, first order wave forces and wave induce motions in centre of gravity for specified wave frequencies.

- (a) Input:
DIFFRAC.INP
DIFFRAC database
- (b) Output:
DIFFRAC.OUT
DIFFRAC database

4. **DBDRIFT:**

DBDRIFT calculates the mean second order wave drift forces.

- (a) Input:
DBDRIFT.INP
DIFFRAC database
- (b) Output:
DBDRIFT.OUT

5. **DBRESP:**

DBRESP computes hydrodynamic data and wave induced motions in centre of gravity. The COG, mass distribution matrix, damping matrix and hydrostatic data can be re-set. The DIFFRAC database is overwritten.

- (a) Input:
DBRESP.INP
DIFFRAC database
- (b) Output:
DBRESP.OUT
DIFFRAC database

6. **DRIFTP:**

The subprogram DRIFTP calculates the second order wave drift force response (QTF) with the data from a specified diffraction database. DRIFTP uses the Pinkster approximation in order to solve the second order potential contribution. The Pinkster approximation is based on first order quantities [12].

- (a) Input:
DRIFTP.INP
DIFFRAC database
- (b) Output:
DRIFTP.OUT

7. **GENHYD:**

GENHYD generates a sequential file with hydrodynamic data. This file is input for time domain simulation programs aNySIM.

- (a) Input:
GENHYD.INP
DIFFRAC database
- (b) Output:
GENHYD.OUT
HYDfile

ANYSIM

aNySim is used in order to perform time domain simulations. The input for the calculation is the .ini - file. In the ini-file the geometric data of the Sleipnir, the duration of the time simulation, the reference position in earth fixed global system, additional linear and quadratic damping matrices, the soft mooring line specifications, wave input and other parameters are set. The calculation output is a .res file. This file is a text structure in which all the output is written.

MATLAB

MathWorks MATLAB R2013b is used for the post processing of the WAMIT, DIFFRAC and aNySIM output. The frequency domain model in order to predict the low frequency second order roll response is programmed in MATLAB.

E

DISCRETIZED SURFACE MODELS

F

ERROR ANALYSES MANUAL

In this appendix a manual on Averaging, Errors and Uncertainty of the Department of Physics & Astronomy from the University of Pennsylvania is presented. This manual provides an quick inside in error analyzes.[30]

Reading instruction: Turn the thesis ninety degrees clockwise, then the pages are structured from left to right.

Averaging, Errors and Uncertainty

Types of Error

There are three types of limitations to measurements:

- 1) **Instrumental limitations**
Any measuring device can only be used to measure to with a certain degree of fineness. Our measurements are no better than the instruments we use to make them.
- 2) **Systematic errors and blunders**
These are caused by a mistake **which does not change** during the measurement. For example, if the platform balance you used to weigh something was not correctly set to zero with no weight on the pan, all your subsequent measurements of mass would be too large. Systematic errors do not enter into the uncertainty. They are either identified and eliminated or lurk in the background producing a shift from the true value.
- 3) **Random errors**
These arise from unnoticed variations in measurement technique, tiny changes in the experimental environment, etc. Random variations affect precision. Truly random effects average out if the results of a large number of trials are combined.

Precision vs. Accuracy

- A **precise** measurement is one where independent measurements of the same quantity closely cluster about a single value that may or may not be the correct value.
- An **accurate** measurement is one where independent measurements cluster about the true value of the measured quantity.

Systematic errors are not random and therefore can never cancel out. They affect the accuracy but not the precision of a measurement.

A. Low-precision, Low-accuracy:

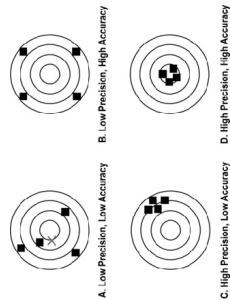
The average (the X) is not close to the center

B. Low-precision, High-accuracy:

The average is close to the true value

C. High-precision, Low-accuracy:

The average is not close to the true value



Writing Experimental Numbers

Uncertainty of Measurements

Errors are quantified by associating an uncertainty with each measurement. For example, the best estimate of a length L is 2.59cm, but due to uncertainty, the length might be as small as 2.57cm or as large as 2.61cm. L can be expressed with its uncertainty in two different ways:

1. **Absolute Uncertainty**
Expressed in the units of the measured quantity: $L = 2.59 \pm 0.02\text{cm}$
2. **Percentage Uncertainty**
Expressed as a percentage which is independent of the units
Above, since $0.02/2.59 \approx 1\%$ we would write $L = 7.7\text{cm} \pm 1\%$

Significant Figures

Experimental numbers must be written in a way consistent with the precision to which they are known. In this context one speaks of **significant figures** or digits that have physical meaning.

1. All definite digits and the first doubtful digit are considered significant.
2. Leading zeros are **not** significant figures.
Example: $L = 2.31\text{cm}$ has 3 significant figures. For $L = 0.0231\text{m}$, the zeros serve to move the decimal point to the correct position. Leading zeros are not significant figures.
3. Trailing zeros are significant figures: they indicate the number's precision.
4. One significant figure should be used to report the uncertainty or occasionally two, especially if the second figure is a five.

Rounding Numbers

To keep the correct number of significant figures, numbers must be rounded off. The discarded digit is called the **remainder**. There are three rules for rounding:

- ✓ **Rule 1:** if the remainder is less than 5, drop the last digit.
Rounding to one decimal place: $5.346 \rightarrow 5.3$
- ✓ **Rule 2:** if the remainder is greater than 5, increase the final digit by 1.
Rounding to one decimal place: $5.798 \rightarrow 5.8$
- ✓ **Rule 3:** if the remainder is exactly 5 then round the last digit to the closest even number. This is to prevent rounding bias. Remainders from 1 to 5 are rounded down half the time and remainders from 6 to 10 are rounded up the other half.
Rounding to one decimal place: $3.55 \rightarrow 3.6$, also $3.65 \rightarrow 3.6$

Statistical Analysis of Small Data Sets

Repeated measurements allow you to not only obtain a better idea of the actual value, but also enable you to characterize the uncertainty of your measurement. Below are a number of quantities that are very useful in data analysis. The value obtained from a particular measurement is x . The measurement is repeated N times. Oftentimes in lab N is small, usually no more than 5 to 10. In this case we use the formulae below:

Mean (\bar{x}_{avg})	The average of all values of x (the “best” value of x)	$\bar{x}_{\text{avg}} = \frac{x_1 + x_2 + \dots + x_N}{N}$
Range (R)	The “spread” of the data set. This is the difference between the maximum and minimum values of x	$R = x_{\text{max}} - x_{\text{min}}$
Uncertainty in a measurement (Δx)	Uncertainty in a single measurement of x . You determine this uncertainty by making multiple measurements. You know from your data that x lies somewhere between x_{max} and x_{min} .	$\Delta x = \frac{R}{2} = \frac{x_{\text{max}} - x_{\text{min}}}{2}$
Uncertainty in the Mean ($\Delta \bar{x}_{\text{avg}}$)	Uncertainty in the mean value of x . The actual value of x will be somewhere in a neighborhood around \bar{x}_{avg} . This neighborhood of values is the uncertainty in the mean.	$\Delta \bar{x}_{\text{avg}} = \frac{\Delta x}{\sqrt{N}} = \frac{R}{2\sqrt{N}}$
Measured Value (x_{m})	The final reported value of a measurement of x contains both the average value and the uncertainty in the mean.	$x_{\text{m}} = \bar{x}_{\text{avg}} \pm \Delta \bar{x}_{\text{avg}}$

The average value becomes **more and more precise** as the number of measurements N increases. Although the uncertainty of any single measurement is always Δx , the **uncertainty in the mean $\Delta \bar{x}_{\text{avg}}$** becomes smaller (by a factor of $1/\sqrt{N}$) as more measurements are made.

Examples

The period of a pendulum is given by $T = 2\pi\sqrt{l/g}$.

Here, $l = 0.24\text{m}$ is the pendulum length and $g = 9.81\text{m/s}^2$ is the acceleration due to gravity.

✘ **WRONG:** $T = 0.983269235922\text{s}$

✔ **RIGHT:** $T = 0.98\text{s}$

Your calculator may report the first number, but there is no way you know T to that level of precision. When no uncertainties are given, report your value with the same number of significant figures as the value with the smallest number of significant figures.

The mass of an object was found to be 3.56g with an uncertainty of 0.032g .

✘ **WRONG:** $m = 3.56 \pm 0.032\text{g}$

✔ **RIGHT:** $m = 3.56 \pm 0.03\text{g}$

The first way is wrong because the uncertainty should be reported with one significant figure

The length of an object was found to be 2.593cm with an uncertainty of 0.03cm .

✘ **WRONG:** $L = 2.593 \pm 0.03\text{cm}$

✔ **RIGHT:** $L = 2.59 \pm 0.03\text{cm}$

The first way is wrong because it is impossible for the third decimal point to be meaningful.

The velocity was found to be 2.45m/s with an uncertainty of 0.6m/s .

✘ **WRONG:** $v = 2.5 \pm 0.6\text{m/s}$

✔ **RIGHT:** $v = 2.4 \pm 0.6\text{m/s}$

The first way is wrong because the first discarded digit is a 5. In this case, the final digit is rounded to the closest even number (i.e. 4)

The distance was found to be 45600m with an uncertainty around 1m

✘ **WRONG:** $d = 45600\text{m}$

✔ **RIGHT:** $d = 4.5600 \times 10^4\text{m}$

The first way is wrong because it tells us nothing about the uncertainty. Using scientific notation emphasizes that we know the distance to within 1m .

Example

You measure the length of an object five times. You perform these measurements twice and obtain the two data sets below.

Measurement	Data Set 1 (cm)	Data Set 2 (cm)
x_1	72	80
x_2	77	81
x_3	8	81
x_4	85	81
x_5	88	82

Quantity	Data Set 1 (cm)	Data Set 2 (cm)
x_{avg}	81	81
R	16	2
Δx	8	1
Δx_{avg}	4	0.4

For Data Set 1, to find the best value, you calculate the mean (i.e. average value):

$$x_{avg} = \frac{72\text{cm} + 77\text{cm} + 82\text{cm} + 86\text{cm} + 88\text{cm}}{5} = 81\text{cm}$$

The range, uncertainty and uncertainty in the mean for Data Set 1 are then:

$$R = 88\text{cm} - 72\text{cm} = 16\text{cm}$$

$$\Delta x = \frac{R}{2} = 8\text{cm}$$

$$\Delta x_{avg} = \frac{R}{2\sqrt{5}} \approx 4\text{cm}$$

Data Set 2 yields the same average but has a much smaller range.

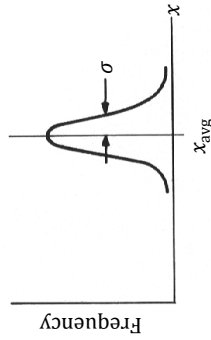
We report the measured lengths x_m as:

Data Set 1: $x_m = 81 \pm 4\text{cm}$
 Data Set 2: $x_m = 81.0 \pm 0.4\text{cm}$

Notice that for Data Set 2, Δx_{avg} is so small we had to add another significant figure to x_m .

Statistical Analysis of Large Data Sets

If only random errors affect a measurement, it can be shown mathematically that in the limit of an infinite number of measurements ($N \rightarrow \infty$), the distribution of values follows a **normal distribution** (i.e. the bell curve on the right). This distribution has a peak at the mean value x_{avg} and a width given by the standard deviation σ .



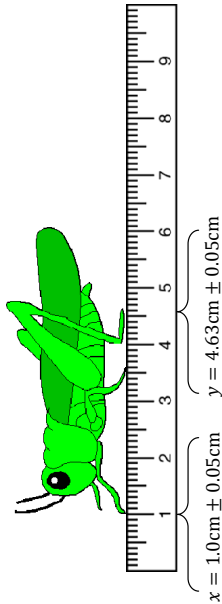
Obviously, we never take an infinite number of measurements. However, for a large number of measurements, say, $N \sim 10 - 10^2$ or more, measurements may be approximately normally distributed. In that event we use the formulae below:

Mean (x_{avg})	The average of all values of x (the "best" value of x). This is the same as for small data sets.	$x_{avg} = \frac{\sum_{i=1}^N x_i}{N}$
Uncertainty in a measurement (Δx)	Uncertainty in a single measurement of x . The vast majority of your data lies in the range $x_{avg} \pm \sigma$	$\Delta x = \sigma = \sqrt{\frac{\sum_{i=1}^N (x_i - x_{avg})^2}{N}}$
Uncertainty in the Mean (Δx_{avg})	Uncertainty in the mean value of x . The actual value of x will be somewhere in a neighborhood around x_{avg} . This neighborhood of values is the uncertainty in the mean.	$\Delta x_{avg} = \frac{\sigma}{\sqrt{N}}$
Measured Value (x_m)	The final reported value of a measurement of x contains both the average value and the uncertainty in the mean.	$x_m = x_{avg} \pm \Delta x_{avg}$

Most of the time we will be using the formulae for small data sets. However, occasionally we perform experiments with enough data to compute a meaningful standard deviation. In those cases we can take advantage of software that has programmed algorithms for computing x_{avg} and σ .

Propagation of Uncertainties

Often times we combine multiple values, each of which has an uncertainty, into a single equation. In fact, we do this every time we measure something with a ruler. Take, for example, measuring the distance from a grasshopper's front legs to his hind legs. For rulers, we will assume that the uncertainty in all measurements is one-half of the smallest spacing.



The measured distance is $d_m = d \pm \Delta d$ where $d = 4.63 \text{ cm} - 1.0 \text{ cm} = 3.63 \text{ cm}$. What is the uncertainty in d_m ? You might think that it is the sum of the uncertainties in x and y (i.e. $\Delta d = \Delta x + \Delta y = 0.1 \text{ cm}$). However, statistics tells us that if the uncertainties are independent of one another, the uncertainty in a sum or difference of two numbers is obtained by quadrature: $\Delta d = \sqrt{(\Delta x)^2 + (\Delta y)^2} = 0.07 \text{ cm}$. The way these uncertainties combine depends on how the measured quantity is related to each value. Rules for how uncertainties propagate are given below.

Addition/Subtraction	$z = x \pm y$	$\Delta z = \sqrt{(\Delta x)^2 + (\Delta y)^2}$
Multiplication	$z = xy$	$\Delta z = xy \sqrt{\left(\frac{\Delta x}{x}\right)^2 + \left(\frac{\Delta y}{y}\right)^2}$
Division	$z = \frac{x}{y}$	$\Delta z = \left \frac{x}{y}\right \sqrt{\left(\frac{\Delta x}{x}\right)^2 + \left(\frac{\Delta y}{y}\right)^2}$
Power	$z = x^n$	$\Delta z = n x^{n-1}\Delta x$
Multiplication by a Constant	$z = cx$	$\Delta z = c \Delta x$
Function	$z = f(x, y)$	$\Delta z = \sqrt{\left(\frac{\partial f}{\partial x}\right)^2 (\Delta x)^2 + \left(\frac{\partial f}{\partial y}\right)^2 (\Delta y)^2}$

Examples
Addition

The sides of a fence are measured with a tape measure to be 124.2cm, 222.5cm, 151.1cm and 164.2cm. Each measurement has an uncertainty of 0.07cm. Calculate the measured perimeter P_m including its uncertainty.

$$P = 124.2 \text{ cm} + 222.5 \text{ cm} + 151.1 \text{ cm} + 164.2 \text{ cm} = 662.0 \text{ cm}$$

$$\Delta P = \sqrt{(0.07 \text{ cm})^2 + (0.07 \text{ cm})^2 + (0.07 \text{ cm})^2 + (0.07 \text{ cm})^2} = 0.14 \text{ cm}$$

$$P_m = 662.0 \pm 0.1 \text{ cm}$$

Multiplication

The sides of a rectangle are measured to be 15.3cm and 9.6cm. Each length has an uncertainty of 0.07cm. Calculate the measured area of the rectangle A_m including its uncertainty.

$$A = 15.3 \text{ cm} \times 9.6 \text{ cm} = 146.88 \text{ cm}^2$$

$$\Delta A = 15.3 \text{ cm} \times 9.6 \text{ cm} \sqrt{\left(\frac{0.07}{15.3}\right)^2 + \left(\frac{0.07}{9.6}\right)^2} = 1.3 \text{ cm}^2$$

$$A_m = 147 \pm 1 \text{ cm}^2$$

Power/Multiplication by Constant

A ball drops from rest from an unknown height h . The time it takes for the ball to hit the ground is measured to be $t = 1.3 \pm 0.2 \text{ s}$. The height is related to this time by the equation $h = \frac{1}{2}gt^2$ where $g = 9.81 \text{ m/s}^2$. Assume that the value for g carries no uncertainty and calculate the height h including its uncertainty.

$$h = \frac{1}{2}(9.8 \text{ m/s}^2)(1.3 \text{ s})^2 \approx 8.281 \text{ m}$$

$$\Delta h = \frac{1}{2}(9.8 \text{ m/s}^2)(2 \times 1.3 \text{ s} \times 0.2 \text{ s}) \approx 2.5 \text{ m}$$

$$h_m = 8 \pm 3 \text{ m}$$

G

COMPANY PROFILES

G.1. HEEREMA MARINE CONTRACTORS



Heerema Marine Contractors (HMC) is a marine contractor in the offshore oil and gas industry. The company is founded in 1948. HMC's core business is transporting, installing and removal of offshore facilities including fixed and floating structures, subsea pipelines and infrastructure in shallow, deep and ultra deep waters.

HMC manages the complete supply chain of offshore constructions with offices and yards in five continents, from design through completion. The services HMC provides include engineering, planning, logistics, project management and project execution. The headquarter is located in Leiden. The amount of employees worldwide consists of approximately 1750 people. In 2014 HMC did realize a turnover of approximately €1.9 billion.

HMC owns a fleet consisting of three heavy lift semi-submersibles, one monohull deepwater construction vessel, two anchor handling tugs and ten cargo/launch barges. Below specifications of HMC's largest vessels are shown:

<p>Thialf The Thialf is a semi-submersible crane vessel (SSCV) with two cranes. The Thialf is a multi-functional deep water crane vessel (DCV) and is customized for the installation of foundations, moorings, SPAR's, TLP's, integrated topsides and pipe- and flowlines.</p> <ul style="list-style-type: none"> • Built in 1985. • Lift capacity: 2 x 7100 t. • Dimensions (Overall length x Width): 202 x 88 m. • Draft: 11.8-31.6 m 	<p>Balder The DCV Balder is customized for the installation of foundations, moorings, SPAR's, TLP's, integrated topsides and pipe- and flowlines.</p> <ul style="list-style-type: none"> • Built in 1978, converted to DCV in 2001/2002. • Lift capacity: 1 x 2700 t and 1 x 3600 t. • Dimensions (Overall length x Width): 154 x 86 m. • Draft: 11-25 m.
<p>Hermod The Hermod is a semi-submersible crane vessel (SSCV).</p> <ul style="list-style-type: none"> • Built in 1978. • Lift capacity: dual lift of 8100 t. • Dimensions (Overall length x Width): 154 x 86 m. • Draft: 11.5-28.2 m. 	<p>Aegir The DCV Aegir is designed for executing complex infrastructure and pipeline projects in ultra-deep water and to install fixed platforms in relatively shallow waters.</p> <ul style="list-style-type: none"> • Built in 2012. • Lift capacity: 4000 t. • Dimensions (Overall length x Width): 210 x 46 m. • Draft: 8-11 m.
<p>Sleipnir The Sleipnir will be a semi-submersible crane vessel. The vessel is mainly designed to perform heavy lifts and to be able to transport and remove large offshore structures.</p> <ul style="list-style-type: none"> • Expected date of delivery end of 2018. • Lift capacity: 2 x 10000 t. • Dimensions (Overall length x Width): 220 x 102 m. • Draft: 12-32 m. 	

For further information: <http://hmc.heerema.com>

G.2. MARITIME RESEARCH INSTITUTE NETHERLANDS



Maritime Research Institute Netherlands (MARIN) is an independent research institute for hydrodynamic and nautical research and development. The institute is founded in 1929. The core business of MARIN is to provide the industry with design solutions and to perform advanced research for the maritime sector. The main office of MARIN is located in Wageningen and other offices are located in Ede and Houston, USA. In total approximately 350 people are working at MARIN.

MARIN is organized in different 'Business Units' in order to efficiently manage knowledge development and to provide the industry a complete range of services. The different business units with their own speciality are:

Business Unit	Expertise
Offshore	Mooring systems, Dynamic Positioning, Complex Installations, Towing of structures, Riser Behaviour, Dredging Equipment in waves, floating civil works, wave run up problems at fixed structures, launching human comfort, downtime analyses and impact loading.
Ships	Resistance & Propulsion, Propulsors & Cavitation, Manoeuvring and Seakeeping with the market teams Cruise & Ferry, Navy, Special Purpose Vessels, Inland Ships, Merchant Vessel & Work Boats and Yachts.
Maritime Simulations & Software Group	Simulators, Design & Engineering tools and Workflow solutions, Technology Transfer and Training, Simulator & Software support.
Nautical centre MSCN	Providing mathematical manoeuvring models for simulators in order to conduct studies and/or trainings comprising Accident investigations, Manoeuvring capability studies, Operational Procedures, Port & Channel design studies, Safety (QRA) using the facilities Fast-time Simulators, Full Mission Bridge Simulators and VTS Simulations.
Research & Development	Resistance & Propulsion, Waves & Workability, Manoeuvring & Nautical Studies, Operations at Sea, CFD Development, Ice and Time Domain Simulations & Control Theory
Trials & Monitoring	Attendance, measurements and analyses of sea trials, , Cavitation observation, Ship and Fleet performance analysis, Hydro-structural analyses, Monitoring Campaigns, On board advisory systems, Long term monitoring of offshore structures.

MARIN is capable of providing services which incorporate combinations of simulations, model testing, full-scale measurements and training programs. MARIN has seven model tank facilities: Seakeeping & Manoeuvring Basin, Offshore Basin, Deepwater Towing Tank, Depressurised Wave Basin, High-speed Basin, Shallow Water Basin and the Cavitation Tunnel.

In general MARIN is an independent institute which provides research, services and consultancy to the maritime sector. In 2014 MARIN did realize a turnover of €42,- million.

For further information: <http://www.marin.nl>

